CAPACITIVE EFFECT OF MICROSTRIP DISCONTINUITIES

Peter Benedek, B.Eng., M.Eng.

INTEGRAL EQUATION SOLUTION OF THE CAPACITIVE EFFECT OF MICROSTRIP DISCONTINUITIES

by

Peter Benedek, B.Eng., M. Eng.

A thesis submitted to the Faculty of Graduate Studies and Research
in partial fulfillment of the requirements for the degree of
Doctor of Philosophy.

Department of Electrical Engineering,
McGill University,
Montreal, Quebec.

June, 1972.

ABSTRACT

The integral equations governing the electrostatics of the excess charge distribution near various microstrip discontinuities are formulated. Discontinuities considered are : open-circuits, gaps, steps, right angle bends, T junctions and crossings. The resulting equations are solved by a projective method, using polynomial approximants. Their solution hinges on the development of computationally efficient techniques for dealing with the singularities and pseudo-singularities that occur, by suitable coordinate transformations and special weighted quadrature formulae. The importance of the discontinuity capacitances in the design of distributed microwave integrated circuits is demonstrated. Also, the integral equation describing the electrostatics of the microstrip is solved by a projective method, using trial functions that preserve the singularity in the charge distribution at the strip edges. The capacitance of rectangular plates on metal backed dielectric substrates is obtained by solving the Fredholm integral equation of the first kind governing the charge distribution on the plates. Extensive results are presented.

ACKNOWLEDGEMENTS

First and foremost I am grateful to Dr. P. Silvester, my thesis advisor, who suggested the problem and acted as a source of inspiration throughout its solution. Although, at time, the obstacles seemed insurmountable, it was through his continuous open-door policy, coupled with the attitude that he was never too busy to discuss a problem, that many of these were overcome. If just a small fraction of his problem solving ability rubbed-off on me, then the few years expended under his guidance were well spent.

Many thanks to my colleagues Z. Csendes, A. Konrad*, K.K. Chan, S. Tymchyshyn and P. Kenton, who in addition to offering a forum and a discussion group for various problems, also provided an extremely pleasant atmosphere to work in. Helpful discussions with Drs. A. Evans, H.S. Cabayan, B. Brown and, in particular, A. Gopinath were much appreciated. Also, informative talks with Drs. D.S. James and R.W. Breithaupt of the Communications Research Centre, are hereby acknowledged.

Acknowledgements are also due to H.E. Stinehelfer, Sr. of Microwave Associates Inc., Burlington, Massachusetts, for his extreme kindness for communicating results and data, as well as to P. Troughton and A. Farrar who were kind enough to correspond with us on matters pertaining to this thesis.

The help provided by A. White by his careful evaluation of Palmer's results and to M.S. Hsieh by his evaluation of the moments with respect to weight $\ln [|x - \xi|/(|x - \xi| + 1)]$ was much appreciated.

---

* The many hours spent by Mr. A. Konrad reading the typed version of the thesis, were instrumental in eliminating numerous errors.

Many thanks are due to Mrs. P. Hyland for expertly typing this thesis.

The financial support of the National Research Council of Canada, in the form of Postgraduate Scholarships, and of the Communications Research Centre in the form of a contract on the study of microstrip transmission lines, is gratefully acknowledged.

And finally, many thanks to my wife, Magda, for putting up with a husband, who during the past years was also married to the computer. Without her encouragement and moral support, this work would not have been possible.

CLAIM OF ORIGINALITY

The original contributions in this thesis are :

(1) A unified theoretical treatment, leading to an efficient numerical method, capable of dealing with the capacitive effect of microstrip discontinuities.

(2) The evaluation of the capacitive effects of the following microstrip discontinuities : (i) open-circuits, (ii) gaps, (iii) steps, (iv) right angle bends, (v) T junctions and (vi) crossings.

(3) The solution of the electrostatic capacitance of rectangular plates on metal backed dielectric substrates by the Rayleigh-Ritz method with biquadratic expansion and projection functions, made possible by the development of computationally efficient techniques capable of dealing with singularities and pseudo-singularities.

TABLE OF CONTENTS

			Page
ABSTRACT			i
ACKNOWLEDGEMENTS			ii
CLAIM OF ORIGINALITY			iv
TABLE OF CONTENTS			v
LIST OF ILLUSTRATIONS			viii
CHAPTER	I	STATE OF THE ART AND OBJECTIVES	1
CHAPTER	II	SOME THEORETICAL BACKGROUND	9
	2.1	Introduction	9
	2.2	Definitions	9
	2.3	Fundamental Solution for the Laplacian Operator and its Relationship to Green's Function	12
	2.4	Charged Thin Metal Plate in an Unbounded Region	13
	2.5	Variational Formulation	18
	2.6	Advantage of the Variational Formulation	21
	2.7	Rayleigh-Ritz Method over Many Subregions	22
	2.8	Galerkin-Petrov Method	24
	2.9	The Integral Operator corresponding to the Laplacian is Positive Definite.	25
CHAPTER	III	INFINITE MICROSTRIP PROBLEM	28
	3.1	Introduction	28
	3.2	Governing Integral Equation	29
	3.3	Treatment of Singularities and Solution of the Integral Equation	31
	3.4	Results and Comparison with Existing Data	36
CHAPTER	IV	CAPACITANCE OF RECTANGULAR PLATES ON METAL-BACKED DIELECTRICS	42
	4.1	Introduction	42
	4.2	Governing Integral Equation	43
	4.3	Solution of the Integral Equation by Rayleigh Ritz Method over Many Subregions	48
	4.4	Evaluation of the Inner Products - Special Treatment of Singularities and Pseudo-singularities	49

			Page
	4.5	Results and Comparison with Existing Data	57
CHAPTER	V	MICROSTRIP DISCONTINUITY CAPACITANCES	67
	5.1	Introduction	67
	5.2	Definitions and Methodology	67
	5.3	Microstrip Open Circuits	70
	5.3.1	Circuit Model and Existing Data	70
	5.3.2	Excess Charge Formulation	73
	5.3.3	Solution for Excess Charge and $C_{o.c.}$	75
	5.3.4	Results and Comparison with Existing Data	78
	5.4	Microstrip Gaps	81
	5.4.1	Circuit Model and Existing Work	81
	5.4.2	Excess Charge Formulation for C_{even} and C_{odd}	85
	5.4.3	Solution for Excess Charge, and C_{even} and C_{odd}	88
	5.4.4	Results and Comparison with Existing Data	90
	5.5	Microstrip Steps	95
	5.5.1	Circuit Model and Existing Work	95
	5.5.2	Excess Charge Formulation	96
	5.5.3	Solution for Excess Charge and C_{step}	99
	5.5.4	Results and Comparison with Existing Data	100
	5.6	Microstrip Right Angle Bends	104
	5.6.1	Circuit Model and Existing Work	104
	5.6.2	Excess Charge Formulation	104
	5.6.3	Solution for Excess Charge and C_{bend}	107
	5.6.4	Results and Comparison with Existing Work	109
	5.7	Microstrip T Junctions	111
	5.7.1	Circuit Model and Existing Work	111
	5.7.2	Excess Charge Formulation	113
	5.7.3	Solution for Excess Charge and C_T	114
	5.7.4	Results and Comparison with Existing Data	115
	5.8	Microstrip Crossings	119
	5.8.1	Circuit Model and Existing Work	119
	5.8.2	Excess Charge Formulation	121
	5.8.3	Solution for Excess Charge and C_+	122
	5.8.4	Results and Comparison with Existing Data	123
CHAPTER	VI	IMPORTANCE OF DISCONTINUITY CAPACITANCES IN THE DESIGN OF OPEN-CIRCUITED MULTISTUB MICROSTRIP FILTERS	127
	6.1	Introduction	127
	6.2	A Two-Port Network Analysis Program	128

			Page
	6.3	Analysis of the Five-Section Ten-Stub Filter	130
	6.4	Results	133
CHAPTER	VII	CONCLUSIONS	140
APPENDIX	I		143
APPENDIX	II		145
REFERENCES			149

LIST OF ILLUSTRATIONS

			Page
Figure	2.4.1	Thin conductor in vacuum	14
Figure	3.2.1	Microstrip cross-section	30
Figure	3.4.1	Microstrip charge density distribution in vacuum for $w/h = 5.0$	38
Figure	3.4.2	Microstrip charge density distribution in vacuum for $w/h = 0.1$	39
Table	3.1	Microstrip capacitance in p F / meter	41
Figure	4.2.1	Conducting plate on metal backed dielectric substrate and equivalent problem	44
Figure	4.2.2	Image representation, valid in the dielectric region, for point charge near an infinite dielectric sheet	44
Figure	4.2.3	8 - way symmetry for the rectangular plate on metal backed dielectric substrate	47
Figure	4.2.4	Region of integration for Equation (4.2.5)	47
Figure	4.4.1	Region of integration in the $x\,x'$ - plane and in the transformed $p\,q$ - plane	52
Figure	4.4.2	Region of integration for Equation (4.4.8)	54
Figure	4.4.3	Region of integration for Equation (4.4.11)	56
Table	4.5.1	$C\,d/\epsilon\,A$, where C is the parallel plate capacitance normalized w. r. t. capacitance of infinite plates	58
Figure	4.5.1	Comparative capacitance values by Harrington [26] and this method	59

			Page
Figure	4.5.2	Comparative capacitance values by Farrar and Adams [20] and this method	59
Table	4.5.2	Parallel square plate ($w = 1$) capacitance in vacuum as obtained by Reitan [50] and this method	60
Figure	4.5.3	Normalized capacitance values for rectangular plates in vacuum some distance h from an infinite ground plane	62
Figure	4.5.4	Effective filling factor η for some commonly used permittivities	62 - 63
Table	4.5.3	Computation times for rectangular plate capacitance calculations	65
Figure	5.3.1.1	Microstrip open circuit together with two equivalent models	72
Figure	5.3.3.1	Potential residual near two open circuits ($w/h = 6.0$, $w/h = 0.2$ and $\epsilon_r = 9.6$)	77
Figure	5.3.4.1	Comparative end effect results obtained by Napoli and Hughes [45], Troughton [65], Farrar and Adams [20,21] and this method.	79
Figure	5.3.4.2	Open circuit capacitances, normalized to strip width, as as a function of width-to-height ratio and permittivity.	82
Figure	5.4.1.1	Stinehelfer's [62] gap capacitance model for a gap in the microstrip	83
Figure	5.4.1.2	Microstrip gap and capacitive π - equivalent network	84
Figure	5.4.1.3	Symmetrically and anti-symmetrically excited π - network resulting in C_{even} and C_{odd}, respectively	86

			Page
Figure	5.4.3.1	Potential residual for the symmetrically (C_{even}) and anti-symmetrically (C_{odd}) excited microstrip gap ($w/h = 1.0$, $s/w = 0.1$ and $\epsilon_r = 9.6$	89
Figure	5.4.4.1	Transmission loss measured by Stinehelfer [62] and calculated by this method, for the gap in microstrip	91
Figure	5.4.4.2	C_{even} and C_{odd} normalized to strip width as a function of gap spacing and substrate permittivity	92 - 94
Figure	5.5.1.1	Microstrip step and shunt discontinuity capacitance model	97
Figure	5.5.1.2	Equivalent circuit for microstrip step incorporating inductive elements	98
Figure	5.5.3.1	Potential residual near a microstrip step ($w_1/h = 1$, $w_2/h = 2$ and $\epsilon_r = 9.6$)	101
Figure	5.5.4.1	Step capacitance normalized to geometric mean width as a function of width-to-height ratio and substrate permittivity	103
Figure	5.6.1.1	Microstrip right angle bend together with equivalent circuit proposed by Stephenson and Easter [60]	105
Figure	5.6.3.1	Potential residual near a microstrip right angle bend ($w_1/h = 1.0$ and $\epsilon_r = 1.0$)	108
Figure	5.6.4.1	Microstrip bend capacitances normalized to strip width as a function of width-to-height ratio and substrate permittivity	110
Figure	5.7.1.1	Microstrip T junction together with its equivalent circuit	112
Figure	5.7.3.1	Potential residual near a microstrip T junction ($w_1/h = 1.0$, $w_2/h = 1.0$ and $\epsilon_r = 9.9$)	116

			Page
Figure	5.7.4.1	Microstrip T junction capacitances, normalized to main line width, as a function of stub line impedance	118
Figure	5.8.1.1	Microstrip crossing together with its equivalent circuit	120
Figure	5.8.3.1	Potential residual near a microstrip crossing ($w_1/h = 3$, $w_2/h = 1$ and $\epsilon_r = 9.9$)	124
Figure	5.8.4.1	Microstrip crossing capacitances, normalized to main line width, as a function of stub line impedance	126
Figure	6.2.1	General two-port network	129
Figure	6.2.2	N cascaded two-ports	129
Figure	6.3.1	Atwood and Stinehelfer's [6] passband filter design	131
Figure	6.3.2	Circuit model and transmission loss for ideal filter design	134
Figure	6.3.3	Filter model, modified for the effect of crossings, and transmission loss	135
Figure	6.3.4	Filter model, modified for the effect of crossings and open circuits, and transmission loss	136
Figure	6.3.5	Filter model, modified for the effect of crossings, open circuits and steps, and transmission loss	138
Figure	6.3.6	Filter transmission loss for the model of Figure 6.3.5 a, including the effect of lossy lines	139
Figure	II.1	Line charge with polarity reversal	146
Figure	II.2	Coordinate system used in the analysis of a microstriplike charge distribution with a polarity reversal	146

CHAPTER I

STATE OF THE ART AND OBJECTIVES

At various stages in the development of the microwave industry, after the wave propagation characteristics of a new form of transmission line are determined and its advantages are recognized, the interest shifts onto modeling its discontinuities. The wave propagating characteristics of microstrip are as well known, as are its numerous advantages. On the other hand, since there is little known about microstrip discontinuities, prototype design is mostly a cut-and-try procedure. The availability of extensive discontinuity data could increase the market penetration of microstrip, by substantially reducing the high cost of design. In this thesis a unified theoretical treatment, capable of dealing with the electrostatic capacitive effects of microstrip discontinuities will be presented.

In the mid - 1940's ; Whinnery and Jamieson published extensive results for parallel plane [70] and coaxial [71] transmission lines. Their approach was one of "matching of electromagnetic wave solutions, across discontinuities" [70] . During World War II, a great deal of work was done on waveguide discontinuities at the Radiation Laboratory of Massachusetts Institute of Technology. As a result of this work, a comprehensive book was compiled by Marcuvitz [39] .

Usually, a transmission line is designed so that, in the frequency band of operation, only one mode is propagated along it. At a discontinuity, however, to describe the field fully an infinite number of non-propagating modes is required. These

modes decay rapidly away from the discontinuity. Whinnery and Jamieson [70] and Marcuvitz [39] showed that such local discontinuity fields can be represented by lumped equivalent circuits.

In the second half of the 1950's Oliner and Altschuler presented lumped models for discontinuities in balanced strip transmission lines [3,46]. They obtained their results using " a small aperture procedure or a Babinet equivalent procedure in conjunction with an approximate model of the line" [3].

Although the electrical properties of microstrip transmission lines have been studied for about twenty years, reliable theoretical data became available only a few years ago. Since then, the microstrip transmission line found extensive uses both in microwave devices and integrated circuits.

The advantages of microstrip over conventional transmission lines are numerous [29] ; among these are :

(i) easy integrability in both monolithic and hybrid circuits (with similar components, semiconductors, ferrites and lumped elements) ,

(ii) low volume and weight,

(iii) broad bandwidth,

(iv) high reliability,

(v) low production cost.

As far as disadvantages are concerned, there are two main ones, namely : very high cost of engineering and relatively low power capability. (Although losses in microstrip are considerably higher than in traditional forms of transmission lines, the greatly reduced size of the circuit makes this loss quite insignificant.) Circuit designers go to great lengths to increase the power capability of microstrip circuits, by improved techniques of heat removal. However, even in low power applications, where heat removal is not a problem, there is a trade-off between the high development cost of microstrip circuits, and their increased reliability and hence lower maintenance costs. For space and military applications, the increased reliability, in addition to the other advantages, overrides cost. On the other hand, for more "every-day" types of microwave applications relatively few inroads have been made.

As far back as 1937, Palmer [47] using the Schwartz-Christoffel transformation, rigorously calculated the capacitance of an infinitely long pair of parallel plates in air. In 1952, Assadourian and Rimai [5] used a simplified theory based on conformal mapping and estimated the characteristic impedance, power flow, together with conductor and dielectric losses. But it was only in 1965, that Wheeler [68, 69] also using an approximate conformal mapping, treated the case of two infinitely long parallel plates separated by a dielectric sheet and gave results accurate to within a few percent for very thin conductors. Caulton, Hughes and Sobol [11], in 1966, repeated Wheeler's calculations, and showed the results to be in good agreement with experiment.

In 1967, Kaupp [33] presented extensive measurements for thick microstrip lines and used these results to produce some empirical formulae. Silvester [53], in early 1968, used the substrip method to solve the integral equation, governing the electrostatics of the microstrip, obtained by partial image theory. This was the first method capable of dealing equally well with both narrow and wide, and thick and thin conductors, with considerable accuracy.

At this point, the rate at which papers appeared on the subject increased rapidly. Still in 1968, Yamashita and Mittra [74] used a variational method in the Fourier transform domain, to obtain the capacitance of a microstrip structure. This was followed by Stinehelfer's [61] paper using a finite difference technique for the microstrip in a box, and by Yamashita's [75] work, again in the Fourier transform domain, treating various microstriplike structures.

Iossel, Kochanov and Strunskiy [30] in 1969, published extensive data on capacitance calculations of n-conductor systems in vacuum. Among the problems solved, mostly by a method equivalent to the method of subareas, was that of two thin infinitely long parallel conductors. In 1970, Mittra and Itoh [44] obtained the charge distribution on and the potential near a shielded microstrip line, while in 1971, Yamashita and Atsuki [73] reported an integral equation formulation for the thick microstrip in a box, where the Green's function was obtained by a Fourier series method.

In addition to the study of the electrostatics of the microstrip, extensive efforts have been conducted into measuring [4, 12, 41, 67] and theoretically predicting [13, 16, 27, 28, 43, 76] its dispersive effects. Losses in microstrip [23, 49]

have also received careful consideration. Similarly, the electrostatics [10] of and dispersion [34, 35] in a coupled pair of microstrip lines has been studied.

From the survey so far presented, it is obvious that in recent years there has been a substantial amount of literature published on microstriplike transmission lines. However, even with the increased use of integrated circuits, there appears to be little data for finite plates on metal-backed dielectric substrates. In 1959, Reitan [50] obtained the capacitance of two parallel square plates in vacuum, using the method of subareas. Harrington [25], in 1968, solved the same problem by the point matching method. Iossel, Kochanov and Strunskiy [30], in a work already mentioned in regard to infinitely long parallel plates ,also calculated the capacitance of two parallel rectangular plates in air, by Reitan's method. In 1969, Adams and Mautz [2] found the capacitance of a rectangular dielectric loaded capacitor, by introducing special matrix elements to account for the air-dielectric interface. Fuller and Chang [22], in 1970, showed that if only the total charge is desired, it is possible to reformulate the problem of the capacitance of a rectangular plate in vacuum in terms of a nonsingular quantity ; the resulting integral equation is solved by Harrington's moment method.

It was 1971 before Farrar and Adams [20] obtained the capacitance of a rectangular section of a microstrip line by the point matching method. Later the same year, Patel [48] solved the capacitance problem of a thin n-conductor system on a dielectric substrate, by a method similar to that used by Farrar and Adams. Still in 1971, Bostian and Wiley [9] claimed that Harrington's method of moments leads to an inherently ill-conditioned matrix. Their argument was that for a square plate, as the

number of subareas is increased, the matrix is no longer strictly diagonally dominant. This, however, is not one of the known criteria for ill-conditioned matrices. As a matter of fact Harrington and Mautz [26] have just published a rebuttal.

Now, to proceed to survey the available literature on microstrip discontinuities, Lewin [38] was the first to consider the problem. His objective was limited to radiation from microstrip open and short circuits, bends and resonators. Interest in radiation from microstrip discontinuities was rekindled recently, when it was shown [15, 19, 58, 66] that a significant fraction of the power loss in a microstrip open circuited stub, is due to radiation at the open circuit.

Attempts, however, to actually model microstrip discontinuities are even more recent. Stinehelfer [62], in 1968, performed measurements on open circuit resonators, gaps and T junctions and crossings. The limited amount of remaining material on microstrip discontinuity models, appeared since the spring of 1971. The first of these was Troughton [65] who conducted experiments on microstrip open-circuits and T junctions. He then proceeded to design successfully, by computer, a multistub filter using the various measured corrections. Then followed the numerical calculations of Farrar and Adams [20] on end-effects at open-circuits, and the measured results of Napoli and Hughes [45] with possible error limits due to dispersion, still on open-circuits. In mid - 1971, Sobol [57] in a review paper, made a one line mention of a simplified theory for the open-circuit effect, but failed to pursue the point. Later in the same year Stephenson and Easter [60] presented preliminary measurements of a resonant technique capable of dealing with microstrip right angle bends.

Still in 1971, Leighton and Milnes [37] in a study on 3 - db directional couplers utilized an approximate model of microstrip, similar to that used by Oliner and Altschuler [3, 46] for balanced stripline, for which the behaviour of a T-junction had been evaluated by Marcuvitz [39].

In 1972, James and Tse [31], using the same approach as Farrar and Adams, presented results for microstrip open-circuits, while Farrar and Adams [21] published a correction to their earlier calculations. Wolff, Kompa and Mehran [72] in a letter in April 1972, matched infinite series of higher order modes at planes of discontinuity in microstrip steps and T junctions, on a waveguide model of the microstrip line. They presented numerically obtained scattering coefficients.

From this literature survey it is readily seen that, although there are numerous papers treating microstrip discontinuities, they mostly deal with open circuits (and even there they show considerable disagreement). For other discontinuities the available data, with two exceptions [37, 72], are all of experimental origin ; and since no two experimentalists consider the same case, there exists no supporting evidence.

The lack of data on microstrip discontinuities necessitates time-consuming and expensive cut-and-try methods in microwave design. Extensive discontinuity data could reduce substantially one of the two main disadvantages of microstrip transmission lines, i.e. the very high cost of engineering. The answer to this problem is not some time-consuming experimental procedure, but rather a general theoretical approach. If large quantities of reliable data were to become available, it is not difficult to visualize

the design of microwave circuits entirely by computer, without any subsequent "tuning" being necessary.

The objective of this thesis is to present a unified theoretical treatment of the electrostatic behaviour of microstrip discontinuities, leading to an efficient numerical method capable of dealing with the capacitive effect of a large number of discontinuities. In particular, microstrip open circuits, gaps, steps, right angle bends, T junctions and crossings will be considered. In the process, two supporting problems will be discussed and solved : the first is the electrostatics of microstrip lines, the second is the electrostatics of rectangular plates on metal backed dielectric substrates.

First, the electrostatic capacitance of microstrip transmission lines is solved, using trial functions which preserve the essential singularity in the charge distribution. This approach provides an efficient means of obtaining electrostatic capacitances, without having to compromise on the accuracy of the charge distribution detail. Second, the problem of thin rectangular plates on metal backed substrates is solved. Instead of the method of subareas with zeroth order approximation on a large number of subareas, the use of a biquadratic trial set with a single subregion will be shown.

CHAPTER II

SOME THEORETICAL BACKGROUND

2.1 Introduction

As entire books have been written on the material in this chapter, it is neither possible nor desirable to go into much detail. Instead, some commonly used definitions are stated, the variational method is introduced and its relationship to the Rayleigh-Ritz and Galerkin-Petrov methods are presented. The fundamental solution for the Laplacian operator is given and used to develop the integral equation governing the charge distribution on a conducting surface. The resulting integral operator is shown to be positive definite, which in turn implies, if the Rayleigh-Ritz equations are used, that the capacitance thus obtained is a maximum on the Hilbert space spanned by the trial functions used. An attempt is made to present as much of a unified treatment as possible of this varied supporting subject matter.

2.2 Definitions [59]

Definition 2.2.1. An inner product, on a real linear space, is a real valued functional of a pair of elements x and y, with the properties

$$\begin{aligned}
&\text{(i)} && \langle x, y \rangle && = && \langle y, x \rangle \\
&\text{(ii)} && \langle a\,x, y \rangle && = && a \langle x, y \rangle \\
&\text{(iii)} && \langle x_1 + x_2, y \rangle && = && \langle x_1, y \rangle + \langle x_2, y \rangle \\
&\text{(iv)} && \langle x, x \rangle && \geq && 0 \quad \text{with } \langle x, x \rangle = 0 \quad \text{iff } x = 0
\end{aligned} \tag{2.2.1}$$

Definition 2.2.2. A norm on a real linear space, is a real valued functional $\| x \|$, with the properties

$$\begin{aligned} &\text{(i)} \quad \| x \| \geq 0 \quad \text{with} \quad \| x \| = 0 \quad \text{iff } x = 0 \\ &\text{(ii)} \quad \| \alpha x \| = | \alpha | \, \| x \| \\ &\text{(iii)} \quad \| x_1 + x_2 \| \leq \| x_1 \| + \| x_2 \| \end{aligned} \tag{2.2.2}$$

Definition 2.2.3. The natural norm of an inner product space is defined by

$$\| x \| = \langle x , x \rangle^{1/2} \tag{2.2.3}$$

Definition 2.2.4. Operator $\mathcal{J}$ is positive definite if

$$\langle \mathcal{J} x, x \rangle > 0 \tag{2.2.4}$$

for all $x \neq 0$ in the domain of the operator $\mathcal{J}$.

Definition 2.2.5. Operator $\mathcal{J}$ is symmetric or self-adjoint if

$$\langle \mathcal{J} x, y \rangle = \langle x , \mathcal{J} y \rangle \tag{2.2.5}$$

for all x and y in the domain of the operator $\mathcal{J}$.

Definition 2.2.6. A metric on a real linear space is a real valued functional of a pair of elements x and y, with the properties

$$\begin{aligned} &\text{(i)} && d(x, y) = d(y, x) \\ &\text{(ii)} && d(x, y) \geq 0 \quad \text{with} \quad d(x, y) = 0 \text{ iff } x = y \\ &\text{(iii)} && d(x, z) \leq d(x, y) + d(y, z) \end{aligned} \tag{2.2.6}$$

Definition 2.2.7. (a) x_k converges to x, if to each $\epsilon > 0$ there exists N such that $d(x, x_k) \leq \epsilon$ whenever $k > N$; (b) a sequence $\{x_k\}$ is a Cauchy sequence if to each $\epsilon > 0$ there exists N such that $d(x_m, x_n) \leq \epsilon$ whenever $m, n > N$; (c) a metric space is complete if every Cauchy sequence is a convergent sequence.

An inner product space complete in its natural metric is a Hilbert space.

Definition 2.2.8. Let S and T be two sets in a metric space with S contained in T. Then S is dense in T if for each $f \in T$ there exists an $e \in S$ such that $d(e, f) < \epsilon$.

Definition 2.2.9. A subspace M of a linear space is called a linear manifold if whenever x and y are in M, so is $\alpha x + \beta y$.

Definition 2.2.10. A normed linear space which is complete in its natural metric is called a Banach space.

Definition 2.2.11. [36] Let E be a Banach space and E_n be a subspace of E. The projection operator P_n from E to E_n satisfies the properties:

$$\text{(i)} \quad P_n E = E_n$$

$$\text{(ii)} \quad P_n^2 = P_n \tag{2.2.7}$$

2.3 Fundamental Solution for the Laplacian Operator and its Relationship to the Green's Functions [59]

Let $\mathfrak{L}$ denote a differential operator, then the fundamental solution of $\mathfrak{L}$ with pole at P' is the solution of the equation,

$$\mathfrak{L}\, E(P ; P') = \delta(P - P') \tag{2.3.1}$$

where P and P' may be points in n-dimensional space. Electrostatically speaking, $E(P ; P')$ is the potential at some point P due to a unit charge at P'. Observe that no boundary conditions are imposed on $E(P ; P')$ in Equation (2.3.1), and two distinct fundamental solutions may differ by the solution of the homogeneous equation corresponding to (2.3.1). When the boundary conditions appropriate to the given problem are imposed on Equation (2.3.1), the solution is called a Green's function and is denoted by $G(P ; P')$.

Stakgold [59] and many others show that the fundamental solution corresponding to the negative Laplacian $\mathcal{L} = -\nabla^2$ is

$$E(P;P') = \begin{cases} \dfrac{1}{2\pi} \ln \dfrac{1}{|P-P'|} & \text{in two dimensions} \\ \dfrac{1}{4\pi |P-P'|} & \text{in three dimensions} \end{cases} \tag{2.3.2}$$

2.4 Charged Thin Metal Plate in an Unbounded Region

The analysis of the charged thin plate in an unbounded region is essentially that presented by Stakgold [59]. In what follows all operators operate with respect to coordinate point P unless otherwise stated.

It is well known that the governing differential equation, for the plate S_p shown in Figure 2.4.1, is

$$-\nabla^2 \varphi(P) = 0 \qquad \text{for} \quad P \notin S_p \tag{2.4.1}$$

$$\varphi(P) = 1 \qquad \text{for} \quad P \in S_p \tag{2.4.2}$$

$$\lim_{|P| \to \infty} \varphi(P) = 0 \tag{2.4.3}$$

The fundamental solution, as defined in Equation (2.3.1), is the solution to

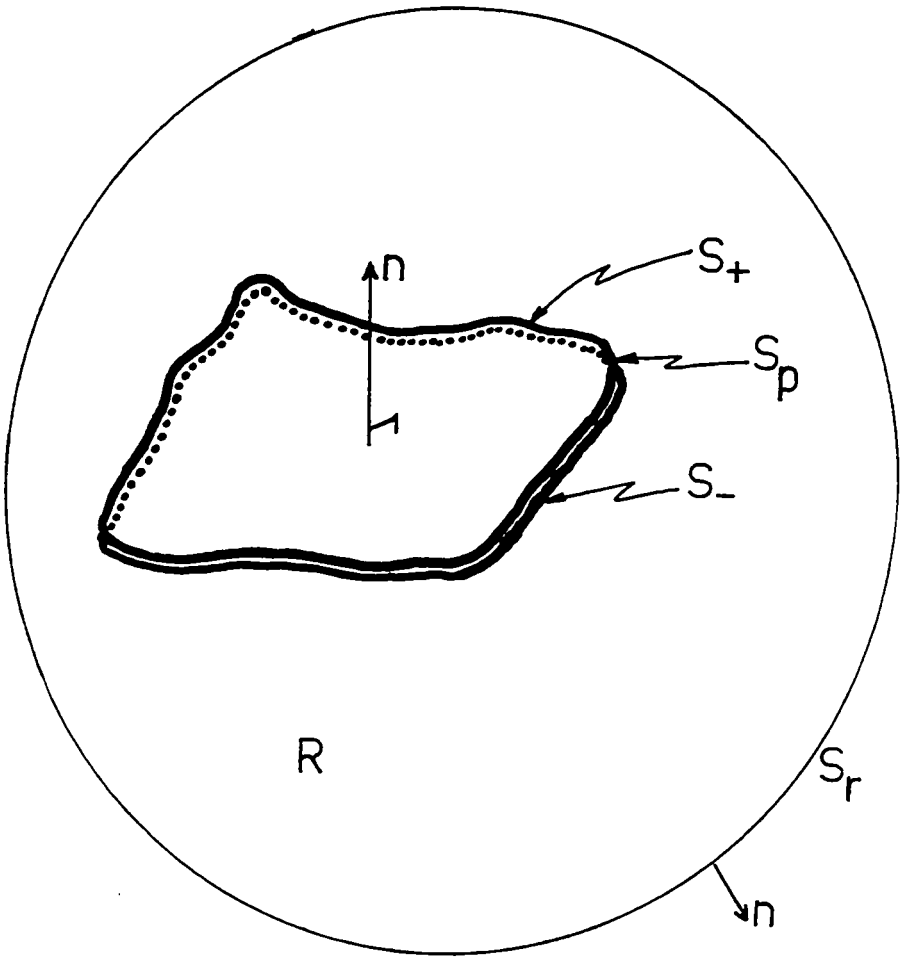

Figure 2.4.1 Thin conductor in vacuum

$$- \nabla^2 E(P ; P') = \delta(P - P') \tag{2.4.4}$$

which, in turn, is given in Equation (2.3.2). As shown in Figure 2.4.1, one side of the plate surface S_p is denoted by S_+, the other by S_-, while the normal to S_+ is denoted by n. The region R is that part of all space, enclosed internally by S_+ and S_- and externally by a sphere S_r.

Multiply Equation (2.4.1) by $E(P ; P')$ and integrate over R,

$$- \int_R E(P ; P') \nabla^2 \varphi(P) \, dR = 0 \tag{2.4.5}$$

Similarly, multiply Equation (2.4.4) by $\varphi(P)$ and integrate over R,

$$- \int_R \varphi(P) \nabla^2 E(P ; P') \, dR = \varphi(P') \tag{2.4.6}$$

Subtract Equation (2.4.5) from Equation (2.4.6) to obtain

$$\varphi(P') = \int_R [E(P ; P') \nabla^2 \varphi(P) - \varphi(P) \nabla^2 E(P ; P')] \, dR \tag{2.4.7}$$

Apply Green's theorem, noting that the positive normal is defined as pointing outward from region R, and is antiparallel to n along S_+.

$$\varphi(P') = \int_{S_r} \left[E(P;P') \frac{\partial \varphi(P)}{\partial n} - \varphi(P) \frac{\partial E(P;P')}{\partial n} \right] dS$$

$$+ \int_{S_+} \left[-E(P;P') \frac{\partial \varphi(P)}{\partial n} + \varphi(P) \frac{\partial E(P;P')}{\partial n} \right] dS$$

$$+ \int_{S_-} \left[E(P;P') \frac{\partial \varphi(P)}{\partial n} - \varphi(P) \frac{\partial E(P;P')}{\partial n} \right] dS \qquad (2.4.8)$$

Stakgold [59] proves that the behaviour of φ and E far from the origin is such as to make the first integral in (2.4.8) zero. Imposing the boundary condition given in (2.4.2), and observing that both $E(P;P')$ and $\frac{\partial E(P;P')}{\partial n}$ are continuous across S_p, so long as $P' \notin S_p$, one obtains

$$\varphi(P') = \int_{S_p} E(P;P') \left[\frac{\partial \varphi(P_-)}{\partial n} - \frac{\partial \varphi(P_+)}{\partial n} \right] dS \qquad (2.4.9)$$

But $-\frac{\partial \varphi(P_+)}{\partial n}$ is just the negative of the gradient of the potential on the S_+ side of the surface S_p, which means that it is the electric field intensity at S_+. This, in turn multiplied by the permittivity ϵ, is the flux density or the surface charge density $\sigma(P_+)$ on S_+. Similarly, $\frac{\partial \varphi(P_-)}{\partial n}$ is proportional to the surface charge density $\sigma(P_-)$ on S_-. Therefore, denoting the total surface charge density on S_p by $\sigma(P)$, Equation (2.4.9) becomes

$$\varphi(P') = \frac{1}{\epsilon} \int_{S_p} E(P;P') \sigma(P) \, dS \qquad (2.4.10)$$

Since $E(P;P')$ is symmetric, coordinates P and P' can be interchanged,

$$\varphi(P) = \frac{1}{\epsilon} \int_{S_p} E(P;P')\,\sigma(P')\,dS \qquad (2.4.11)$$

where the integration is performed with respect to the primed variable over S_p.

An analogous procedure can be used to prove that, for the two dimensional case of an infinitely long thin strip, the form of Equation (2.4.11) is still valid subject to the following interpretation : (a) $E(P;P')$ is the two dimensional fundamental solution, (b) integration is over a line segment, rather than a surface and (c) $\sigma(P')$ is charge density per unit length along the line segment.

In order to determine the surface charge density $\sigma(P')$ on the plate, let P approach some point on S_p. Then using the continuity of simple layer potential [59] together with the boundary condition in Equation (2.4.2), the resulting Fredholm integral equation of the first kind to be solved is

$$\frac{1}{4\pi\epsilon} \int_{S_p} \frac{\sigma(P')}{|P-P'|}\,dS = 1 \qquad (2.4.12)$$

and this is valid for all $P \in S_p$.

2.5 Variational Formulation

Let $\mathcal{J}$ be a symmetric and positive definite operator defined on a linear manifold $D_{\mathcal{J}}$, dense in a real Hilbert space. Consider the operator equation

$$\mathcal{J} u = f \tag{2.5.1}$$

together with the associated functional

$$\mathcal{F}(v) = 2 \langle f, v \rangle - \langle \mathcal{J} v, v \rangle \tag{2.5.2}$$

where $v \in D_{\mathcal{J}}$. Then the following theorems can be proved [59] :

Theorem 2.5.1. Equation (2.5.1) has at most one solution.

Theorem 2.5.2. (a) If Equation (2.5.1) has a solution u, then $\mathcal{F}(v)$ attains its maximum value for $v = u$.

(b) If $\mathcal{F}(v)$ attains its maximum value for some function u, then u is the solution of Equation (2.5.1).

Note that the maximum value of the functional $\mathcal{F}(v)$ is $\mathcal{F}(u) = \langle f, u \rangle$.

By Theorems 2.5.1 and 2.5.2, there exists only one $v \in D_{\mathcal{J}}$, which maximizes $\mathcal{F}$. Suppose that one is willing to settle for an approximate solution in E_n, some n-dimensional subspace of $D_{\mathcal{J}}$. Then

$$\max_{v \in E_n} \mathcal{F}(v) \leq \max_{v \in D_{\mathcal{J}}} \mathcal{F}(v) = \mathcal{F}(u) \tag{2.5.3}$$

Hence, $\max_{v \in E_n} \mathcal{F}(v)$ is a lower bound to the true solution. Let P_n be the (symmetric) projection operator onto E_n. If $v \in E_n$, then $P_n v = v$ and

$$\begin{aligned} \mathcal{F}(v) &= 2\langle f, v\rangle - \langle \mathcal{J} v, v\rangle \\ &= 2\langle f, P_n v\rangle - \langle \mathcal{J} v, P_n v\rangle \\ &= 2\langle P_n f, v\rangle - \langle P_n \mathcal{J} v, v\rangle \end{aligned} \tag{2.5.4}$$

By Theorem 2.5.2, the function $u_n \in E_n$ which maximizes $\mathcal{F}(v)$ is the solution of the equation

$$P_n \mathcal{J} u_n = P_n f \quad ; \quad u_n \in E_n \tag{2.5.5}$$

Observe that Equation (2.5.5) could also be obtained by simply projecting Equation (2.5.1) onto E_n. In the space E_n

$$\max_{v \in E_n} \mathcal{F}(v) = \langle f, u_n\rangle \leq \max_{v \in D_{\mathcal{J}}} \mathcal{F}(v) \tag{2.5.6}$$

Let the set $\{ v_n \}$ be a basis for E_n ; since $u_n \in E_n$

$$u_n = \sum_{i=1}^{n} a_i v_i \tag{2.5.7}$$

Perform the projection indicated in Equation (2.5.5), in this case, taking inner products with the basis function set $\{ v_n \}$

$$< \mathcal{J} u_n , v_i > \quad = \quad < f, v_i > \qquad (2.5.8)$$

$$i = 1, 2, \ldots, n$$

and substitute (2.5.7) into (2.5.8)

$$\sum_{i=1}^{n} a_i \; < \mathcal{J} v_i , v_i > \quad = \quad < f , v_i > \qquad (2.5.9)$$

$$i = 1, 2, \ldots, n$$

This equation may be written in matrix form

$$[I_{ij}] \underline{a}_i \quad = \quad \underline{f}_i \qquad (2.5.10)$$

where $I_{ij} = < \mathcal{J} v_i , v_j > = I_{ji}$

$$\underline{a}_i^T = [a_1 , a_2 , \ldots, a_n]$$

$$\underline{f}_i^T = [< f , v_1 >, < f , v_2 >, \ldots, < f , v_n >]$$

This system of linear equations is called the Rayleigh-Ritz or Galerkin equations.

It is appropriate to note that the form of Equation (2.5.10) is the same, irrespective of whether it was obtained variationally or by projections. While the variational approach, applicable only under special circumstances, guarantees the

maximality of some functional, projections, having considerably fewer restrictions on both the operator and the function space, have wider applicability.

2.6 Advantage of the Variational Method

The variational solution is particularly advantageous if one is interested, in the actual maximum of the related functional $\mathfrak{F}$, not just obtaining the solution of the operator equation. It will be shown that an error of order ϵ in the solution yields only order ϵ^2 error in the maximum value of the functional.

Define the function

$$F(\epsilon) = \mathfrak{F}(u + \epsilon \eta) \tag{2.6.1}$$

where u is the exact solution,

η is some element in the domain $D_{\mathfrak{F}}$,

ϵ is some real parameter.

Expand Equation (2.6.1) in a Taylor series about $\epsilon = 0$

$$F(\epsilon) = F(0) + \epsilon \left.\frac{dF}{d\epsilon}\right|_{\epsilon=0} + \epsilon^2 \left.\frac{d^2F}{d\epsilon^2}\right|_{\epsilon=0} + \cdots$$

$$= \mathfrak{F}(u) + \epsilon \left.\frac{d\mathfrak{F}(u+\epsilon\eta)}{d\epsilon}\right|_{\epsilon=0} + \epsilon^2 \left.\frac{d^2\mathfrak{F}(u+\epsilon\eta)}{d\epsilon^2}\right|_{\epsilon=0} + \cdots \tag{2.6.2}$$

In the case of the variational method

$$\left.\frac{d\,\mathfrak{F}(u+\epsilon\,\eta)}{d\,\epsilon}\right|_{\epsilon=0} = 0$$

implying that

$$F(\epsilon) = \mathfrak{F}(u) + \epsilon^2 \left.\frac{d^2\,\mathfrak{F}(u+\epsilon\,\eta)}{d\,\epsilon^2}\right|_{\epsilon=0} + \ldots \qquad (2.6.3)$$

Therefore, if the error in the solution of $\mathcal{J}u = f$ is of order ϵ, then the error in F is of order ϵ^2. So that for small errors, F is likely to have twice as many good significant figures as the approximate solution.

2.7 Rayleigh-Ritz Method over many Subregions

Consider the projected operator equation

$$P_n \mathcal{J} u_n = P_n f \qquad (2.5.5)$$

and let E_n, the subspace of $D_{\mathcal{J}}$, be defined on a region of space denoted by S. Subdivide S into m non-overlapping subregions $S_1, S_2, \ldots, S_m$ such that $S = \bigcup_{i=1}^{m} S_i$, so that one ends up with corresponding subdivisions, $E_n^1, E_n^2, \ldots E_n^m$, of E_n.

Let $\{ v_n^i \}$ be basis functions with local support for E_n^i on S_i, and $E_n = \bigcup_{i=1}^{m} E_n^i$. Hence, if u_n^i denotes the approximate solution in the ith subregion, then

$$u_n^i = \sum_{j=1}^{n} a_j^i \, v_j^i \tag{2.7.1}$$

$$u_n = \sum_{i=1}^{m} u_n^i \tag{2.7.2}$$

Let f^i denote the forcing function with local support in the ith subregion, then

$$f = \sum_{i=1}^{m} f^i \tag{2.7.3}$$

Substitute Equations (2.7.1), (2.7.2) and (2.7.3) into (2.5.5)

$$\sum_{i=1}^{m} \sum_{j=1}^{n} a_j^i \, P_n \, \mathcal{J} \, v_j^i = \sum_{i=1}^{m} P_n \, f^i \tag{2.7.4}$$

Perform the indicated projections, onto the set $\{ v_n^k \}$ for $k = 1, 2, \ldots, m$.

$$\sum_{i=1}^{m} \sum_{j=1}^{n} a_j^i < \mathcal{J} v_j^i , v_l^k > = \sum_{i=1}^{m} < f^i , v_l^k > \tag{2.7.5}$$

$$k = 1, 2, \ldots m \; ; \; l = 1, 2, \ldots n.$$

Using the product integral definition of an inner product, $< f^i , v_l^k > = 0$ when $i \neq k$; whereas, for the integral operator given in Equation (2.4.12), $< \mathcal{J} v_j^i , v_l^k > \neq 0$ when $i \neq k$. Hence a full matrix results.

2.8 Galerkin - Petrov Method [36 , 42]

Although not variationally stationary, this generalization of the Rayleigh-Ritz method is worth mentioning. Consider, again, Equation (2.5.1)

$$\mathcal{J} u = f \tag{2.5.1}$$

where $u \in D_{\mathcal{J}}$ while $f \in R_{\mathcal{J}}$ where $D_{\mathcal{J}}$ and $R_{\mathcal{J}}$ are Banach spaces. Let E_n be a subspace of the domain $D_{\mathcal{J}}$, while G_n is a subspace of the range $R_{\mathcal{J}}$. Also, let $\{ v_n \}$ be a basis set in E_n and $\{ w_n \}$ a basis set in G_n.

Expand $u_n \in E_n$ on the subspace basis set $\{ v_n \}$

$$u_n = \sum_{i=1}^{n} a_i v_i \tag{2.8.1}$$

Use the approximation given by (2.8.1) in Equation (2.5.1)

$$\sum_{i=1}^{n} a_i \mathcal{J} v_i = f \tag{2.8.2}$$

For the Galerkin-Petrov method project both sides of Equation (2.8.2) on the subspace G_n,

$$\sum_{i=1}^{n} a_i P_{G_n} \mathcal{J} v_i = P_{G_n} f \tag{2.8.3}$$

where P_{G_n} is the projection operator onto subspace G_n. When inner product projections can be used, (2.8.3) becomes

$$\sum_{i=1}^{n} a_i < \mathcal{J} v_i , w_j > \quad = <f, w_j> \qquad (2.8.4)$$

$$j = 1, 2, \ldots n$$

If $\{ w_n \} = \{ v_n \}$, possible when the range space is contained in the domain space, the Bubnov-Galerkin method results. If, in addition, the operator $\mathcal{J}$ is positive definite and symmetric, Equation (2.8.4) is equivalent to the Rayleigh-Ritz equations.

2.9 The Integral Operator Corresponding to the Laplacian is Positive Definite

The three dimensional electrostatic problem, to be solved in Chapter IV, is formulated in terms of Rayleigh-Ritz equations using product integral inner products. Therefore if the integral operator can be shown to be positive definite then the capacitance obtained is guaranteed to be a lower bound to the exact value. The integral operator under consideration is given in Equation (2.4.12) to be

$$\mathcal{J} u = \int_{S_p} \frac{u(P')}{|P-P'|} \, dS(P') \qquad (2.9.1)$$

where $dS(P')$ indicates integration with respect to the primed coordinate over the plate surface S_p. The inner product definition to be used is

$$<u, v> = \int_{S_p} u(P) \, v(P) \, dS(P) \qquad (2.9.2)$$

Thus, consider the inner product

$$< \mathcal{J} u,\ v > = \int_{S_p} v(P) \int_{S_p} \frac{u(P')}{|P-P'|}\, dS(P')\ dS(P) \tag{2.9.3}$$

Apply the mean value theorem for multiple integrals [51] to the integration in the primed coordinate

$$< \mathcal{J} u,\ v > = \int_{S_p} v(P)\ u(P_o) \int_{S_p} \frac{1}{|P-P'|}\, dS(P')\ dS(P) \tag{2.9.4}$$

where P_o is some point in S_p. Change the order of integration, as permitted by Fubini's theorem [24],

$$< \mathcal{J} u,\ v > = u(P_o) \int_{S_p} \int_{S_p} \frac{v(P)}{|P-P'|}\, dS(P)\ dS(P') \tag{2.9.5}$$

and, now, apply the mean value theorem to the integration in the unprimed coordinate, which incidentally is identical in form to the earlier integration in the primed coordinate. Then

$$< \mathcal{J} u,\ v > = u^2(P_o) \int_{S_p} \int_{S_p} \frac{1}{|P-P'|}\, dS(P)\ dS(P') \tag{2.9.6}$$

Therefore,

$$< \mathcal{J} u, u > \quad > 0 \tag{2.9.7}$$

for all real $u \neq 0$. Hence by Definition 2.2.4, the integral operator in question is positive definite.

Incidentally, the fact that the operator is symmetric is obvious. Therefore, if the Rayleigh-Ritz method is used, to solve the integral equation given in (2.4.12), then the functional which is being maximized is

$$\max \mathfrak{F}(v) = < f, u > = \int_{S_p} \sigma(P') \, dS(P') \tag{2.9.8}$$

i.e. the total charge on the plate. This in turn is proportional to the electrostatic capacitance. Hence the capacitance thus obtained is a lower bound and is variationally stationary.

CHAPTER III

THE INFINITE MICROSTRIP PROBLEM [55]

3.1 Introduction

Numerous solutions have appeared in the literature for the electrostatic capacitance of microstrip transmission lines : a simplified theory [5], conformal mappings [47, 68, 69], substrip approximations to the integral equation formulation of the problem [10, 53], polynomial trial functions in the Fourier transform domain [74], as well as others. All these methods produced quite good approximations to the capacitance values on the strip, since the electrostatic capacitance is variationally stationary. Hence even relatively large errors in the computed charge distributions, yield acceptably good values of C . To obtain local charge distributions of reasonable accuracy, especially in the neighbourhood of the strip edge, the existing matrix methods result in large systems of equations and therefore time-consuming computation.

Since in the analysis of discontinuity effects an accurate knowledge of the charge distribution itself becomes important, it would be highly desirable to develop a method which has accuracy comparable to the substrip method, with a large number of subdivisions, yet possibly requiring shorter computing times. Therefore, it is not inappropriate to take time to discuss another, more economical, approach to obtain microstrip transmission line parameters. The method described below, which, incidentally, is equally well suited to deal with the electrostatics of coupled strips, takes relatively little computing time, but yields good charge distribution accuracy, including preserving the all important singularity at the strip edge.

It is appropriate, at this time, to point out that dispersion in microstrip, especially at frequencies above 5 GHz, is a factor to be contended with. Various investigators published results in this area [4, 12, 13, 16, 27, 28, 41, 43, 67, 76]. Typically, over the range of 5 - 12 GHz for a characteristic impedance $Z_o = 50\ \Omega$ on alumina substrate ($\epsilon_r \approx 10$) of 0.025 inch thickness, there is a 2.2 % dispersion in the phase velocity [67]. However, as the microstrip discontinuities are to be discussed from the electrostatic point of view, only the electrostatic solution is of immediate interest.

3.2 Governing Integral Equation

As in much previous work, the TEM formulation of the microstrip problem is used. The integral equation which governs the electrostatic charge distribution on the infinite strip is given in [53] to be

$$\varphi_\infty(y) = \int_{-1}^{1} \sigma_\infty(y')\, G_\infty(y\,;\,y')\, dy' \qquad (3.2.1)$$

where $\varphi_\infty(y) = \varphi_\infty$ for $y \in [-1, 1]$. $\varphi_\infty(y)$ is the electrostatic potential on the line $z = h$ while φ_∞ denotes the constant potential on the line segment $z = h$ and $y \in [-1, 1]$. $\sigma_\infty(y')$ is the charge distribution and $G_\infty(y\,;\,y')$ is the Green's function for the problem (see Figure 3.2.1). y and y' are potential and charge coordinates, respectively. It can be shown, using extended image theory, that

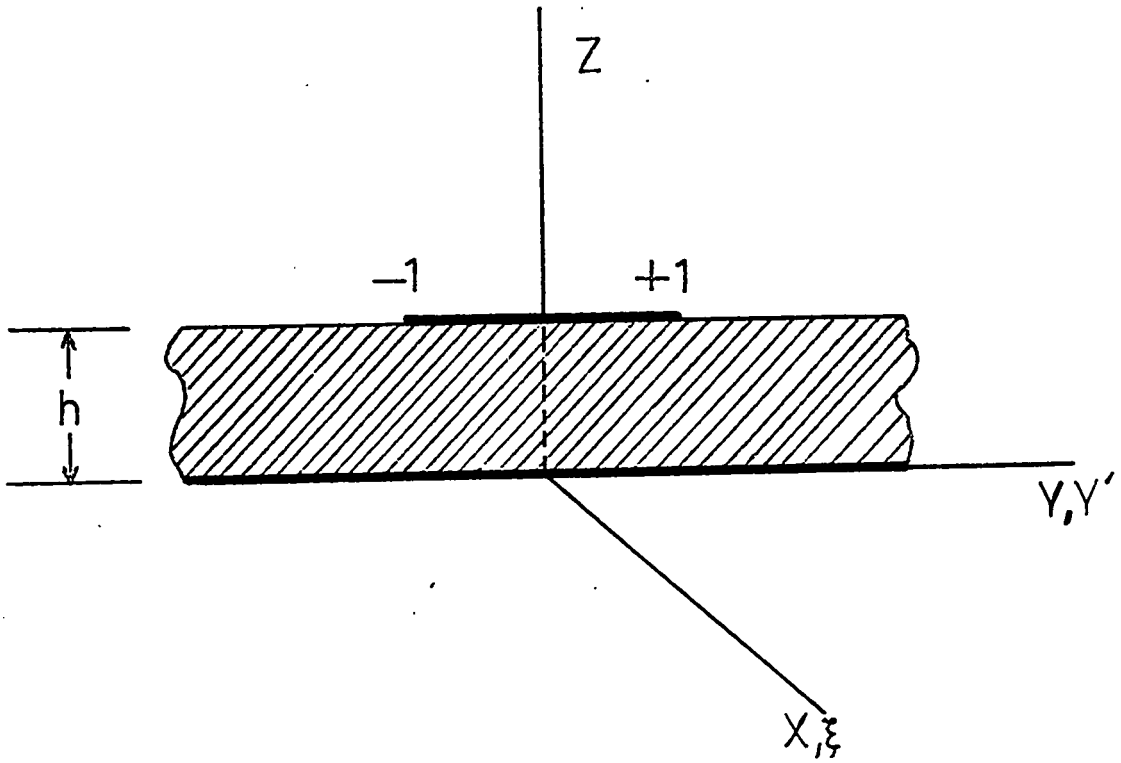

Figure 3.2.1 Microstrip cross-section

the necessary Green's function is

$$G_{\infty}(y\,;y') = \frac{1}{2\pi(\epsilon_0+\epsilon_1)} \sum_{n=1}^{\infty} K^{n-1} \ln\left\{ \frac{4n^2 + (\frac{y-y'}{h})^2}{4(n-1)^2 + (\frac{y-y'}{h})^2} \right\} \qquad (3.2.2)$$

where $K = (\epsilon_0 - \epsilon_1)/(\epsilon_0 + \epsilon_1)$. The potential due to a charged wire of radius r, near a metal backed dielectric substrate, was obtained by Kaden [32] in a form similar to that given in Equation (3.2.2).

3.3. Treatment of Singularities and Solution of the Integral Equations

It should be noted that the Green's function in Equation (3.2.2) contains a singularity of the form $\ln|y-y'|$. Also, it is well known [1, 52] that the charge distribution $\sigma_{\infty}(y')$ on the strip in vacuum is continuous but singular at the edges, and it may be written in the form

$$\sigma_{\infty}(y') = \frac{c(y')}{\sqrt{1-y'^2}} \qquad (3.3.1)$$

where $c(y')$ is a slowly varying continuous function. Assume, that even when a dielectric is present the charge density can still be written in the form given by Equation (3.3.1). According to the Weierstrass approximation theorem [59], such functions are well approximated by polynomials. Therefore, a good family of functions

for approximating the charge distribution is $\{ \psi_i (y') \}$ given by

$$\psi_i (y') = \frac{f_i (y')}{\sqrt{1 - y'^2}} \tag{3.3.2}$$

$$f_i (y') = \begin{cases} \prod_{i=1}^{i-1} \left[\left(\frac{i}{i-1} \right) - y'^2 \right] , & i > 1 \\ 1 , & i = 1 \end{cases} \tag{3.3.3}$$

Approximating the charge distribution by the k - term sum

$$\sigma_\infty (y') = \sum_{i=1}^{k} a_i \psi_i (y') \tag{3.3.4}$$

the integral equation (3.2.1) assumes the form

$$\varphi (y) = \sum_{i=1}^{k} a_i \int_{-1}^{1} \psi_i (y') G_\infty (y ; y') \, dy' \tag{3.3.5}$$

To solve for the coefficients a_i , one variant of the Galerkin-Petrov method [36, 42] can be used. Projecting both sides of Equation (3.3.5) onto a finite set of even order Legendre polynomials $P_{2i} (y)$ yields

$$\int_{-1}^{1} \varphi (y) P_{2i} (y) \, dy = \sum_{i=1}^{k} a_i \int_{-1}^{1} \int_{-1}^{1} \psi_i (y') P_{2i} (y) G_\infty (y ; y') \, dy' \, dy \tag{3.3.6}$$

It might be noted, in passing, that the integral projection in Equation (3.3.6) cannot be regarded as a moment method [26] - not all members of the set $\{ \psi_i \}$ are square integrable and therefore do not belong to any normed space on which the product integral constitutes an inner product. (As a matter of fact the expansion and projection sets do not even span the same space.) This also implies that the result is not variationally stationary and the capacitance thus obtained is not a lower bound to the true solution. Nevertheless, Equation (3.3.6) may be regarded as a non-symmetric matrix equation which is solved readily for the coefficients a_i.

No difficulty is encountered in evaluating the integral on the left side of Equation (3.3.6) ; for the microstrip of constant potential, $\varphi_\infty (y) = \varphi_\infty$ for $y \in [-1, 1]$, all Legendre polynomials except the zeroth are orthogonal to the constant potential function φ_∞. Therefore no actual calculations are required to obtain the forcing vector for the matrix equation corresponding to (3.3.6) .

However, the double integral contains a singular kernel in addition to the singularity in ψ_i. Its evaluation may, therefore, cause some concern. Fortunately, the integral can be shown to be convergent, so it may readily be evaluated, provided suitable weighted quadrature formulae are available. Such formulae may be constructed in the manner indicated by Silvester and Hsieh [54] ; alternately, suitable product quadrature rules may be obtained as described in Appendix I . The latter approach is to be followed here.

The double integral on the right hand side of Equation (3.3.6) can be designated by I and rewritten as

$$I = \int_{-1}^{1} \int_{-1}^{1} \frac{f_i(y')}{\sqrt{1-y'^2}} P_{2i}(y) \ln\left[\frac{|y-y'|}{|y-y'|+1}\right] \frac{G_\infty(y;y')}{\ln\left[\frac{|y-y'|}{|y-y'|+1}\right]} dy' dy \tag{3.3.7}$$

by simply substituting the expression in Equation (3.3.2) for $\psi_i(y')$ and multiplying and dividing $G_\infty(y;y')$ by $\ln[|y-y'|/(|y-y'|+1)]$. Note, that the ratio

$$r(y,y') = \frac{G_\infty(y;y')}{\ln\frac{|y-y'|}{|y-y'|+1}} \tag{3.3.8}$$

is no longer singular when $y = y'$. Also, observe that simply dividing by $\ln|y-y'|$ would not be acceptable as $r(y,y')$ would be singular when $|y-y'| = 1$.

The integral in Equation (3.3.7) can be rearranged to read

$$I = \int_{-1}^{1} \frac{1}{\sqrt{1-y'^2}} f_i(y') \int_{-1}^{1} \ln\frac{|y-y'|}{|y-y'|+1} P_{2i}(y)\, r(y,y')\, dy\, dy' \tag{3.3.9}$$

To perform the integration in the y' direction, Gaussian quadrature formulae with weight $(1-y')^{-1/2}$ are easily obtained from Stroud and Secrest [63], so that I in Equation (3.3.9) becomes

$$I = \sum_{n=1}^{N} A_n f_i(y'_n) \int_{-1}^{1} \ln\frac{|y-y'_n|}{|y-y'_n|+1} P_{2i}(y)\, r(y,y'_n)\, dy \tag{3.3.10}$$

where A_n and y'_n are quadrature weights and points, respectively. To evaluate the integral in the y-direction, Gaussian quadrature formulae with weight $\ln [| y - y'_n | / (| y - y'_n | + 1)]$ for each quadrature point y'_n, can be obtained so that

$$I = \sum_{n=1}^{N} A_n f_i (y'_n) \sum_{m=1}^{M} B_{mn} P_{2j} (y_{mn}) r (y_{mn}, y'_n) \qquad (3.3.11)$$

where B_{mn} and y_{mn} are quadrature weights and points corresponding to the indicated logarithmic weight, for each of the N quadrature points in the y'-direction. Note that this weight function does not change sign within the interval of integration, a property required to be able to obtain Gaussian quadrature formulae by the method described in Appendix I. Ten point quadratures in both directions have been found adequate to give good accuracy where the width to height ratio of the strip does not exceed three. For wider strips, the formulation appears to be entirely adequate, but ten point quadratures no longer suffice for accurate integrations, i.e. this is a program limitation rather than a limitation in the method and may be removed, if desired, by using quadrature formulae of higher precision. (For the few instances in which very wide strip capacitances were required, rather than increase the number of quadrature points, good success was obtained by projecting the results from the substrip approximation onto the set $\{ \psi_i \}$ given in Equation (3.3.2).)

It is worth noting that the approximation involved in Equations (3.3.2) and (3.3.3) is in fact in polynomial with a Chebyshev weight. Since any polynomials of a given degree span exactly the same function space, they may readily be

converted to another family of polynomials of the same degree. It is appreciated, that this approximation is in fact equivalent to an approximation in Chebyshev polynomials, with the equal ripple properties of the latter.

A note regarding the evaluation and convergence of the infinite series in Equation (3.2.2) is appropriate. In vacuum $\epsilon_1 = \epsilon_0$ and $K = 0$ and the series becomes finite, in fact only the $n = 1$ term exists. When the dielectric is other than vacuum $-1 < K < 0$, Silvester [53] noted that "each term in the series is smaller than K^{n-1} by the logarithmic factor, so that the series must not only converge, but must converge more quickly than a geometric series." He also observed, that since this is an alternating series, an overestimate of the number of terms required for convergence within an error limit E is

$$M = \frac{\ln E}{\ln |K|} . \tag{3.3.12}$$

This is a consequence of the fact that truncating an alternating geometric series at the Mth term results in an error of at most $|K|^M$.

3.4 Results and Comparison with Existing Data

Unfortunately, no exact results - that is to say results of known superior accuracy - are available for strips on substrates of high permittivity. On the other hand, for parallel strips in free space, Palmer [47] presents a detailed analysis, by

means of conformal mapping, which permits computation of the capacitance to arbitrary accuracy. The analysis given by Palmer is sufficiently complicated to preclude finding analytic expressions for the charge density. On the other hand, the positions of successive flux lines on the strips themselves may be determined from his analysis. Since these positions are known to high accuracy, it is possible to perform numerical differentiation so as to plot the charge density on the strip surfaces.

Figure 3.4.1 shows comparative results obtained by conformal mapping and the present method, for a strip five times as wide as its height above ground plane, in vacuum. The charge distribution, it is noted, is very similar for both the conformal mapping solution and the numerical approximation ; however the average charge densities differ sufficiently to lead to a capacitance error under 2 % . Similar comments apply to the width-to-height ratio of about 0.1 , a quite narrow strip, shown in Figure 3.4.2. The essential feature to note is that the small matrix size (the two cases illustrated were obtained using 2×2 matrices) results in short computing times. In this case $8 / 60$ seconds are required, as opposed to $56 / 60$ seconds for the substrip method using a 50×50 matrix required to model accurately the local charge distribution. The singularity near the edges is still modeled accurately. In actual fact the saving in computation time is not quite as great as it appears. In the substrip method a large fraction of the time is consumed by matrix solving, while in this method virtually the whole time is taken up by integrating the Green's function. Requiring an error in the infinite series of not more than 10^{-7} puts the break even point at about 45×45 matrix for $\epsilon_1 = 10.0$. However, if fewer terms are taken in the series the computa-

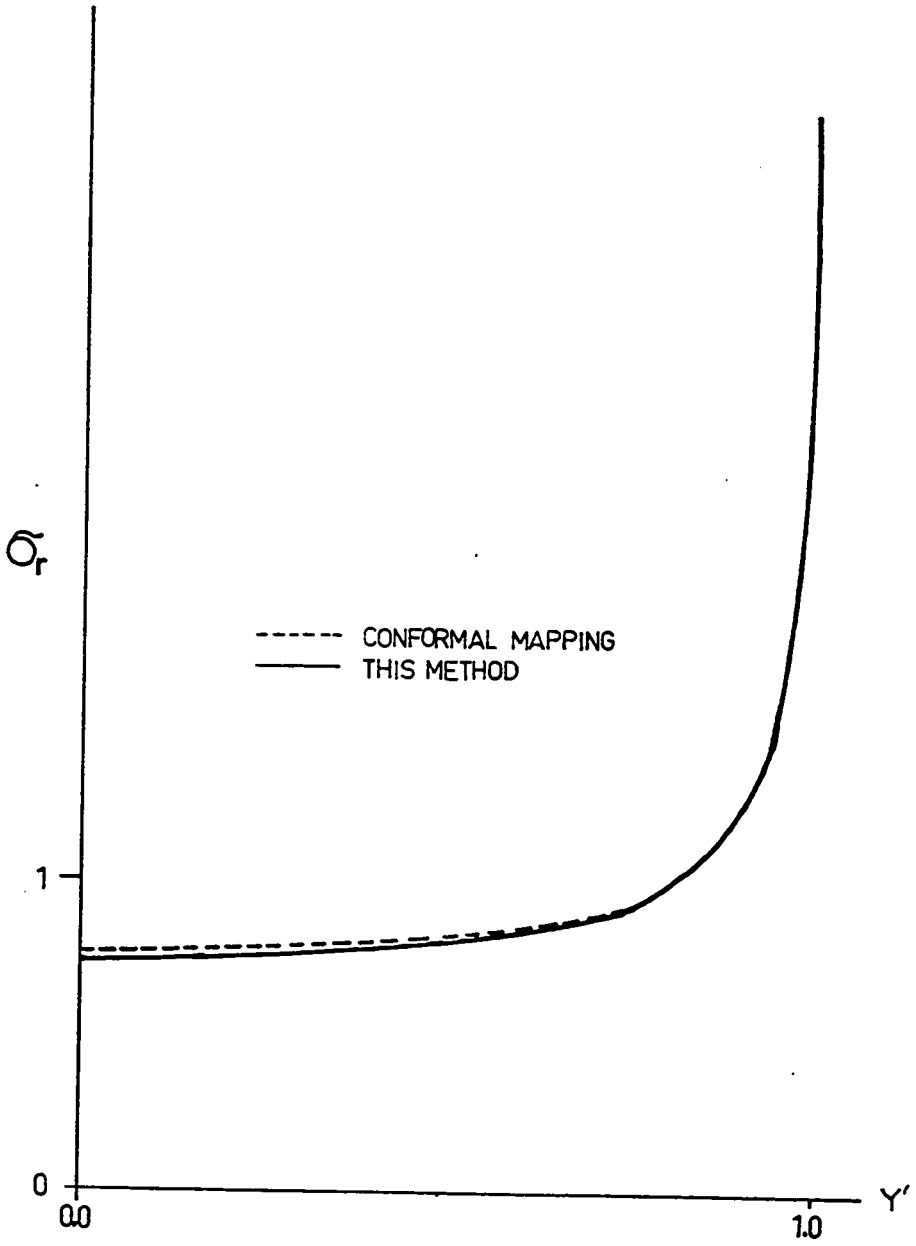

Figure 3.4.1 Microstrip charge density distribution in vacuum for $w/h = 5.0$

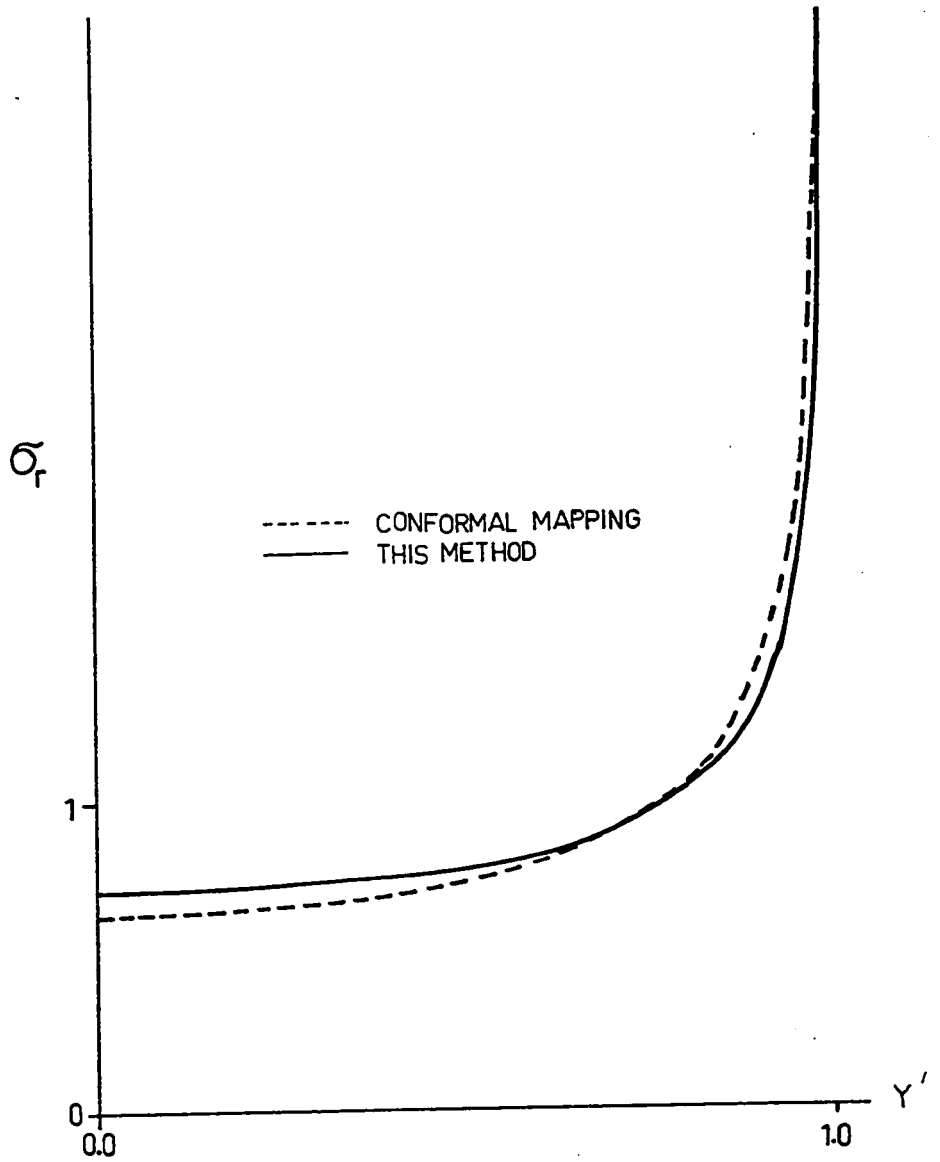

Figure 3.4.2 Microstrip charge density distribution in vacuum for w / h = 0.1

tion time for this method falls considerably. Table 3.1 shows comparative values of microstrip capacitance obtained by this method, as opposed to the results obtained by Silvester [53] by the substrip approximation. This program, with N substrips specified, also recalculates with N/2 substrips and using quadratic Aitken extrapolation produces a capacitance equivalent to about 2 N substrip approximation. It should also be mentioned here that since the new method is not variationally stationary, the fact that the capacitances are higher than those obtained by the substrip method is not necessarily an indication of better accuracy.

Therefore the task of obtaining an economical means of solving the microstrip capacitance problem, while still preserving the singularity in the charge density at the strip edge has been accomplished. A further improvement in the solution of this problem would be the use of linear or quadratic expansion functions near the center of the strip, while still maintaining singular functions near the edge.

TABLE 3. 1.

Microstrip capacitance in p F / meter

w / h	ϵ_r	Substrip [37] 30 x 30 Matrix	This Method 2 x 2 Matrix
0.2	2.5	28.2	28.6
2.667	2.5	92.2	92.5
0.2	4.2	42.9	43.5
2.667	4.2	145.9	146.0
0.2	9.0	84.1	85.4
2.667	9.0	296.8	296.5
0.2	16.0	144.2	146.4
2.667	16.0	516.5	515.7
0.2	51.0	444.6	451.3
2.667	51.0	1614.6	1611.0

CHAPTER IV

CAPACITANCE OF RECTANGULAR PLATES ON METAL-BACKED DIELECTRICS [8]

4.1 Introduction

In recent years a substantial amount of literature has become available for microstriplike and related structures. But even with the increased use of integrated circuits there appears to be very little data for finite plates on dielectric substrates. Reitan [50] and Harrington [26] obtained the capacitance of two parallel square plates in vacuum. Adams and Mautz [2] found the capacitance of a rectangular dielectric loaded capacitor, while Farrar and Adams [20] obtained the capacitance of a rectangular section of a microstrip line.

Initially, the rectangular plate problem was tackled with the intention of obtaining the discontinuity capacitance at an open circuited microstrip by the same method as used by Farrar and Adams [20]. This involves successively increasing the length of a rectangular section of a microstrip line until the difference, between the capacitance of the rectangular section and capacitance of an equal length of infinite microstrip line, converges. Ideally this difference represents twice the open circuit capacitance. This approach, however, entails serious numerical problems, to be discussed in Section 5.3, and was abandoned. Nevertheless, the problem of rectangular plates on metal backed dielectrics is worthwhile in its own right, particularly in the design of lumped element integrated circuitry. Also, the method used to solve the

governing integral equation for the rectangular plate, will be used to directly obtain the excess charges at various microstrip discontinuities.

For a charged rectangular plate in vacuum, the governing differential equation and the appropriate boundary conditions are given in Equations (2.4.1) , (2.4.2) and (2.4.3). Normally, one would proceed to solve the differential equation directly ; however, this being a three dimensional exterior problem, it is not well suited to be approached from this point of view. Instead the equivalent integral equation was obtained in Equation (2.4.12).

4.2 Governing Integral Equation

The rectangular conducting plate on metal backed dielectric substrate is shown in Figure 4.2.1 a . To facilitate the analysis, the equivalent problem, shown in Figure 4.2.1 b is considered.

In Chapter II, it was pointed out that a fundamental solution becomes a Green's function when boundary conditions are satisfied. The boundary condition imposed by the ground plane was satisfied by using an image plate as given in Figure 4.2.1 b. To satisfy the air dielectric boundary condition, Silvester [53] used partial image theory in the case of the microstrip problem. He showed that for a line charge at a distance a from a dielectric sheet of thickness 2 h, the image representation valid in the dielectric region is as shown in Figure 4.2.2. This representation is equally valid in the case of a point charge, required for three dimensional problems. Therefore, the potential at a

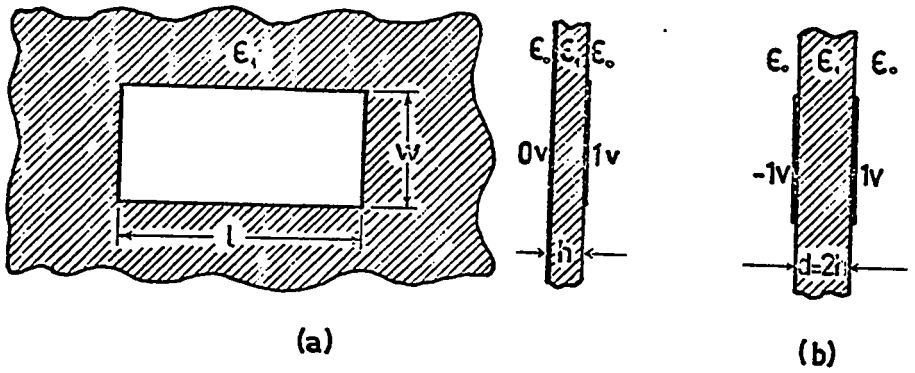

Figure 4.2.1 Conducting plate on metal backed dielectric substrate and equivalent problem

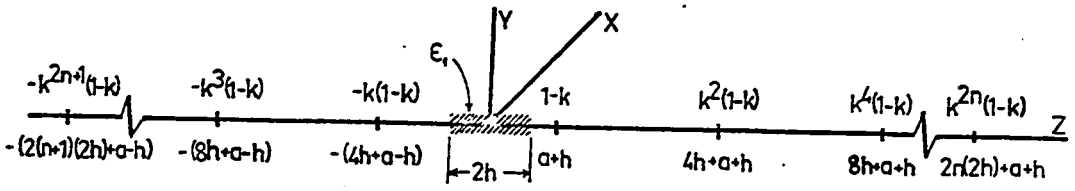

Figure 4.2.2 Image representation, valid in the dielectric region, for point charge near an infinite dielectric sheet

point (x, y, z) where $-h \le z \le h$, due to a unit point charge at $(x', y', h+a)$, by superposition of the partial images, is

$$\varphi(x,y,z) = \frac{1-K}{4\pi\epsilon_1}\sum_{n=0}^{\infty} K^{2n} \frac{1}{\sqrt{(x-x')^2+(y-y')^2+[z-(4n+1)h-a]^2}}$$

$$-\frac{K(1-K)}{4\pi\epsilon_1}\sum_{n=0}^{\infty} K^{2n} \frac{1}{\sqrt{(x-x')^2+(y-y')^2+[z+(4n+3)h+a]^2}} \qquad (4.2.1)$$

where $K = (\epsilon_0 - \epsilon_1)/(\epsilon_0 + \epsilon_1)$ is the image coefficient. For a thin plate $a = 0$, so that the potential in the $z = h$ plane is given by

$$\varphi(x,y) = \frac{1-K}{4\pi\epsilon_1}\sum_{n=0}^{\infty} K^{2n} \frac{1}{\sqrt{(4nh)^2+(x-x')^2+(y-y')^2}}$$

$$-\frac{K(1-K)}{4\pi\epsilon_1}\sum_{n=0}^{\infty} K^{2n} \frac{1}{\sqrt{[4(n+1)h]^2+(x-x')^2+(y-y')^2}} \qquad (4.2.2)$$

Equation (4.2.2) represents the potential at a point (x, y, h) due to a point charge located at point (x', y', h) on top of an infinitely extending dielectric slab of thickness $2h$. This was obtained by a superposition of fundamental solutions to satisfy the air dielectric boundary condition. Therefore Equation (4.2.2) represents the Green's

function for the problem. To simplify the computations to follow, the 8 - way symmetry inherent in the configuration shown in Figure 4.2.3, is included in the Green's function, which becomes

$$G(x, y ; x', y') = \frac{1}{2\pi(\epsilon_0 + \epsilon_1)h} \left[f(0) - (1-K) \sum_{n=1}^{\infty} K^{n-1} f(n) \right] \tag{4.2.3}$$

where

$$f(n) = \left[(2n)^2 + \left(\frac{x - x'}{h}\right)^2 + \left(\frac{y - y'}{h}\right)^2 \right]^{-1/2} + \left[(2n)^2 + \left(\frac{x+x'}{h}\right)^2 + \left(\frac{y - y'}{h}\right)^2 \right]^{-1/2} \tag{4.2.4}$$

$$+ \left[(2n)^2 + \left(\frac{x - x'}{h}\right)^2 + \left(\frac{y+y'}{h}\right)^2 \right]^{-1/2} + \left[(2n)^2 + \left(\frac{x+x'}{h}\right)^2 + \left(\frac{y+y'}{h}\right)^2 \right]^{-1/2}$$

Using the Green's function given in Equation (4.2.3), with all the image points built into it, only the positive quadrant of the top plate, shown in Figure 4.2.4, needs to be considered. A similar Green's function, containing only half the terms of Equation (4.2.3), has recently been obtained by Patel [48] for the case when the ground plane is at infinity.

Therefore, referring to Figure 4.2.4, the integral equation to be solved is

$$\int_{y=0}^{b} \int_{x=0}^{a} G(x, y ; x', y') \, \sigma(x', y') \, dx' \, dy' = \varphi(x, y) \tag{4.2.5}$$

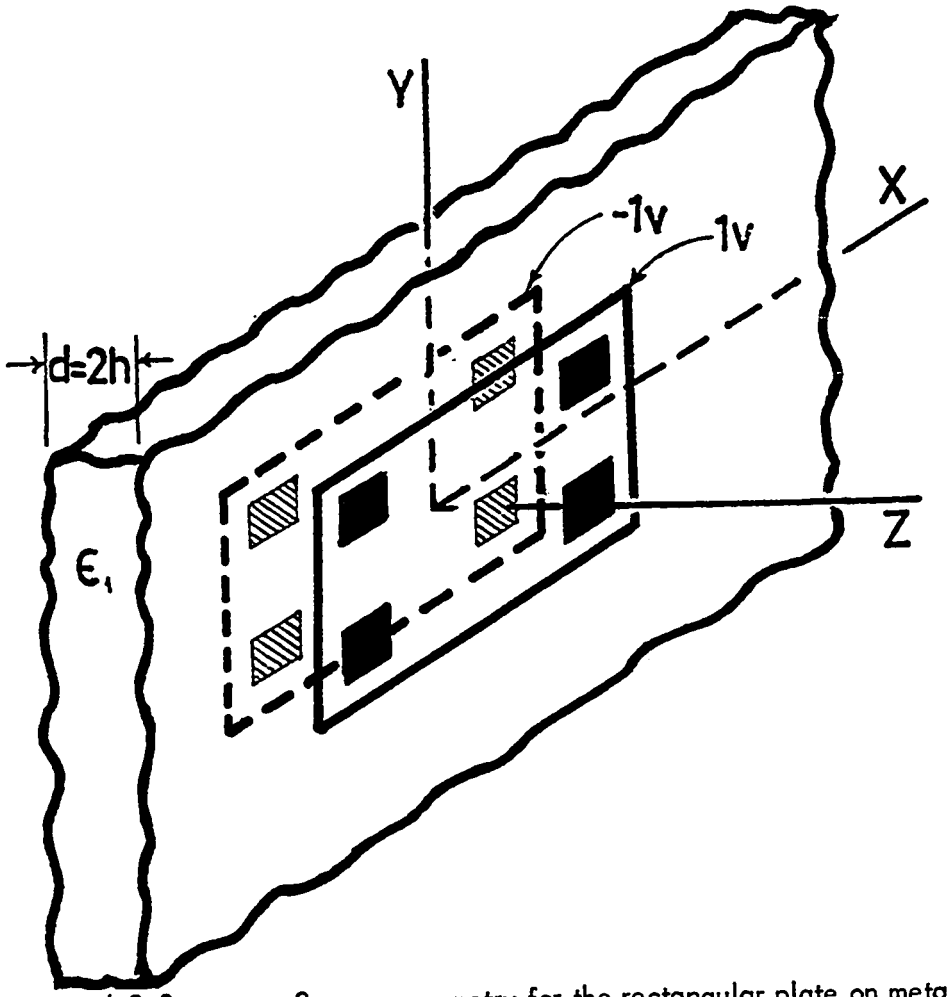

Figure 4.2.3 8 - way symmetry for the rectangular plate on metal backed dielectric substrate

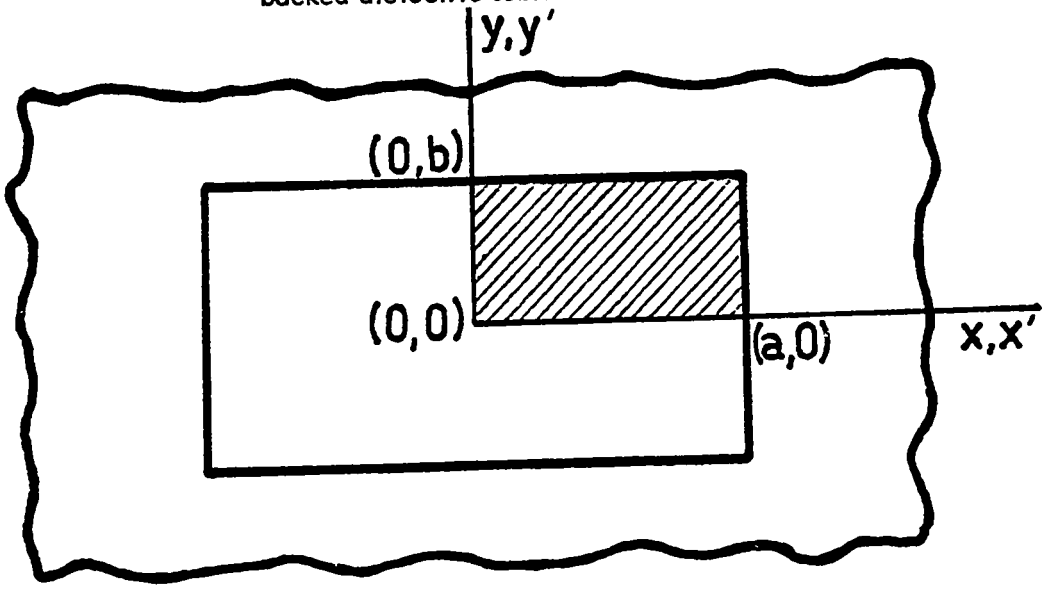

Figure 4.2.4 Region of integration for Equation (4.2.5)

Even prior to proceeding to solve this equation, the matter of evaluation and convergence of the infinite series should be disposed of. On examining $f(n)$, given by Equation (4.2.4), it is readily noted that $f(n) < \frac{2}{n}$. Therefore, subject to the change that each term in the alternating geometric series is smaller than K^{n-1} by the factor $\frac{2}{n}$, the rest of the argument, regarding convergence and the number of terms required for convergence to within a specified error limit for the infinite microstrip problem, is also applicable here.

4.3 Solution of Integral Equation by Rayleigh-Ritz Method over Many Subregions

Observe that the three-dimensional boundary value problem has been reduced to a two-dimensional integral equation. The question asked in Equation (4.2.5) is : "What charge distribution $\sigma(x', y')$ is required on the plate to produce some given potential $\varphi(x, y)$ on it ?" To solve Equation (4.2.5) the Rayleigh-Ritz method over many subregions, described in Section 2.5, is used. In the present context Equation (2.7.5) can be written as

$$\sum_{i=1}^{m} \sum_{j=1}^{n} a_j^i \, \langle \vartheta \, v_j^i(x', y'), \, v_l^k(x, y) \rangle = \langle \varphi^k(x, y), v_l^k(x, y) \rangle \qquad (4.3.1)$$

$$l = 1, 2, \ldots n \; ; k = 1, \ldots, m$$

This is an $m\,n \times m\,n$ matrix equation which can be solved for the unknown

coefficeints a_j^i by any standard technique. Once the a_j^i are known, the total charge on the plate is readily calculated as

$$Q_T = 4 \int_{y'=0}^{b} \int_{x'=0}^{a} \sigma(x', y')\, dx'\, dy'$$

$$= 4 \int_{y'=0}^{b} \int_{x'=0}^{a} \sum_{i=1}^{m} \sum_{j=1}^{n} a_j^i\, v_j^i(x', y')\, dx'\, dy' \qquad (4.3.2)$$

Since the charge distribution was calculated for the case when $\varphi(x, y) = 1$ v on the plate with respect to the ground plane, the capacitance of the rectangular plate is

$$C = \frac{Q_T}{1\text{ v}} = Q_T \quad \text{farads} \qquad (4.3.3)$$

4.4 Evaluation of Inner Products - Special Treatment of Singularities and Pseudo-singularities

The typical matrix element in Equation (4.3.1) is an inner product of the form

$$\langle \mathcal{L} v_j^i(x', y'),\, v_l^k(x, y) \rangle \qquad (4.4.1)$$

$$= \int_{\substack{k\text{-th} \\ \text{region}}} \int \int_{\substack{i\text{-th} \\ \text{region}}} \int G(x, y; x', y')\, v_j^i(x', y')\, v_l^k(x, y)\, dx'\, dy'\, dx\, dy$$

where $G(x, y ; x', y')$ is given in Equation (4.2.3). Three distinct cases need to be examined in some detail.

To perform the integration in (4.4.1), when the integrand contains no singularities, a four-dimensional Cartesian product rule is used. This involves considering the integration as an iterated integral and applying a Gaussian quadrature formula in each coordinate direction [14]. The use of a three point Gaussian quadrature formula in each direction, yields 81 quadrature points for the four-dimensional region. Although, in principle, fewer points may be sufficient to integrate four-dimensional complete polynomials of 5th degree (i.e. all polynomials $x_1^i\, x_2^j\, x_3^k\, x_4^l$ such that $i + j + k + l \leq 5$) the extra points are not wasted as these permit the exact integration of all polynomials $x_1^i\, x_2^j\, x_3^k\, x_4^l$ such that i, j, k and $l \leq 5$.

The second case, which is necessary to consider, arises when $i = k$ in Equation (4.4.1). In this case the Green's function contains a singularity ; the integral, with the singular kernel, is of the form

$$I_1 = \int_{y=c}^{d} \int_{x=a}^{b} \int_{y=c}^{d} \int_{x=a}^{b} \frac{v_i(x', y')\, v_l(x, y)}{\sqrt{(x - x')^2 + (y - y')^2}}\, dx'\, dy'\, dx\, dy \qquad (4.4.2)$$

This integration is once again over a hypercube, but here there is a singularity at $x = x'$ and $y = y'$. However, performing two coordinate transformations the singularity sheet can be shown to have a point projection on the sheet formed by the remaining two coordinates. First, let the order of integration in (4.4.2) be changed to

$$I_1 = \int_{y=c}^{d} \int_{y'=c}^{d} \left[\int_{x=a}^{b} \int_{x'=a}^{b} \frac{v_i(x', y')\, v_l(x, y)}{\sqrt{(x-x')^2 + (y-y')^2}}\, dx'\, dx \right] dy'\, dy \qquad (4.4.3)$$

Now perform the transformation $x - x' = p$ and $x + x' = q$ as suggested for the logarithmic singularity [54]. Referring to Figures 4.4.1 a and b, and using the symmetry about the q - axis in Figure 4.4.1 b, I_1 may be written as

$$I_1 = \int_{y=c}^{d} \int_{y'=c}^{d} \left[\frac{1}{2} \int_{p=0}^{b-a} \int_{q=2a+p}^{2b-p} \frac{v_i\left(\frac{-p+q}{2}, y'\right) v_l\left(\frac{p+q}{2}, y\right) + v_i\left(\frac{p+q}{2}, y'\right) v_l\left(\frac{-p+q}{2}, y\right)}{\sqrt{p^2 + (y-y')^2}} dq\, dp \right] dy'\, dy \qquad (4.4.4)$$

A similar procedure can now be repeated in the $y\,y'$ - plane, setting $y - y' = r$ and $y + y' = s$, to yield

$$I_1 = \frac{1}{4} \int_{p=0}^{b-a} \int_{r=0}^{d-c} \frac{1}{\sqrt{p^2 + r^2}} \int_{q=2a+p}^{2b-p} \int_{s=2c+r}^{2d-r} F(p, r, q, s)\, ds\, dq\, dr\, dp \qquad (4.4.5)$$

where

$$F(p,r,q,s) = v_i\left(\frac{-p+q}{2}, \frac{-r+s}{2}\right) v_l\left(\frac{p+q}{2}, \frac{r+s}{2}\right) + v_i\left(\frac{p+q}{2}, \frac{-r+s}{2}\right) v_l\left(\frac{-p+q}{2}, \frac{r+s}{2}\right)$$

$$+ v_i\left(\frac{-p+q}{2}, \frac{r+s}{2}\right) v_l\left(\frac{p+q}{2}, \frac{-r+s}{2}\right) + v_i\left(\frac{p+q}{2}, \frac{r+s}{2}\right) v_l\left(\frac{-p+q}{2}, \frac{-r+s}{2}\right)$$

The integration indicated by Equation (4.4.5) can be performed if the following integrals can be evaluated :

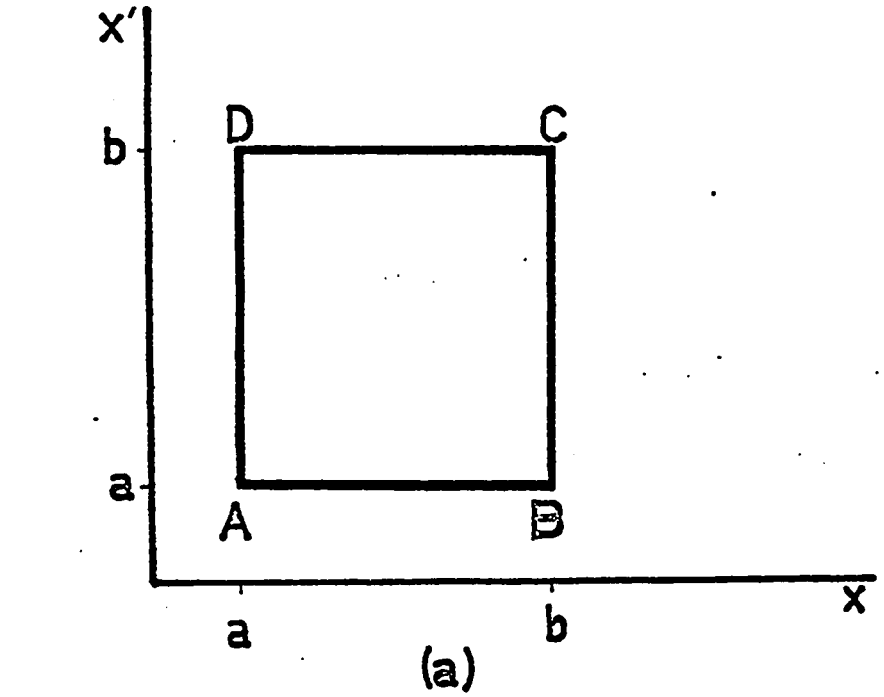

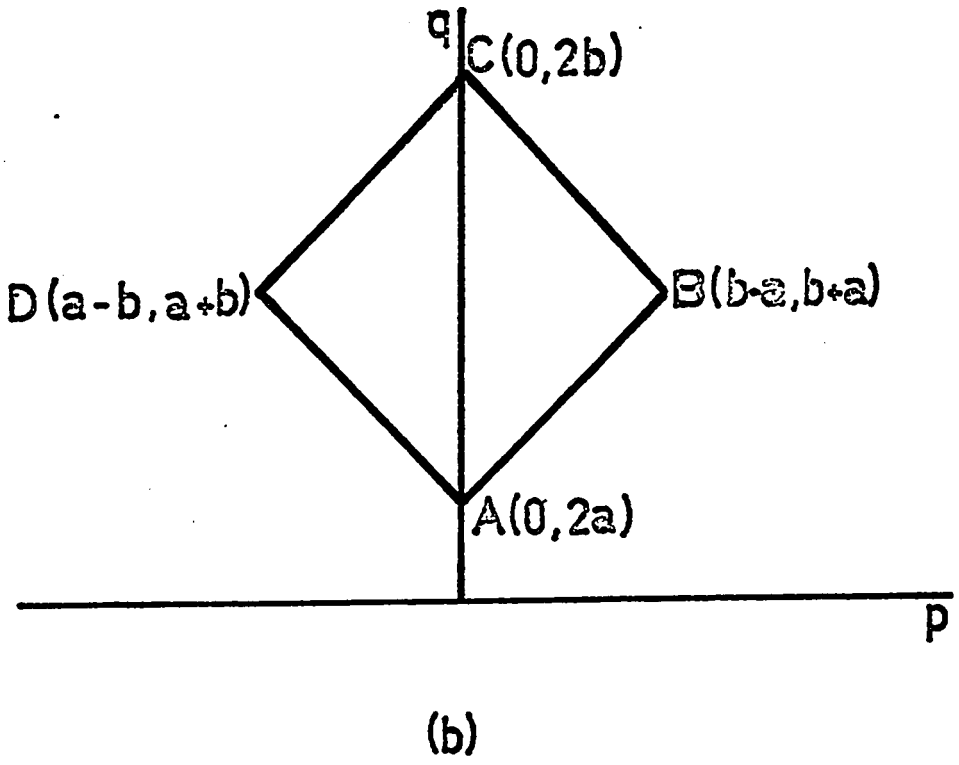

Figure 4.4.1 Region of integration in the $x\,x'$ - plane and in the transformed $p\,q$ - plane

$$I_1 = \int_{p=0}^{b-a} \int_{r=0}^{d-c} \frac{H(p, r)}{\sqrt{p^2 + r^2}} \, dr \, dp \qquad (4.4.6)$$

where

$$H(p, r) = \int_{q=2a+p}^{2b-p} \int_{s=2c+r}^{2d-r} F(p, r, q, s) \, ds \, dq \qquad (4.4.7)$$

The integral in (4.4.6) can be evaluated by performing the transformation $p = R \cos\theta$ and $r = R \sin\theta$. Referring to Figure 4.4.2

$$I_1 = \int_{\theta=0}^{a} \int_{R=0}^{(b-a)\sec\theta} \frac{H(R, \theta)}{R} R \, dR \, d\theta + \int_{\theta=a}^{\pi/2} \int_{R=0}^{(d-c)\,\mathrm{cosec}\,\theta} \frac{H(R, \theta)}{R} R \, dR \, d\theta \qquad (4.4.8)$$

Note that in the integrations in Equation (4.4.8) the singularity is no longer present. Each integral in (4.4.8) can be evaluated using a Cartesian product of Gaussian quadrature formulae in the $R - \theta$ plane. Once the quadrature nodes for the integrations in Equation (4.4.8) are known, the integrations indicated by (4.4.7) become a definite integral, which can be evaluated by a Cartesian product rule in the $s\,q$ - plane.

The third case to be considered is a pseudo-singularity which takes the form

$$I_2 = \int_{y=c}^{d} \int_{x=a}^{b} \int_{y'=c}^{d} \int_{x'=a}^{b} \frac{v_i(x', y') \, v_j(x, y)}{\sqrt{k^2 + (x - x')^2 + (y - y')^2}} \, dx' \, dy' \, dx \, dy \qquad (4.4.9)$$

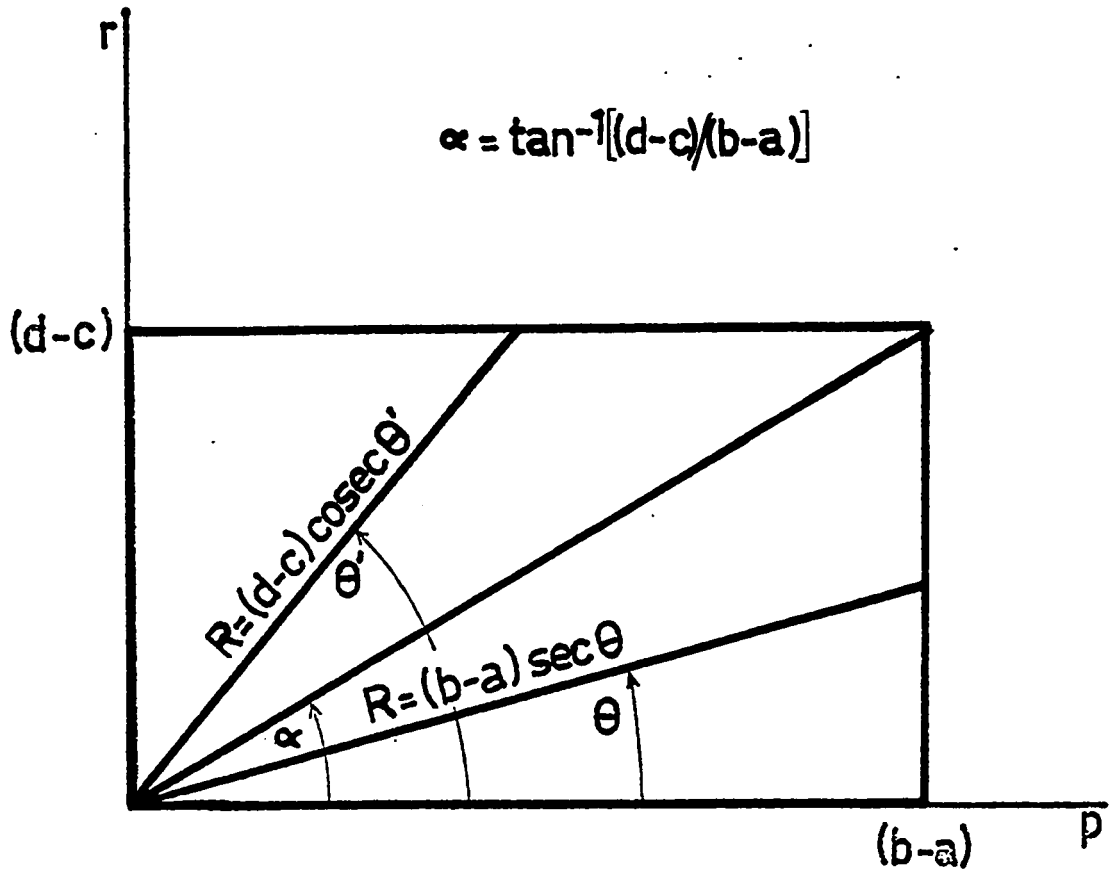

Figure 4.4.2 Region of integration for Equation (4.4.8)

The integrand here is in fact continuous throughout the region of integration, but has very large derivatives as well as values if k is small ; straightforward use of Gauss-Legendre quadratures, therefore, leads to bounded but very large error. From the numerical point of view, this integral is difficult and requires special treatment similar to true singular integrands. In this case the equation equivalent to (4.4.6) is of the form

$$I_2 = \int_{p=0}^{b-a} \int_{r=0}^{d-c} \frac{H(p,r)}{\sqrt{k^2+p^2+r^2}}\, dr\, dp \qquad (4.4.10)$$

Perform the same polar transformation as before, i.e. $p = R\cos\theta$ and $r = R\sin\theta$. Now referring to Figure 4.4.3 I_2 can be rewritten as

$$I_2 = \int_{\theta=0}^{\pi/2} \int_{R=0}^{3k} \frac{R}{\sqrt{k^2+R^2}}\, H(R,\theta)\, dR\, d\theta$$

$$+ \int_{\theta=0}^{a} \int_{R=3k}^{(b-a)\sec\theta} \frac{R}{\sqrt{k^2+R^2}} H(R,\theta)\, dR\, d\theta + \int_{\theta=a}^{\pi/2} \int_{R=3k}^{(d-c)\operatorname{cosec}\theta} \frac{R}{\sqrt{k^2+R^2}} H(R,\theta)\, dR\, d\theta \qquad (4.4.11)$$

To evaluate the first integral in Equation (4.4.11) a Gaussian quadrature formula is developed with weight $R/\sqrt{k^2+R^2}$ for the R-direction, while a Gauss-Legendre quadrature is used in the θ direction. This ensures that the pseudo-singular part of the integral is evaluated rather accurately. The second and third integrals in Equation (4.4.11) do not have pseudo-singular integrands and straightforward Cartesian products of Gauss-Legendre formulae may be taken.

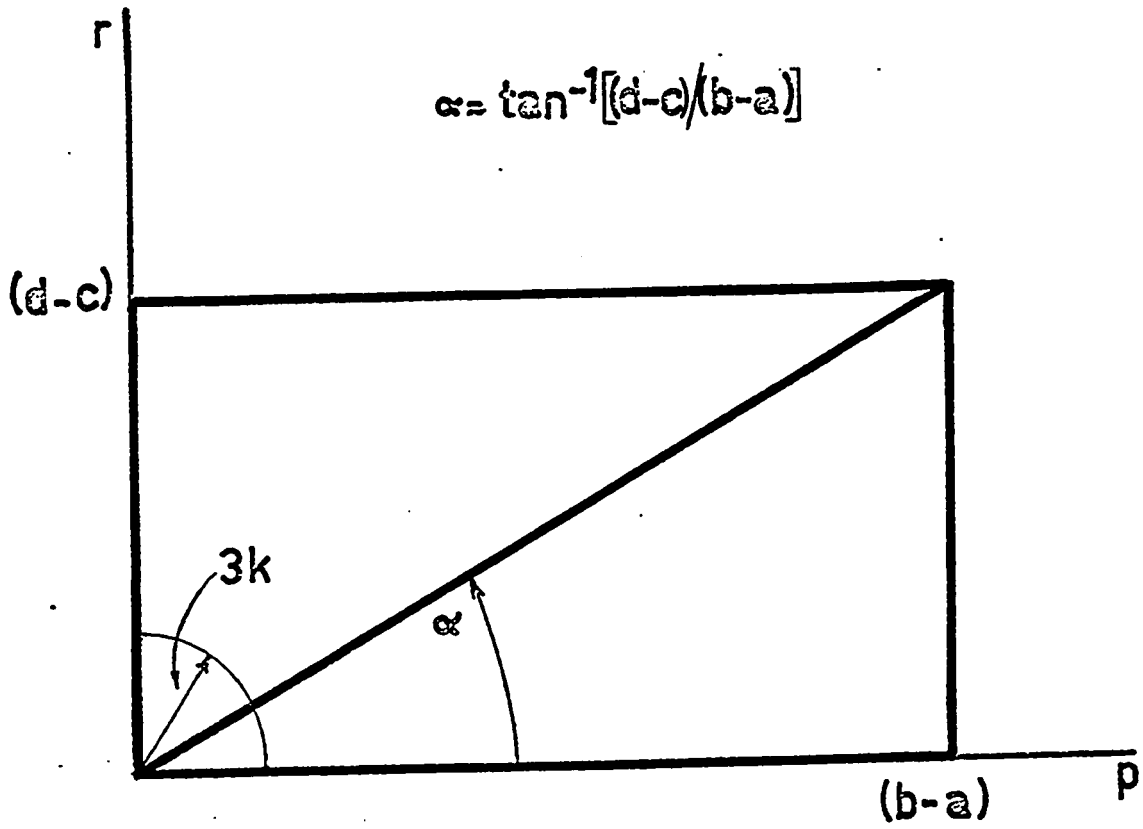

Figure 4.4.3 Region of integration for Equation (4.4.11)

The inner product on the right of Equation (4.3.1) is, simply, a two-dimensional integral with nonsingular integrand, so that its evaluation is done very simply using a Cartesian product of Gauss-Legendre formulae.

4.5 Results and Comparison with Existing Data

Since Equation (4.3.1) is the Rayleigh-Ritz equation over many subregions and the integral operator in it is obtained by the superposition of a number of positive definite operators, the method is variationally stationary. The corresponding functional, which is in effect maximized, was shown in Equation (2.9.8) to be the capacitance of the rectangular plate.

In all the present calculations the basis functions used are $\{ v_i (x, y) \} = \{ 1, x, y, x^2, y^2 \}$. Although it is well known that the charge distribution on a rectangular plate contains singularities at the plate edge, so that the polynomial basis set used is not well suited to reproduce these singularities, nevertheless relatively high accuracy is expected for the total charge and hence the capacitance of the plate for the reason described in Section 2.6. Also in Chapter II, it was pointed out that the capacitance thus obtained is a lower bound to the exact value.

As a result of the variational nature of the solution, increasing the number of basis functions or using more subregions, the capacitance value obtained should increase or stay unchanged. This type of behaviour is readily seen in Table 4.5.1 for $\epsilon_r = 2.5$ and $w / l = 1.0$.

TABLE 4.5.1

$C d / \epsilon A$, where C is the parallel plate capacitance normalized w. r. t. capacitance of infinite plates

d / l \ Number of Subregions	1	2	3	5
1.0	6.17	6.20	6.25	6.30
0.2	3.26	3.26	3.33	3.34

It is appropriate at this point to compare the results obtained by the present method with those in [20, 26, 50]. Reitan [50] calculated the parallel square plate capacitance in vacuum using constant basis functions over 36 subregions on the plate, which is equivalent to using 9 subregions on one quarter of the plate. A comparison of his results with those obtained by the present method, using the bi-quadratic basis set over one subregion, is shown in Table 4.5.2. Harrington [26] solved the same problem by the point matching method. His results together with those obtained by this method are shown in Figure 4.5.1. Farrar and Adams [20] calculated the electrostatic capacitance of square and rectangular plates on a metal backed dielectric substrate. They also use a number of subregions with constant basis functions ; however they do not indicate how many subregions were used. Figure 4.5.2 a and b

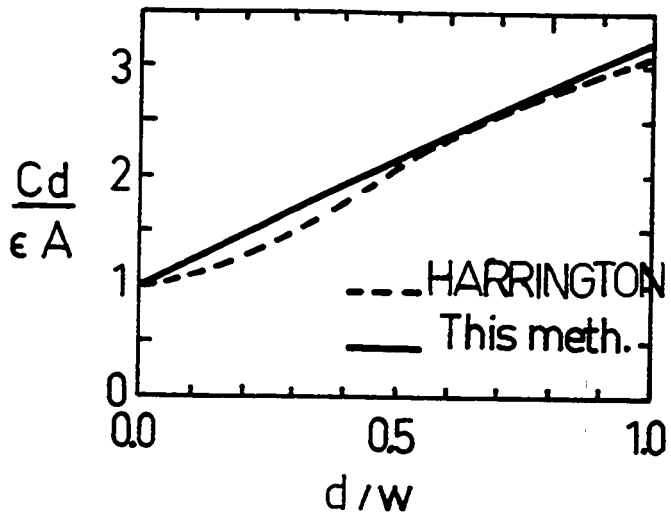

Figure 4.5.1 Comparative capacitance values by Harrington [26] and this method

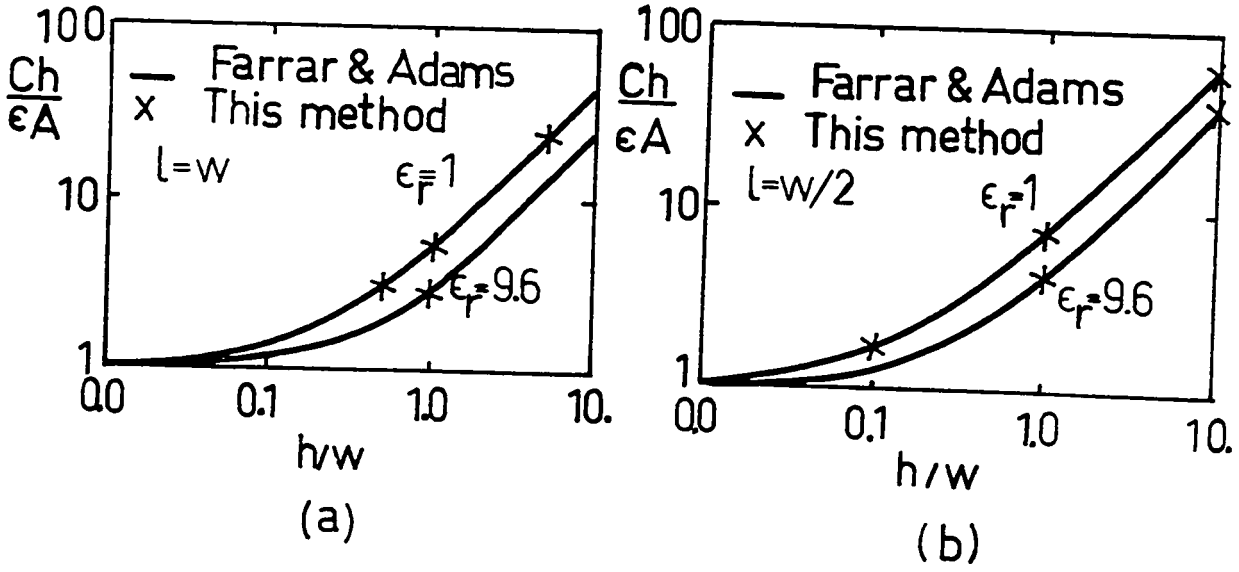

Figure 4.5.2 Comparative capacitance values by Farrar and Adams [20] and this method

TABLE 4.5.2

Parallel Square Plate (w = 1) Capacitance in Vacuum

d/w	C/w (pf/cm)	
	Reitan - 9 const Subregions	This Method One Subregion
0.005	17.74	18.8
0.025	3.7892	3.93
0.05	2.0295	2.07
0.10	1.1324	1.14
0.20	0.6629	0.671
0.50	0.3750	0.385
1.0	0.2801	0.289

show their results together with those obtained by this method. Note that the results obtained by the present method are equal to or higher than the others. Since this method produces a lower bound to the true capacitance, the higher values thus obtained are closer to the exact solution.

A sufficiently large number of computations has been carried out using the above method to permit determining, within a small percentage error, the electrostatic capacitance of virtually any rectangular plate separated by a dielectric sheet

from an infinite conducting sheet (or, what is equivalent, any rectangular plate pair separated by an infinite dielectric sheet). The results of these calculations are given in Figures 4.5.3 and 4.5.4.

In Figure 4.5.3 extensive results are shown for a thin rectangular plate of width w and length l a distance h from an infinite conducting sheet in vacuum. (The same curves apply for two parallel rectangular plates spaced $d = 2h$ apart with the ordinate relabeled $C d / \epsilon_0 A$). The capacitance values as given have been normalized to the capacitance of a similar configuration, calculated on the assumption that there is no fringing. It will be noted that the range w / l shown covers all possible cases : $w / l = 0$ corresponds to infinitely long strip, while $w / l = 1$ represents a square plate over a ground plane. The parameter of Figure 4.5.3, d / w, has been used in preference to d / l for two reasons. First, this choice makes the left-hand endpoints ($w / l = 0$) of all curves represent strips with specified ratio of width-to-height above ground plane, directly comparable with the microstrip results given in Chapter III. Secondly, it has been found that Figures 4.5.4 a - e are rendered most easily legible by this choice.

If a dielectric sheet of relative permittivity ϵ_r is inserted between the ground plane and the rectangular plate, the capacitance rises from its original free-space value C_o to some higher value C . This value, however, is always lower than the value C_r that would be achieved by filling all space with dielectric of permittivity ϵ_r . One may define effective filling factor η as the ratio of capacitance with dielectric sheet in place, to capacitance obtained in a space of homogeneous relative permittivity ϵ_r .

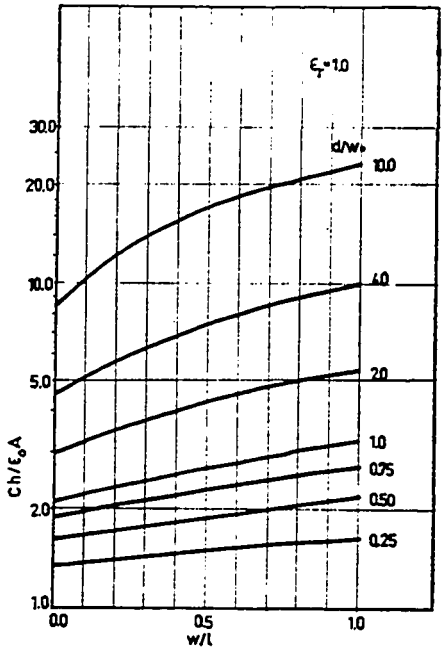

Figure 4.5.3 Normalized capacitance values for rectangular plates in vacuum some distance h from an infinite ground plane

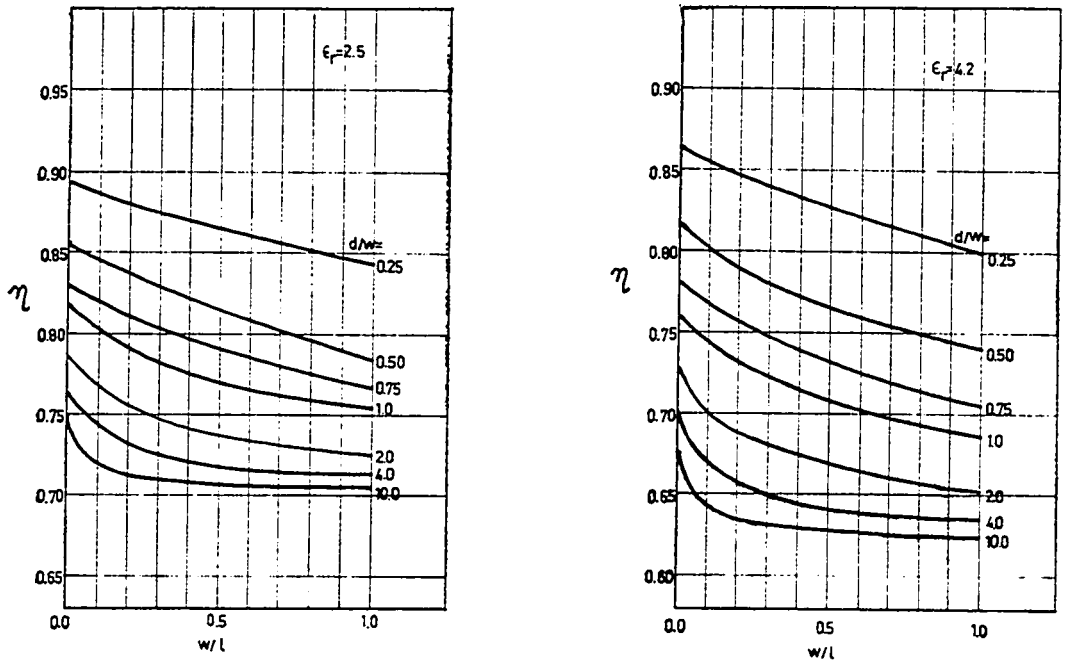

Figure 4.5.4 Effective filling factor η for some commonly used permittivities

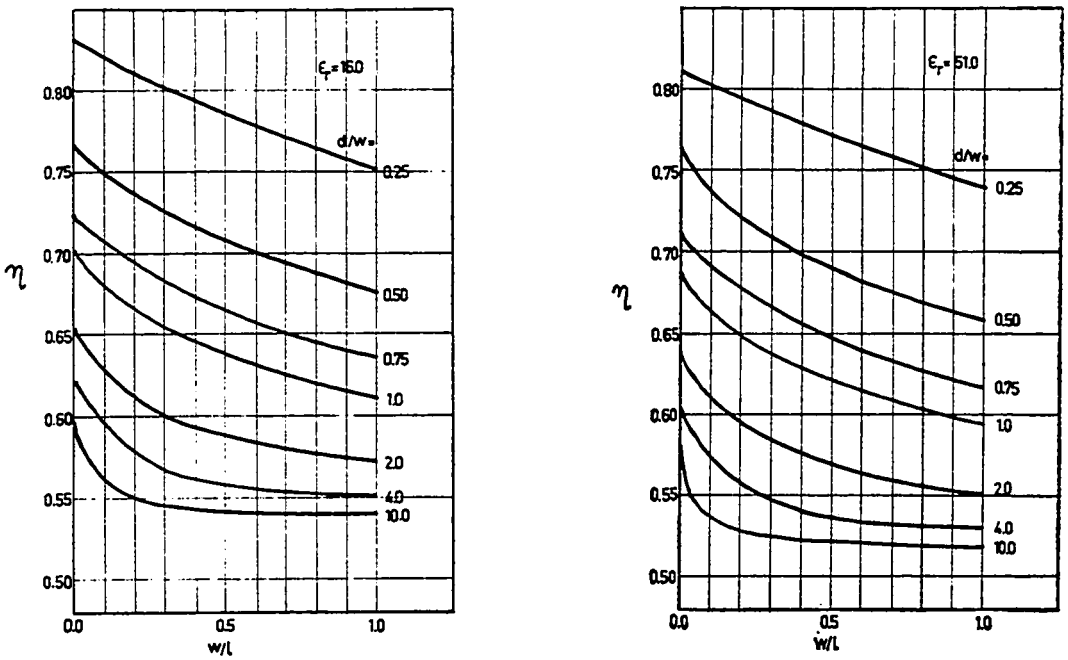

(d)

(e)

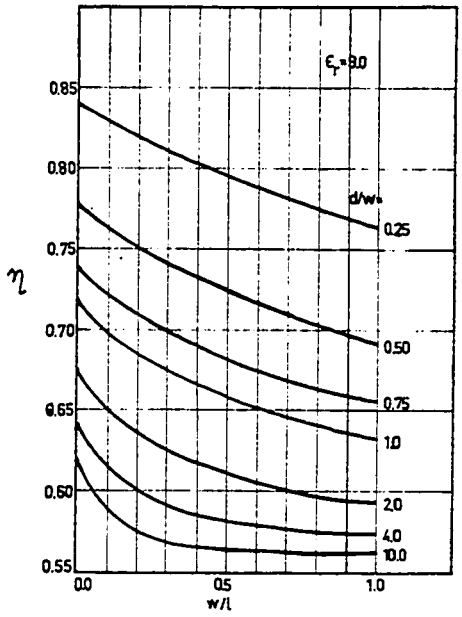

(c)

Figure 4.5.4 Effective filling factor η for some commonly used permittivities

$$\eta = C / C_r \tag{4.5.1}$$

Since $C_r = \epsilon_r C_o$, the actual capacitance C can be found from

$$C = \eta \epsilon_r C_o \tag{4.5.2}$$

provided η is known.

Values of effective filling factor η are given in Figures 4.5.4 a - e for $\epsilon_r = 2.5, 4.2, 9, 16, 51$; these choices are appropriate to some of the commonly employed dielectric materials. While η is obviously dependent on ϵ_r as well as on the geometric parameters, its variation with ϵ_r is not very rapid. Therefore very little accuracy is lost by, for example, using Figure 4.5.4 d for all $14 \leq \epsilon_r \leq 18$ without modification or correction.

If capacitance values are required for relative permittivities not close to one of the tabulated values, linear interpolation has been found quite effective. As an extreme example, suppose $w / l = 0.4$, $d / w = 0.5$ and $\epsilon_r = 4.2$. Using Figure 4.5.4 b , $\eta = 0.772$ is obtained. Were this curve not available, it would be necessary to interpolate between Figure 4.5.4 a (from which $\eta = 0.822$) and Figure 4.5.4 c (where $\eta = 0.731$) . The interpolation yields $\eta = 0.798$, in error by less than four percent, despite the very large range of relative permittivities spanned by the interpolation. Various numerical tests have shown that interpolation between adjacent pairs of computed curves, ordinarily yields errors of about one percent, and occasionally two percent. It is believed that this accuracy level is entirely adequate

for practical work, where neither permittivities, nor geometric parameters are likely to be known much more accurately.

In conclusion, the use of the Rayleigh-Ritz method with biquadratic basis functions, as opposed to a large number of zeroth order subregions, indicates that electrostatic capacitance values accurate to within a few percent can be achieved using one subregion. The computing times required by this method have been found sufficiently short to permit presentation of a set of universal curves, from which the capacitance of a rectangular plate on a conductively backed substrate, or of a pair of rectangular plates separated by a dielectric sheet, may be found. Typical computation times are given in Table 4.5.3. The computation time, as a consequence of

TABLE 4.5.3

No. of Subregions \ ϵ_1	1.0	9.9 46 Terms
1	4.2 sec	5.4 sec
3	15.9 sec	22.1 sec
5	29.3 sec	47.6 sec

Computation times for rectangular plate capacitance calculations

Equation (3.3.12), which is also applicable here, increases with increasing ϵ_1 (decreasing K) for a specified value of the truncation error in the infinite series.

An important advance on this problem, would be the development of efficient quadrature formulae required for the evaluation of the four-dimensional singular integrals generated by the Cartesian product of triangular, rather than rectangular, subregions. The use of high-order triangular subregions would not only reduce the number of subregions required for a Manhattan type rectangular geometry, and hence permit the solution of larger systems of conductors, but would also allow the treatment of conductors of virtually any shape.

CHAPTER V

MICROSTRIP DISCONTINUITY CAPACITANCES

5.1 Introduction

Although numerous papers have been published on microstrip discontinuities, mostly during the past year and almost exclusively treating microstrip open circuits, the results show a great deal of disagreement.

Many discontinuities are well represented by capacitive models. In other discontinuities, the capacitive component is dominant, though it forms an incomplete model. In this chapter a method is presented capable of dealing with the capacitive effects of the discontinuity of any junction of microstrip transmission lines. Its simplicity and inherently high accuracy, in addition to its versatility will be demonstrated.

5.2 Definitions and Methodology

The approaches so far utilized in obtaining discontinuity capacitance values, both numerically and experimentally, run into considerable difficulties with numerous errors. The most important of these errors is invariably due to the subtraction of two numbers of almost equal magnitude.

The method presented here, determines excess capacitance directly. Subtraction of almost equal numbers is avoided, so that the overall accuracy realized

is that of the resulting excess capacitance. The best way to introduce the methodology utilized is by actually obtaining the governing integral equations for the excess charges, and hence excess capacitances, at various discontinuities. But prior to that, a number of commonly used symbols are defined and a key artifice is described. As in Equation (3.2.1), let $\varphi_{\infty}^{(1)}(P_x)$ denote the potential, in the plane of the microstrip, corresponding to an infinite microstriplike charge distribution $\sigma_{\infty}^{(1)}(P'_x)$. The subscript x on the charge and potential coordinates, P'_x and P_x, indicates that the axis of the microstrip is parallel to the x-axis; while the superscript 1 indicates a microstrip of width-to-height ratio $(w/h)_1$. When the meaning is obvious both of these will be omitted. Therefore as in Equation (3.2.1)

$$\varphi_{\infty}^{(1)}(P_x) = \int \sigma_{\infty}^{(1)}(P'_x)\, G_{\infty}(P_x ; P'_x)\, d P'_x \qquad (5.2.1)$$

In the case when P_x is on the microstrip, $\varphi_{\infty}^{(1)}(P_x) = \varphi_{\infty}^{(1)} = \text{constant}$.

Now, let $\varphi_{\xi}^{(1)}(P_x)$ represent the potential, in the plane of the microstrip, associated with a microstriplike charge density distribution $\sigma_{\infty}^{(1)}(P'_x)$ with a sudden polarity reversal in the charge at $x = \xi$. It is shown in Appendix II that

$$\varphi_{\xi}^{(1)}(P_x) = \int \sigma_{\infty}^{(1)}(P'_x)\, G_{\xi}(P_x ; P'_x)\, d P'_x \qquad (5.2.2)$$

The Green's function required in Equation (5.2.1) is given by Equation (3.2.2) while that required in (5.2.2), with reference to Figure 3.2.1, is

$$G_{\xi}(x, y ; y') = \frac{1 - K}{4 \pi \epsilon_0} \left[f(0) - (1 - K) \sum_{n=1}^{\infty} K^{n-1} f(n) \right] \qquad (5.2.3)$$

where

$$f(n) = \log \frac{\sqrt{(x - \xi)^2 + (y - y')^2 + 4 n^2 h^2} + (x - \xi)}{\sqrt{(x - \xi)^2 + (y - y')^2 + 4 n^2 h^2} - (x - \xi)} \qquad (5.2.4)^*$$

and K is the image coefficient defined in Section 4.2.

The charge distribution that causes $\varphi_{\xi}^{(1)}$ is exactly the same as $\sigma_{\infty}^{(1)}(P'_x)$ over the interval $x \in (\xi, \infty)$ and equal to $-\sigma_{\infty}^{(1)}(P'_x)$ over the interval $(-\infty, \xi)$. While this situation may be physically difficult to realize, there is no mathematical objection to it. This simple artifice holds the key to the useful formulation of the excess charge problem, as will be shown in the following sections.

To evaluate the integral in Equation (5.2.2), recall that the charge distribution resulting from (5.2.1) is of the form given by

$$\sigma_{\infty}(y') = \frac{1}{\sqrt{1 - y'^2}} \sum_{i=1}^{k} a_i f_i(y') \qquad (3.3.4)$$

Note that the Green's function in (5.2.3) has a singularity at $y = y'$, while the ratio

$$r_{\xi}(y ; y') = \frac{G_{\xi}(x, y ; y')}{\log \dfrac{|y - y'|}{|y - y'| + 1}} \qquad (5.2.5)$$

is no longer singular. Substituting into the integration to be performed in (5.2.2), then

---

* The notations log and ln are used interchangeably in the thesis, both implying natural logarithm.

$$\phi^{(1)}_{\xi}(x, y) = \sum_{i=1}^{k} a_i \int_{-1}^{1} \frac{\log \dfrac{|y - y'|}{|y - y'| + 1}}{\sqrt{1 - y'^2}} \, f_i(y') \, r_{\xi}(y ; y') \, dy' \qquad (5.2.6)$$

In this integrand $f_i(y')\, r_{\xi}(y ; y')$ is nonsingular over the interval $y' \in [-1, 1]$, all the singularities are packed in the weight $\log [|y - y'| / (|y - y'| + 1)] / \sqrt{1 - y'^2}$. Gaussian quadrature formulae, with this weight, can be developed for each y, by the procedure described in Appendix I. The work in this chapter, as in the previous ones, is confined to microstrips assumed to be of zero thickness.

5.3 Microstrip Open Circuits [56]

5.3.1 Circuit Model and Existing Data

A fact generally true for almost all wave-guiding structures is that, unlike for short circuits, physical terminations which closely correspond to mathematical open circuits are almost impossible to realize. For a microstrip open circuit, i.e. a microstrip line terminated by simply cutting it off square, a number of phenomena may occur. At the end region a charge accumulation is expected ; corresponding to this charge, there may be some local currents ; and, finally, there may be some energy loss due to radiation at the open circuit. Each of these can, respectively, be accounted for in terms of capacitive, inductive and resistive components. Consequently the physical open circuit may be modeled by an R-L-C termination.

In practical work, judging by published experimental data for alumina substrates, the radiative and inductive components are almost wholly negligible up to 1 GHz. In the 1 to 20 GHz range the inductive and in particular the radiative component is measurable, but the capacitive aspect is still the dominant component. To date, therefore, two models have been proposed as practically usable for the open termination : a pure equivalent capacitance and a length of transmission line electrostatically equivalent to that capacitance (see Figure 5.3.1.1).

Attempts have been made to determine the termination parameters experimentally. Stinehelfer [62] performed some measurements as far back as 1969. Troughton [65] has, recently published results for two width to height ratios which appear to have been very carefully conducted. Napoli and Hughes [45] have given a much more extensive set of data, most laudably together with an indication of possible error limits due to dispersion. Concurrently, some theoretical attempts have been made. Farrar and Adams [20] have published computed results for the open circuit pair formed by a rectangular finite piece of strip. Sobol [57] in a review paper alludes to a "simple" theory for wide strips, but surprisingly omits to indicate where it has been published or what its basic assumptions may be. And finally James and Tse [31] using a method similar to that of Farrar and Adams present considerably more extensive results.

Experimental work in this area is made particularly difficult by the existence of dispersion on the line. On the theoretical side, even in the electrostatic assumption, great difficulties arise since analytic solution is impossible and all

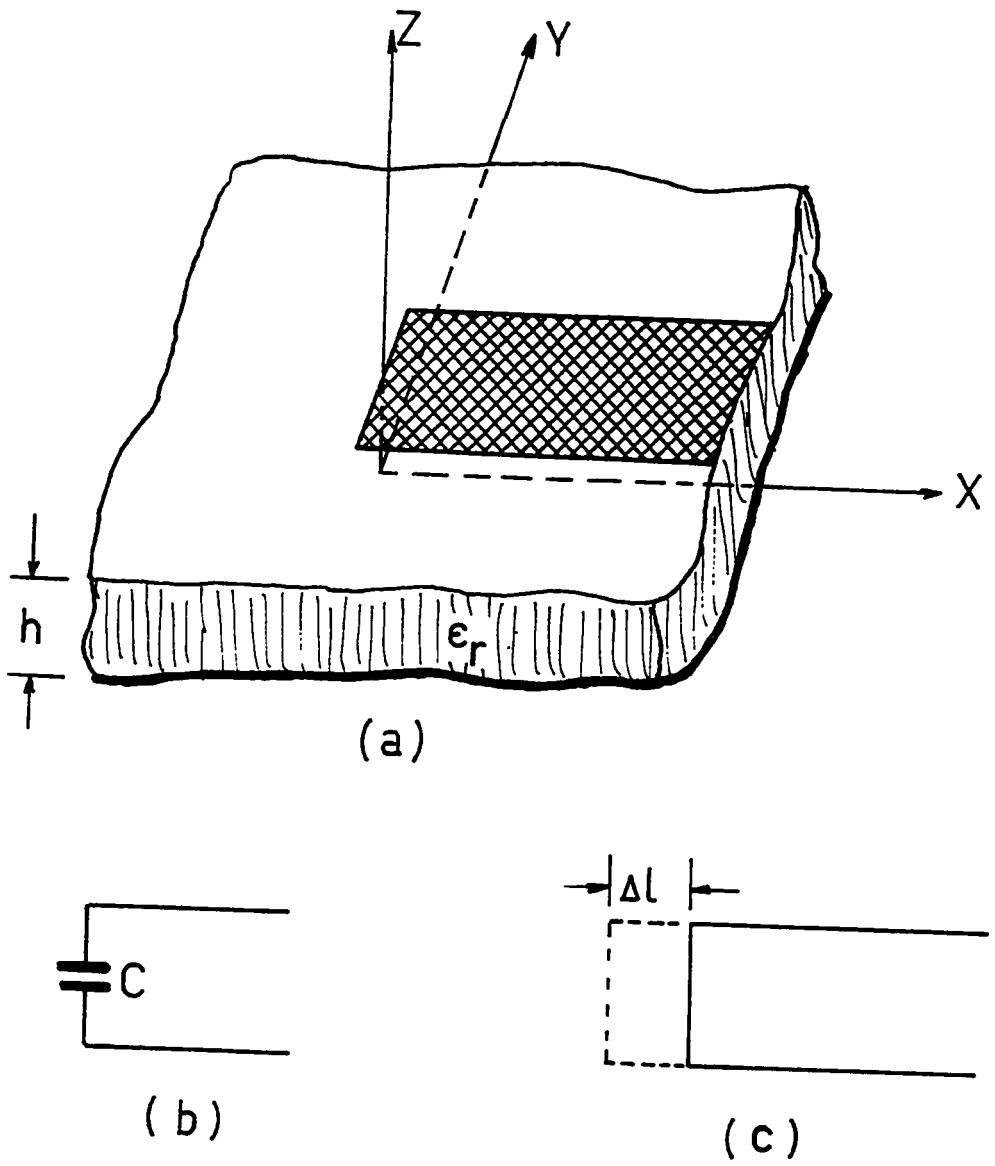

Figure 5.3.1.1 Microstrip open circuit together with two equivalent models

numerical approaches lead to two dimensional integral equations with singular kernels. The approaches tried so far encountered numerous errors, since they have involved the subtraction of two numbers of almost equal size ; this holds true for both analytic and numerical approaches. As already mentioned, the method proposed here determines the excess charge directly so that the above problem is not encountered.

5.3.2 Excess Charge Formulation

To formulate the excess charge problem usefully, consider an infinite microstriplike charge distribution, as given in Equation (5.2.1), of $\frac{1}{2}\,\sigma_\infty\,(P'_x)$ with its associated potential $\frac{1}{2}\,\varphi_\infty\,(P_x)$. Also, consider a charge distribution $\frac{1}{2}\,\sigma_\infty\,(P'_x)$ with a polarity reversal at $x = 0$, as given by Equation (5.2.2), with its corresponding potential $\frac{1}{2}\,\varphi_o\,(P_x)$. By the superposition of these two charge distributions, there results the hypothetical distribution exactly equal to the charge on an infinite strip for $x \in [0, \infty]$ and zero for $x \in [-\infty, 0]$. The potential corresponding to such a distribution is $\frac{1}{2}[\varphi_\infty\,(P_x) + \varphi_0\,(P_x)]$.

It is readily seen that this potential distribution cannot satisfy the requirement of constant potential everywhere on the half-strip. Indeed, were it to satisfy this condition, the desired end capacitance would be zero ! To raise the potential everywhere on the half-strip to the constant value φ_∞, a certain amount of extra charge $\sigma_x = \sigma_t - \sigma_\infty$ must be placed on it. Here σ_t denotes the total charge

density on the actual open circuited semi-infinite microstrip. Therefore, the potential residual annihilated by the extra charge σ_x on the half-strip is

$\varphi_\infty - \frac{1}{2}[\varphi_\infty + \varphi_0 (P_x)]$, or

$$\varphi_x^{oc} (P) = \frac{1}{2} [\varphi_\infty - \varphi_0 (P)] \qquad (5.3.2.1)$$

Since both φ_∞ and $\varphi_0 (P)$ are known (φ_∞ is chosen as unity, while $\varphi_0 (P)$ can be calculated from Equation (5.2.2)), φ_x^{oc} can be obtained. In order to find the unknown excess charge σ_x^{oc} corresponding to φ_x^{oc}, a three dimensional problem, analogous to the rectangular plate of Chapter IV, must be solved. Therefore, as in Equation (4.2.5),

$$\varphi_x^{oc} (P) = \int_{\text{half-strip}} \sigma_x^{oc} (P') \, G^{oc} (P ; P') \, d P' \qquad (5.3.2.2)$$

where $G^{oc} (P ; P')$ is the three-dimensional Green's function given in Equation (4.2.4) except, now there is no symmetry about the y-axis.

Although this equation requires integration over the semi-infinite strip, computationally effective ways can be devised for its solution since both the potential and the excess charge approach zero asymptotically (and rather rapidly) for points at increasing distances from the strip end.

5.3.3 Solution for Excess Charge and C_{oc}

It should be observed, that Equation (5.3.2.2) permits the solution for excess charge directly, without further arithmetic manipulation or approximation. The only subtraction in the entire formulation is that required for the potential residual φ_x^{oc} in Equation (5.3.2.1) ; these numbers are numerically very different near the strip end, where the excess charge resides ; their difference, therefore, is determinable to high accuracy. The region in which the potential residual is known only with poor accuracy, i.e. far away from the termination is an area of no interest in any case, since it contains little if any of the excess charge.

To solve Equation (5.3.2.2) the following steps need to be taken :

(i) assume $\varphi_\infty = 1$ and evaluate $\sigma_\infty (P')$ as in Chapter III ,

(ii) use $\sigma_\infty (P')$ in Equation (5.2.2) to solve for $\varphi_0 (P)$,

(iii) evaluate the potential residual φ_x^{oc} ,

(iv) use the Green's function as given in Equation (4.2.3) with

$$f^{oc}(n) = \left[(2n)^2 + \left(\frac{x - x'}{h}\right)^2 + \left(\frac{y - y'}{h}\right)^2 \right]^{-1/2} + \left[(2n)^2 + \left(\frac{x - x'}{h}\right)^2 + \left(\frac{y + y'}{h}\right)^2\right]^{-1/2} \qquad (5.3.3.1)$$

(v) solve Equation (5.3.2.2) using the Rayleigh-Ritz method over many subregions, in a manner similar to that employed in Chapter IV for the rectangular plates,

(vi) evaluate the total excess charge and hence the open circuit capacitance .

$$C_{oc} = \int_{s} \sigma_x^{oc} (P') \, d P' \qquad (5.3.3.2)$$

For $\epsilon_r = 9.6$ and two relatively extreme strip widths the potential residual appears plotted in Figure 5.3.3.1. This figure also shows the typical subregions used in the excess charge calculations. As may be seen from Figure 5.3.3.1 the potential residual does not extend far back from the open circuited end, so that integration over the semi-infinite strip is in fact not required ; carrying integrations back about two substrate thicknesses for alumina substrates, appears to be adequate for most width-to-height ratios. While it is possible to develop quadrature formulae to integrate over the semi-infinite strip, this has not appeared worthwhile since the potential residual dies off very rapidly. The exact distance how far back from the strip end the integration is carried is not critical. This geometric truncation has been tested by repeated recomputation using larger and larger regions of integration.

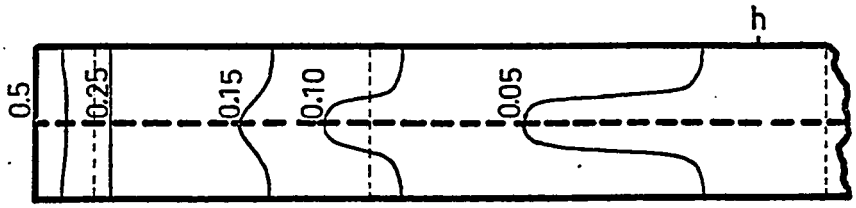

(b)

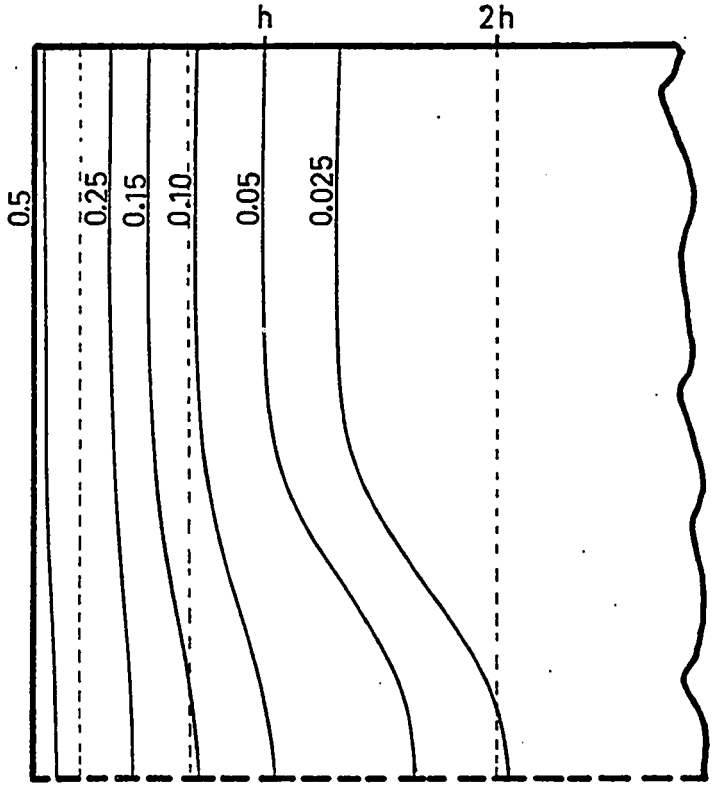

(a)

Figure 5.3.3.1 Potential residual near two open circuits ($w/h = 6.0$, $w/h = 0.2$ and $\epsilon_r = 9.6$)

5.3.4 Results and Comparison with Existing Data

There have appeared in the literature, both experimental and theoretical, results for the open circuit capacitance of a microstrip line. The results given by Napoli and Hughes [45] are of considerable importance in this regard as are those of Farrar and Adams [20]. Both were concerned with alumina substrates, results being presented for relative permittivities of 9.6 and 10.4. Detailed comparison has been made with both sets of results as well as with those by Troughton [65].

Figure 5.3.4.1 shows the comparison between the present method and those indicated above. The open circuit capacitance is represented by the electrostatic capacitance of a length Δl from an infinite microstrip line. It is interesting to note that in the center portion, around $w/h = 1$, all four groups of investigators agree substantially. Above and below this portion some disagreement is evident. The Farrar and Adams curve was computed using a method in which the capacitance of a finite section of infinite microstrip is subtracted from the computed capacitance of a finite rectangle. This procedure is fraught with error accumulation ; it represents the classical difficulty of subtracting two large, and nearly equal, numbers. Because this difficulty obtrudes particularly badly for wide strip widths, it is held that the Farrar and Adams curve may be considered reliable for narrow strip widths but not for broad ones. This discrepancy has been communicated to the authors and very recently, they published a correction to their results [21], which shows much better agreement with the present method for wide strips. Their corrected results are also shown in Figure 5.3.4.1. Further support is lent to this view by the Napoli and Hughes curve, which, as may be

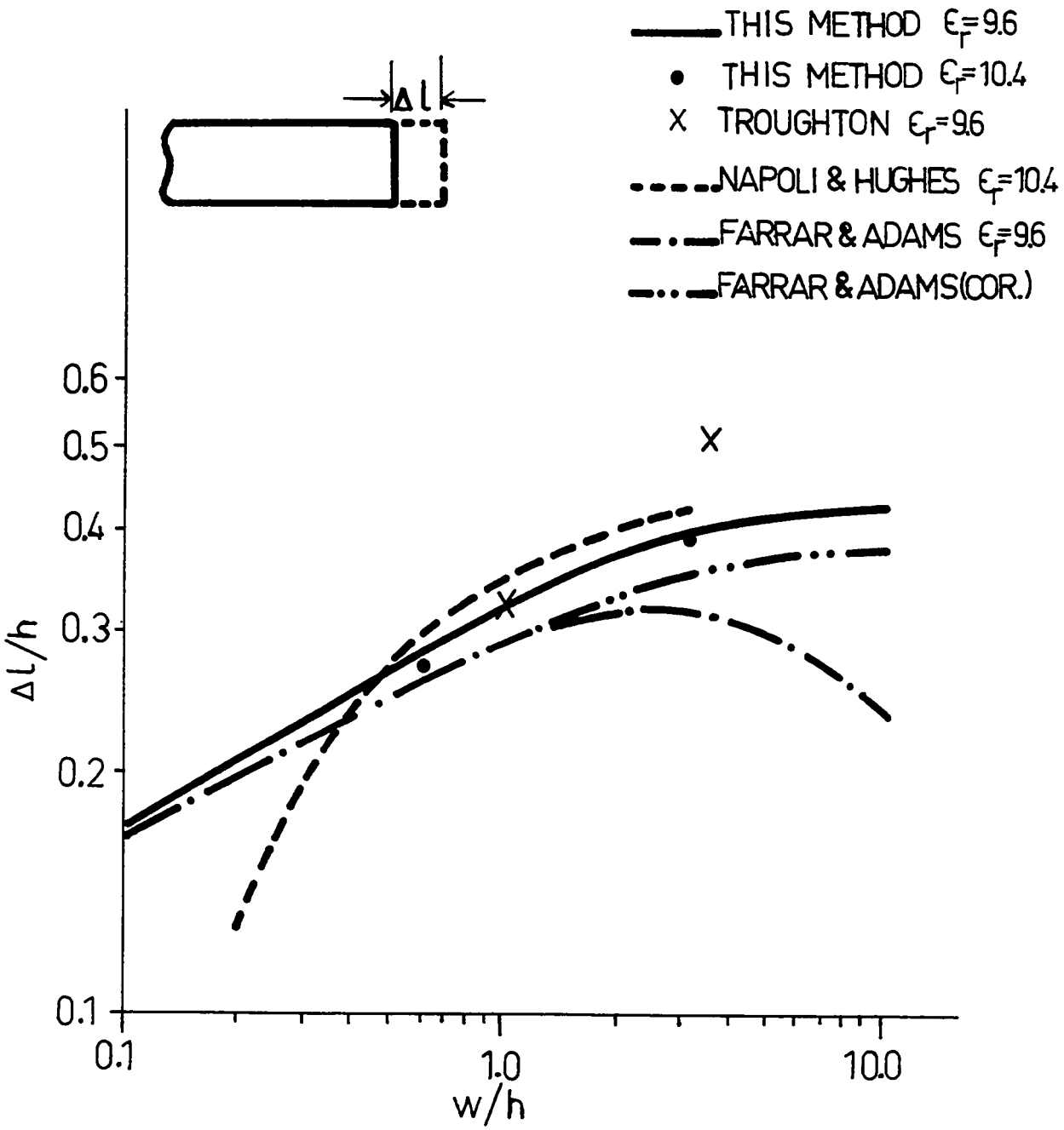

Figure 5.3.4.1 Comparative end effect results obtained by Napoli and Hughes [45], Troughton [65], Farrar and Adams [20,21] and this method.

seen, follows the computed ones well through the mid-range and up to broad strip widths. Troughton has only given two points : for $w/h = 1$ there is good agreement with Napoli and Hughes while for $w/h = 3.44$ the results are about 20 % higher.* The reasons why Napoli and Hughes' experimental results should not agree with calculations for narrow strip widths are not evident. However, it is noteworthy that the shape of their curve at small widths is predicated on one point only, so that an experimental error of unusually large magnitude in the measurement of that point could well alter the shape of their results, as presented, quite markedly.

Stinehelfer's [62] results are not shown in Figure 5.3.4.1 since they are higher by more than a factor of two. All the evidence available points to the fact that the disagreement must be resolved in favour of the results calculated by the method proposed here. James and Tse, being in possession of a preprint of [56], have indicated in [31] that their results are in good agreement with those calculated by this method.

A rudimentary error analysis of the numerical method presented here has been made. It has been found that the calculated results are in error probably on the low side ; and it will be noted that this expectation is borne out by comparison with experimental results.

---

* It should be noted that the curve given in Figure 2 of Troughton's paper [65] has an error of one order of magnitude in the admittance coordinate [64] ; the points plotted in Figure 5.3.4.1 have been corrected.

Figure 5.3.4.2 shows curves of the excess capacitance of an open circuit microstrip termination normalized to strip width as a function of strip width-to-height ratio and substrate permittivity. Typical CPU times required for $\epsilon_r = 1.0$ and $\epsilon_r = 9.6$ on the IBM S 360/75 with three subregions are 16 seconds and 30 seconds, respectively. This compares favorably with the 5 - 20 minutes reported by Farrar and Adams [20] on a GE 635, a computer of roughly comparable speed. The permittivity values have been chosen essentially arbitrarily, but in keeping with some of the fairly common substrate materials. These open-circuit capacitance curves have been fitted with quartic polynomials [56], to enable users to write function subroutines capable, with little arithmetic, of returning the required discontinuity data.

5.4 Microstrip Gaps [7]

5.4.1 Circuit Model and Existing Work

Unlike for the microstrip open circuit there is hardly any published literature, theoretical or experimental, on gaps in microstrip. Stinehelfer [62] performed transmission loss measurements on gaps in microstrip and used the results to model the discontinuity by a series gap capacitance (see Figure 5.4.1.1).

A more complete model, to be utilized here, for this discontinuity is a symmetric two port capacitive π network (see Figures 5.4.1.2 a and b). This model, of course, assumes that there is no radiation due to or delay through the gap.

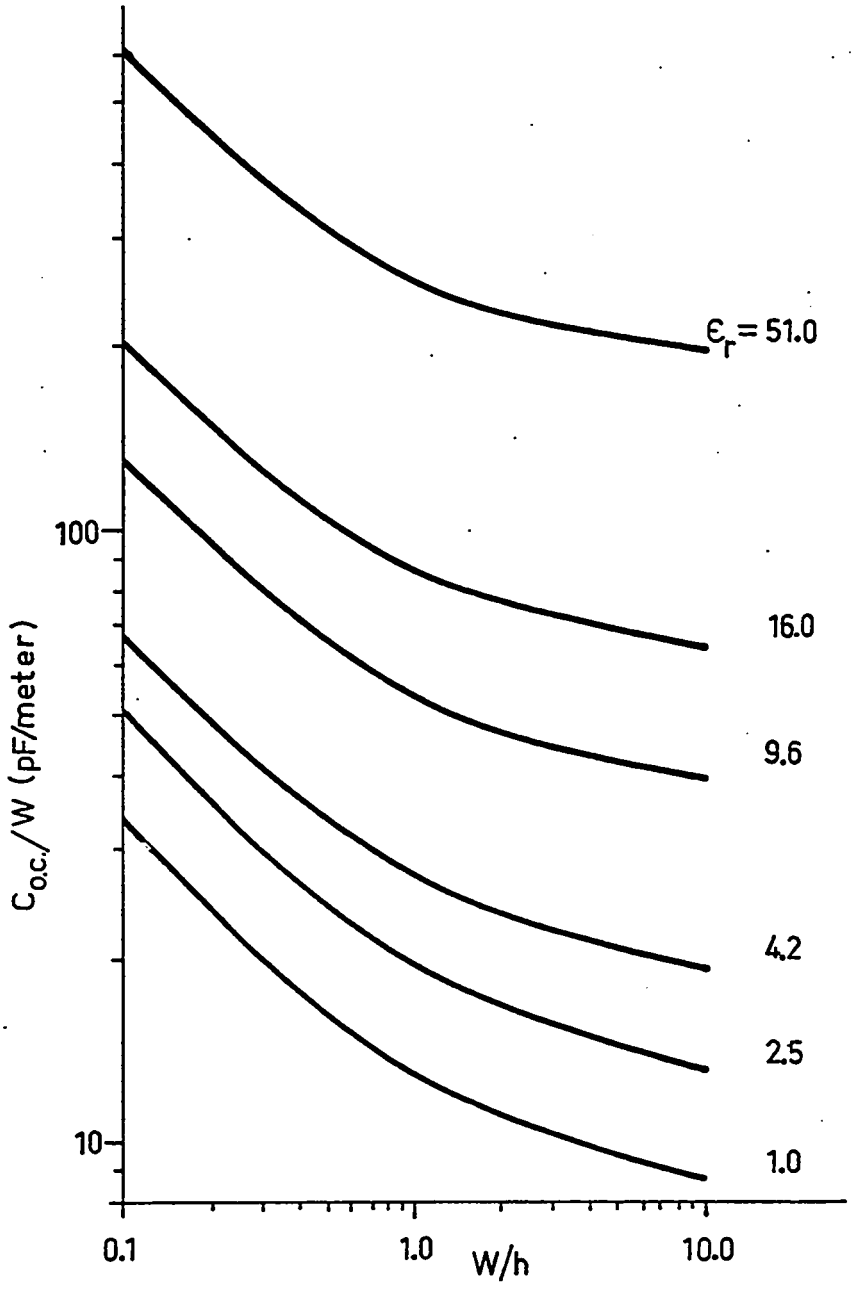

Figure 5.3.4.2 Open circuit capacitances, normalized to strip width, as as a function of width-to-height ratio and permittivity.

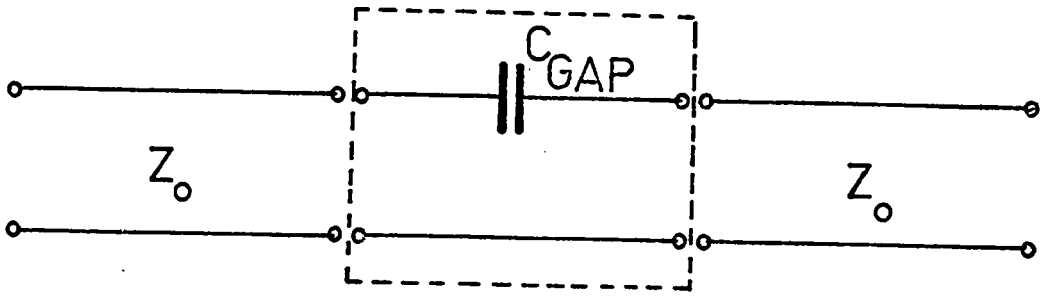

Figure 5.4.1.1 Stinehelfer's [62] gap capacitance model for a gap in the microstrip

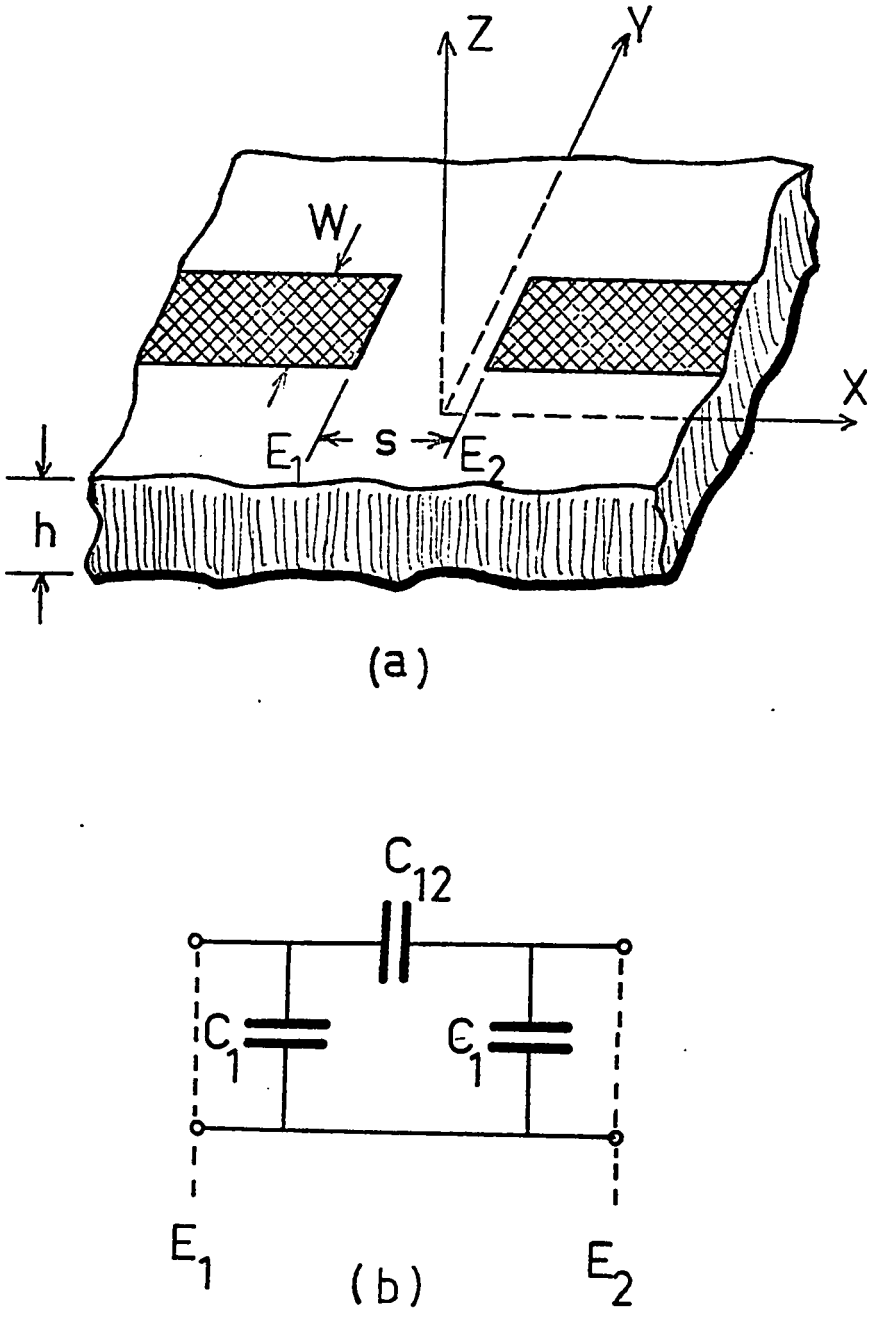

Figure 5.4.1.2 Microstrip gap and capacitive π - equivalent network

The inclusion of these would add some resistive and inductive components respectively.

In the capacitive π model shown in Figure 5.4.1.2 b it is well known that at least two measurements are required for the determination of the parameters C_1 and C_{12}. Figures 5.4.1.3a and b illustrate two such measurements. The capacitance values thus obtained are denoted by C_{even} and C_{odd}, respectively.

5.4.2 Excess Charge Formulation for C_{even} and C_{odd}

To obtain the excess charge for C_{even}, defined by Figure 5.4.1.3 a, an infinitely extending microstriplike charge distribution $\sigma_\infty (P_x')$, of the type defined by Equation (5.2.1), is considered. Two other charge distributions each $\frac{1}{2}\sigma_\infty (P_x')$, one having a polarity reversal at $x = s/2$ and the other at $x = -s/2$, are required. The potentials, as defined by Equation 5.2.2, corresponding to these three charge distributions are $\varphi_\infty (P)$, $\frac{1}{2}\varphi_{s/2} (P)$ and $\frac{1}{2}\varphi_{-s/2} (P)$, respectively.

Superposing the infinite microstriplike charge distribution with the one with polarity reversal at $x = s/2$ and subtracting the third charge distribution, one is left with a microstriplike charge over the intervals $|x| > s/2$ and zero charge elsewhere. The corresponding potential is $\varphi_\infty (P) + \frac{1}{2}[\varphi_{s/2} (P) - \varphi_{-s/2} (P)]$.

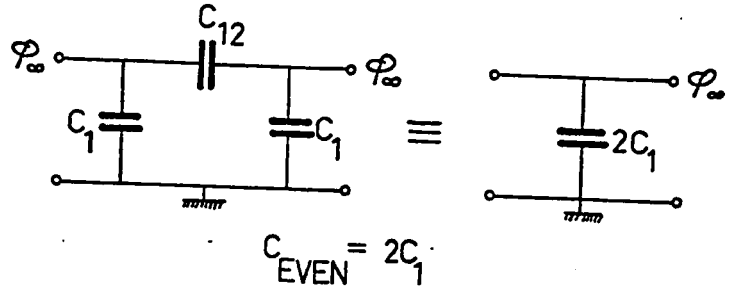

$C_{EVEN} = 2C_1$

(a)

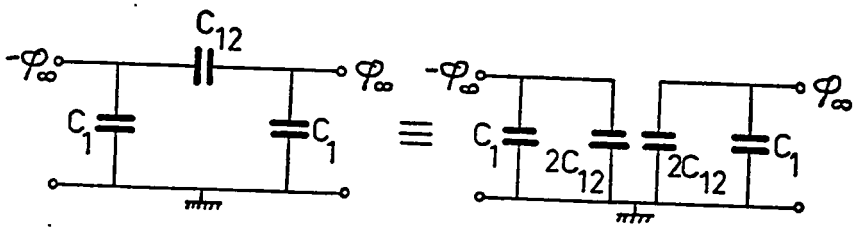

$C_{ODD} = 2C_{12} + C_1$

(b)

Figure 5.4.1.3 Symmetrically and anti-symmetrically excited π - network resulting in C_{even} and C_{odd}, respectively

Now, arguing as in the open circuit case, a certain amount of extra charge $\sigma_x^{even} = \sigma_t - \sigma_\infty$ must be added to each of these microstriplike distributions in order to raise the potential on them to φ_∞, as required by Figure 5.4.1.3 a. Therefore the potential residual on the strip, corresponding to the extra charge σ_x^{even}, is $\varphi_\infty - \{\varphi_\infty + \frac{1}{2}[\varphi_{s/2}(P) - \varphi_{-s/2}(P)]\}$, i.e.

$$\varphi_x^{even}(P) = \frac{1}{2}[\varphi_{-s/2}(P) - \varphi_{s/2}(P)] \qquad (5.4.2.1)$$

Therefore, as in the open circuit case, the governing integral equation is

$$\varphi_x^{even}(P) = \int \sigma_x^{even}(P')\, G^{even}(P ; P')\, dP' \qquad (5.4.2.2)$$

To obtain the excess charge formulation for C_{odd}, as defined in Figure 5.4.1.3 b, it can be shown by an analogous procedure that to raise (lower) the potential on the semi-infinite strip at $x > s/2$ ($x < -s/2$) to φ_∞ ($-\varphi_\infty$) an extra charge σ_x^{odd} ($-\sigma_x^{odd}$) is required. The governing integral equation is

$$\varphi_x^{odd}(P) = \int \sigma_x^{odd}(P')\, G^{odd}(P ; P')\, dP' \qquad (5.4.2.3)$$

where

$$\varphi_x^{odd}(P) = \varphi_\infty - \frac{1}{2}[\varphi_{s/2}(P) + \varphi_{-s/2}(P)] \qquad (5.4.2.4)$$

In Equations (5.4.2.2) and (5.4.2.3) both the potential residual and excess charge approach zero asymptotically at increasing distances from the strip ends.

5.4.3 Solution for Excess Charges, and C_{even} and C_{odd}

The comments made in Section 5.3.3, for open circuits, also apply here, subject to the following modifications :

The Green's function is the same as given in Equation 4.2.3 with

$$f^{even}_{odd}(n) = \left[(2n)^2 + \left(\frac{x-x'}{h}\right)^2 + \left(\frac{y-y'}{h}\right)^2 \right]^{-1/2} + \left[(2n)^2 + \left(\frac{x-x'}{h}\right)^2 + \left(\frac{y+y'}{h}\right)^2 \right]^{-1/2} \tag{5.4.3.1}$$

$$\pm \left[(2n)^2 + \left(\frac{x+x'}{h}\right)^2 + \left(\frac{y-y'}{h}\right)^2 \right]^{-1/2} \pm \left[(2n)^2 + \left(\frac{x+x'}{h}\right)^2 + \left(\frac{y+y'}{h}\right)^2 \right]^{-1/2}$$

Note that full advantage is taken of the symmetry about the x-axis, and symmetry or anti-symmetry about the y-axis for the even and odd cases.

The desired capacitance values are

$$C_{even} = 2 \int \sigma_x^{even}(P')\, dP' \tag{5.4.3.2}$$

$$C_{odd} = \int \sigma_x^{odd}(P')\, dP' \tag{5.4.3.3}$$

where the indicated integrations are over the half-strips located at $x > s/2$.

For $\epsilon_r = 9.6$, $w/h = 1$ and $s/w = 0.1$ the potential residuals are shown in Figures 5.4.3.1 a and b ; also shown are the typical subdivisions used for excess charge calculation.

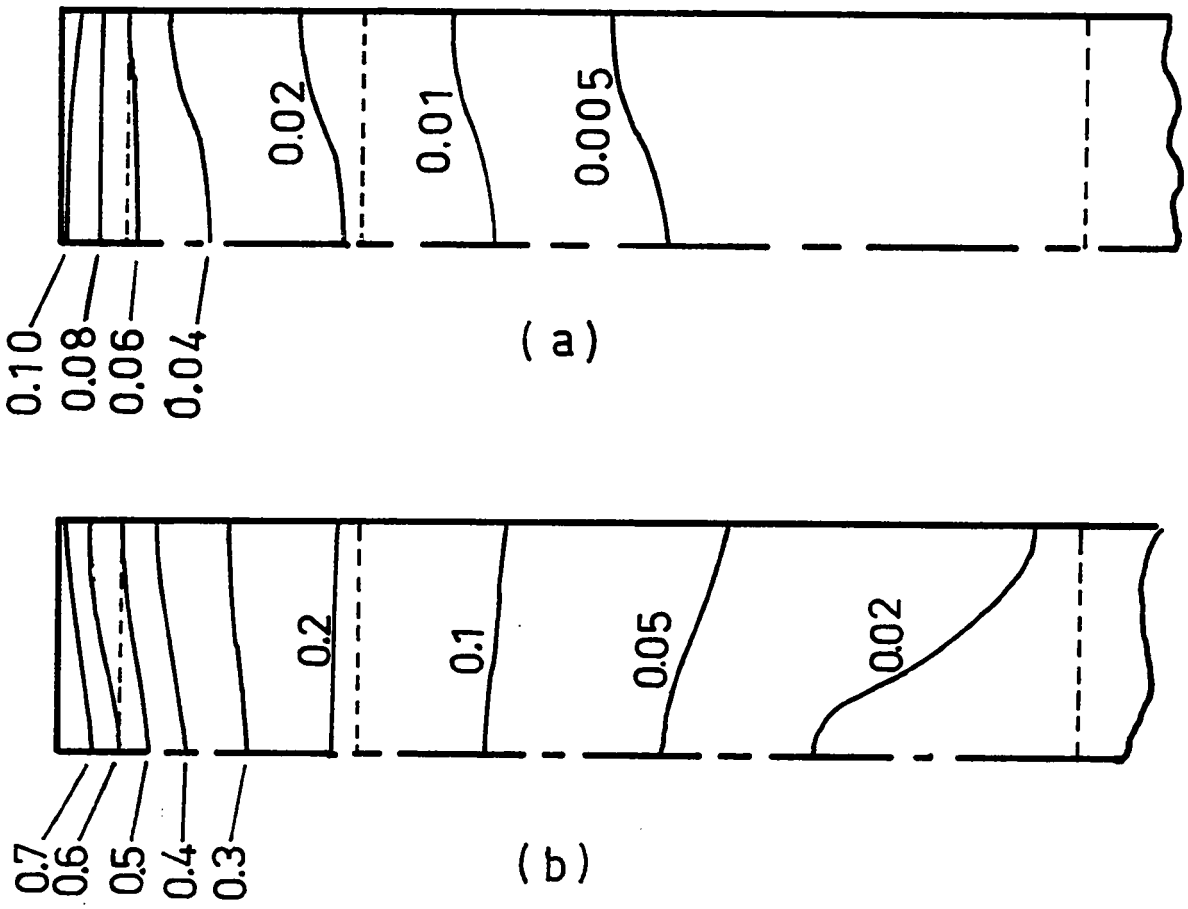

Figure 5.4.3.1 Potential residual for the symmetrically (C_{even}) and anti-symmetrically (C_{odd}) excited micro-strip gap ($w/h = 1.0$, $s/w = 0.1$ and $\epsilon_r = 9.6$

5.4.4 Results and Comparison with Existing Data

The only published data available for microstrip gaps appear to be those due to Stinehelfer [62] * . He performed transmission loss measurements on single gaps in uniform 50 Ω microstrip lines, and compared the results with the theoretical loss calculated for a capacitive gap in a 50 Ω line. The measurements were made at 2 GHz on a substrate of relative permittivity of 8.875 of thickness $h = 0.020$ inches and $w/h = 1$, with a metallic cover placed some distance from the substrate. Gap capacitance versus spacing-to width ratio curves are given for both cover off and cover on cases. As the theory proposed here is developed for the cover off case, it is appropriate that comparison be made with measurements under the same conditions.

The most meaningful comparison is to plot transmission loss against spacing-to-width ratio from Stinehelfer's measurements on the same graph as loss predicted by the π equivalent circuit given here. The measured and calculated results are shown in Figure 5.4.4.1 ; the close agreement is indeed reassuring.

C_{even} and C_{odd} , normalized to strip width, are plotted in Figure 5.4.4.2 for $0.1 \leq s/w \leq 2.0$, substrate dielectric constants of $\epsilon_r = 1.0$, 2.5, 4.2, 9.6 and 15.0 and width-to-height ratios $w/h = 0.5$, 1.0 and 2.0. The capacitances C_1 and C_{12} to be used in the π model of the microstrip gap, may be

---

* In June 1972, M. Maeda [78] published some results on the gap in microstrip. His formulation is for total charge for the microstrip in a box, and results are presented for the walls "sufficiently removed" to have negligible effect. The excess capacitance was then obtained from the total capacitance by the same argument as used by Farrar and Adams [20, 21] . There appears to be good agreement between his results and those presented here.

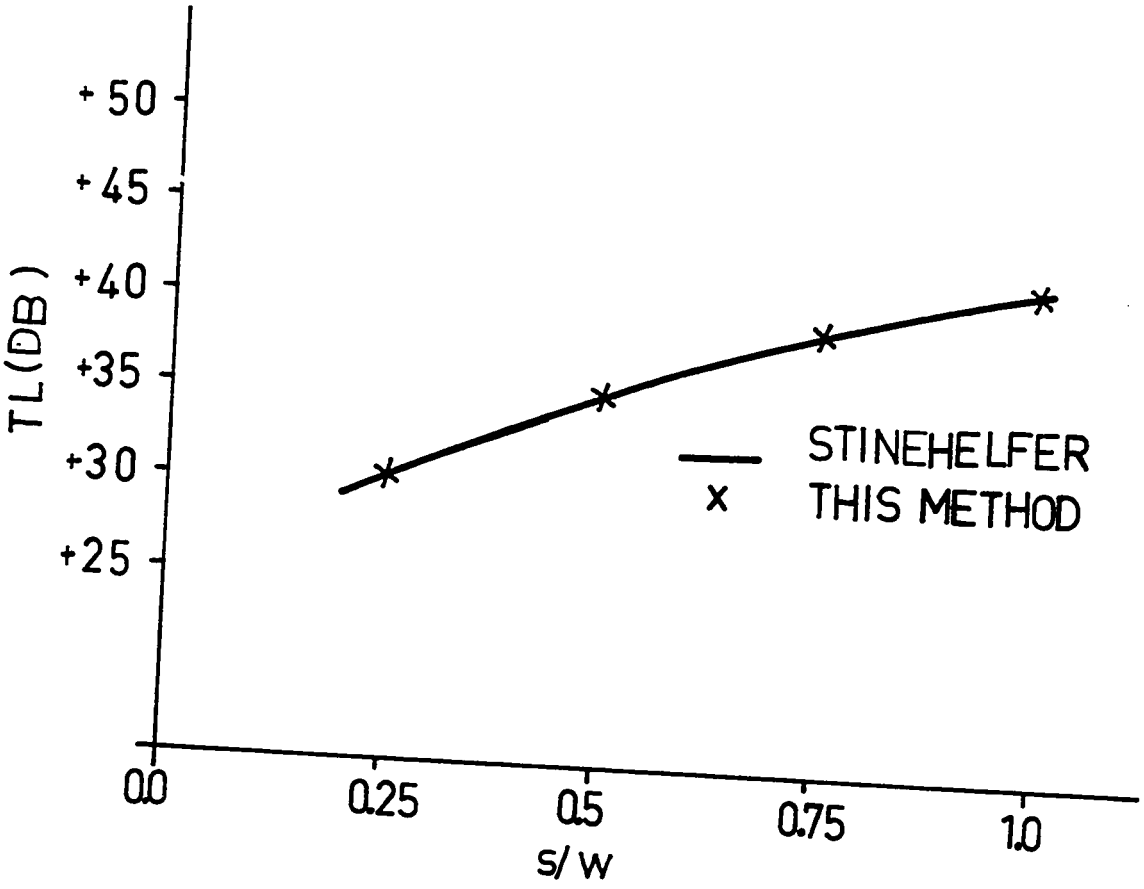

Figure 5.4.4.1 Transmission loss measured by Stinehelfer [62] and calculated by this method, for the gap in microstrip

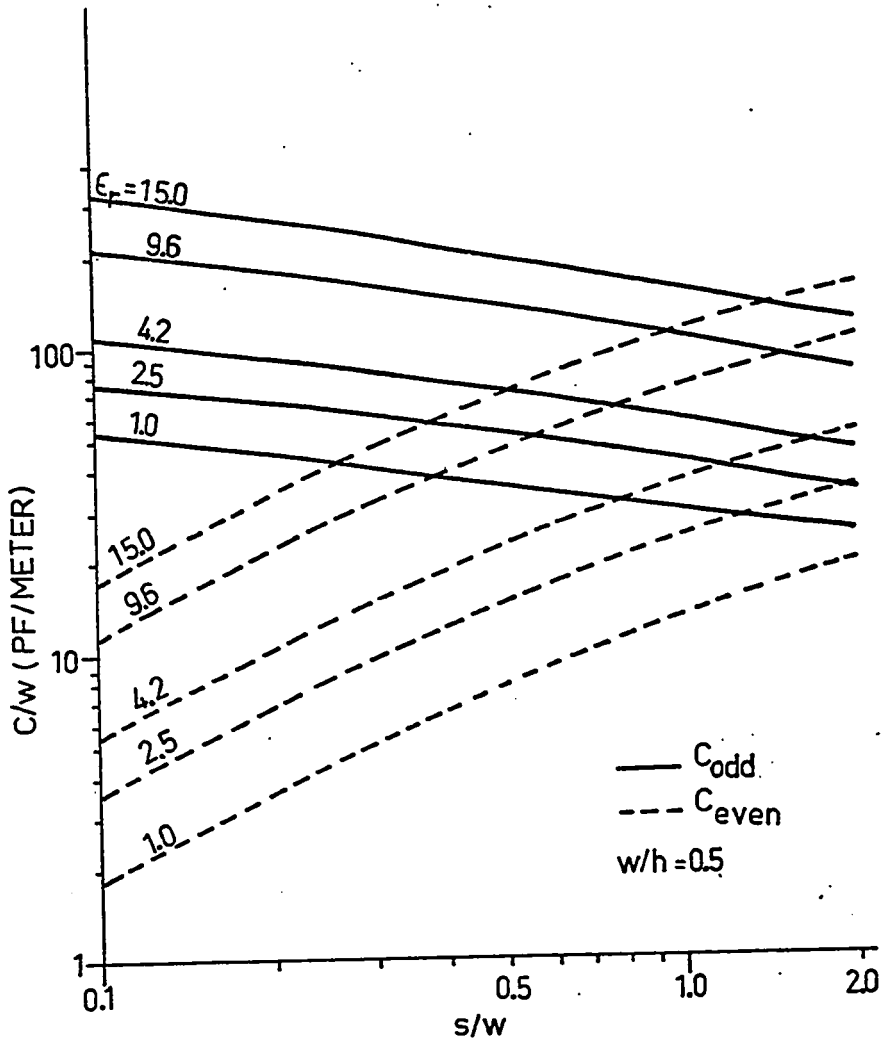

(a)

Figure 5.4.4.2 C_{even} and C_{odd} normalized to strip width as a function of gap spacing and substrate permittivity

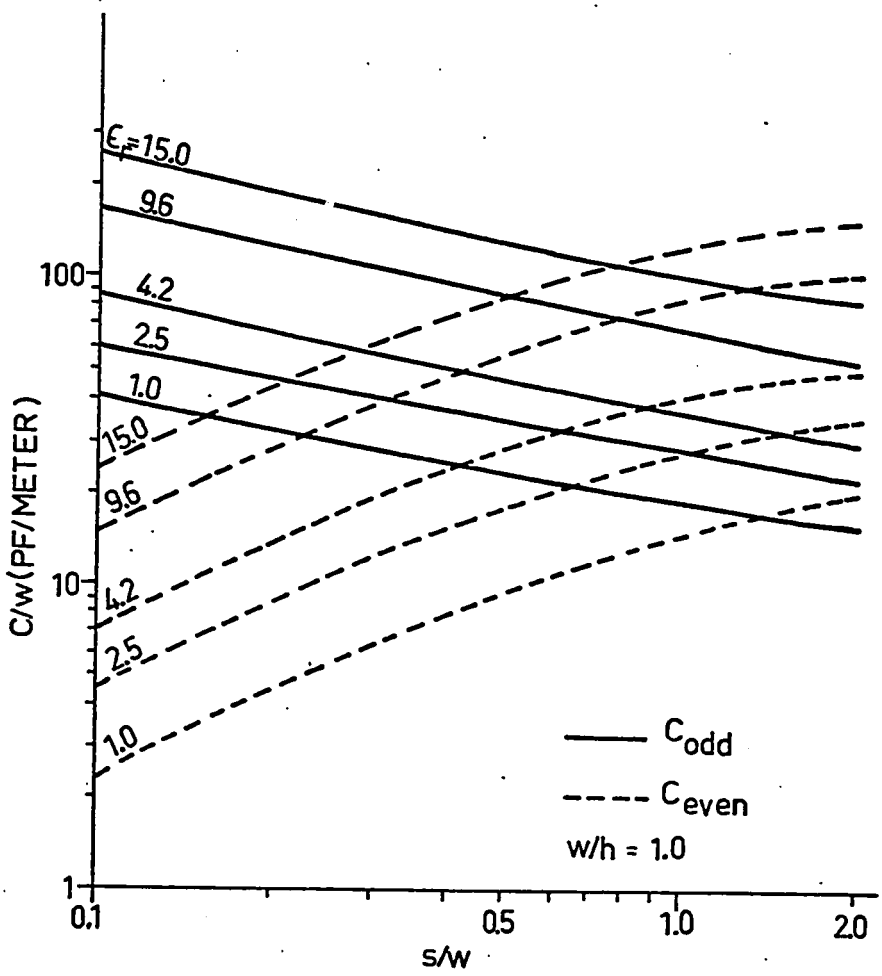

(b.)

Figure 5.4.4.2 C_{even} and C_{odd} normalized to strip width as a function of gap spacing and substrate permittivity

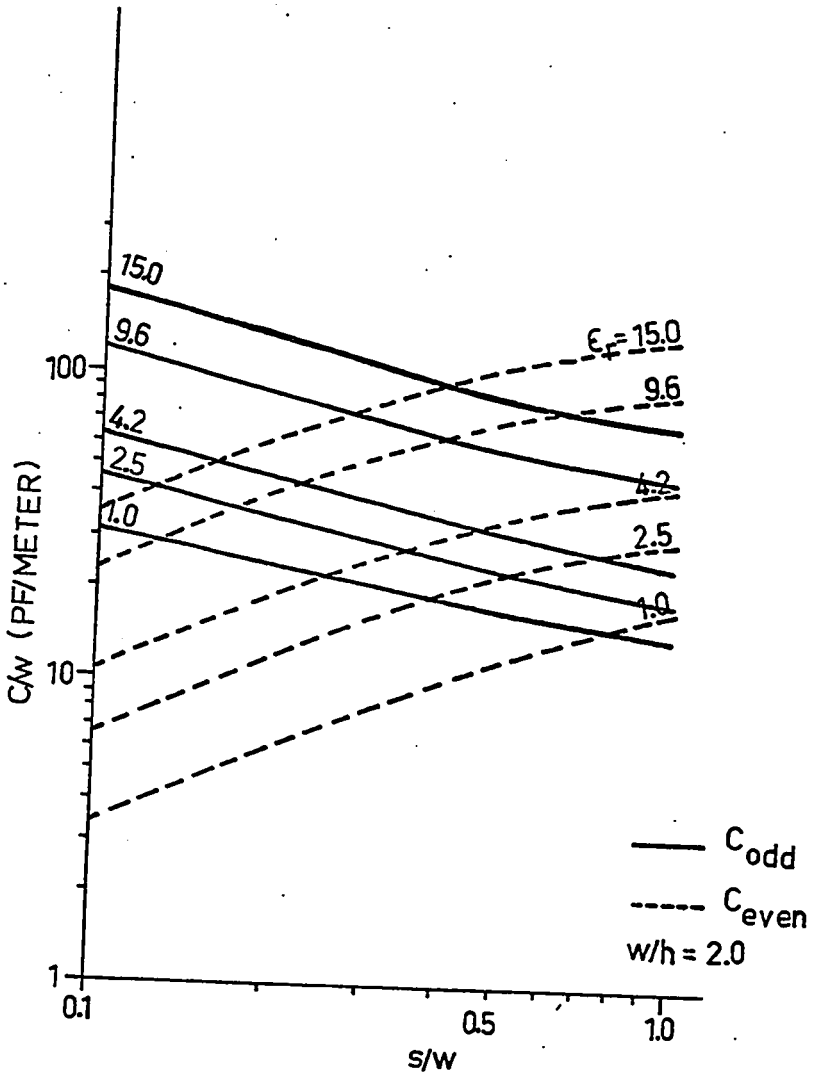

(c)

Figure 5.4.4.2 C_{even} and C_{odd} normalized to strip width as a function of gap spacing and substrate permittivity

easily calculated using

$$C_1 = \frac{1}{2} C_{even} \qquad (5.4.4.1)$$

$$C_{12} = \frac{1}{2} [C_{odd} - C_1] \qquad (5.4.4.2)$$

These two relations follow readily from Figures 5.4.1.3 a and b. As expected, for large values of s/w, C_{odd} approaches C_1 which in turn approaches the open circuit capacitance value calculated in Section 5.3. Also as s/w approaches zero, C_{even} approaches zero.

The calculated values of C_{even} and C_{odd}, as was the case for the open circuit capacitance, are expected to be on the low side ; in these calculations the error introduced by subtraction of nearly equal numbers has been eliminated. Typical CPU times required on the IBM 360/75 for $\epsilon_r = 9.6$ are 33 seconds for each of C_{even} and C_{odd}. For $\epsilon_r = 1.0$, of course, the time required is considerably shorter.

5.5 Microstrip Steps [7]

5.5.1 Circuit Model and Existing Work

In the case of a sudden change of width of the microstrip line, it appears that, there are no published experimental data. The only theoretical data available are due to Wolff, Kompa and Mehran [72], who used an approximate waveguide

model of the microstrip and then proceeded to match local expansions of wave components at the discontinuity. They only presented preliminary results of scattering coefficients for $\epsilon_r = 2.33$, with more results to be published later.

A typical microstrip step is shown in Figure 5.5.1.1 together with the shunt capacitance discontinuity model to be evaluated here. Of course, a resistive component could be included in the model, to account for losses due to radiation at the junction ; however, what would be more important is inductive components in a two port model, as shown in Figure 5.5.1.2, to account for local currents in the discontinuity region.

5.5.2 Excess Charge Formulation

The excess charge associated with a sudden change of width of the microstrip line may be handled in much the same way as was the C_{even} case for the gap. Consider two infinite microstriplike charge distributions of $\frac{1}{2}\sigma_{\infty}^{(1)}(P'_x)$ and $\frac{1}{2}\sigma_{\infty}^{(2)}(P'_x)$ having width-to-height ratios $(w/h)_1$ and $(w/h)_2$, respectively. The corresponding potentials are $\frac{1}{2}\varphi_{\infty}^{(1)}(P_x)$ and $\frac{1}{2}\varphi_{\infty}^{(2)}(P_x)$. Also, take two microstriplike charge distributions of $\frac{1}{2}\sigma_{\infty}^{(1)}(P'_x)$ and $\frac{1}{2}\sigma_{\infty}^{(2)}(P'_x)$, each with a polarity reversal at $x = 0$. The corresponding potentials are $\frac{1}{2}\varphi_0^{(1)}(P_x)$ and $\frac{1}{2}\varphi_0^{(2)}(P_x)$. Note that superposing the first three charge distributions and subtracting the last one, to the left of the discontinuity plane there results a microstriplike distribution $\sigma_{\infty}^{(2)}(P'_x)$ while to the right $\sigma_{\infty}^{(1)}(P'_x)$ is obtained.

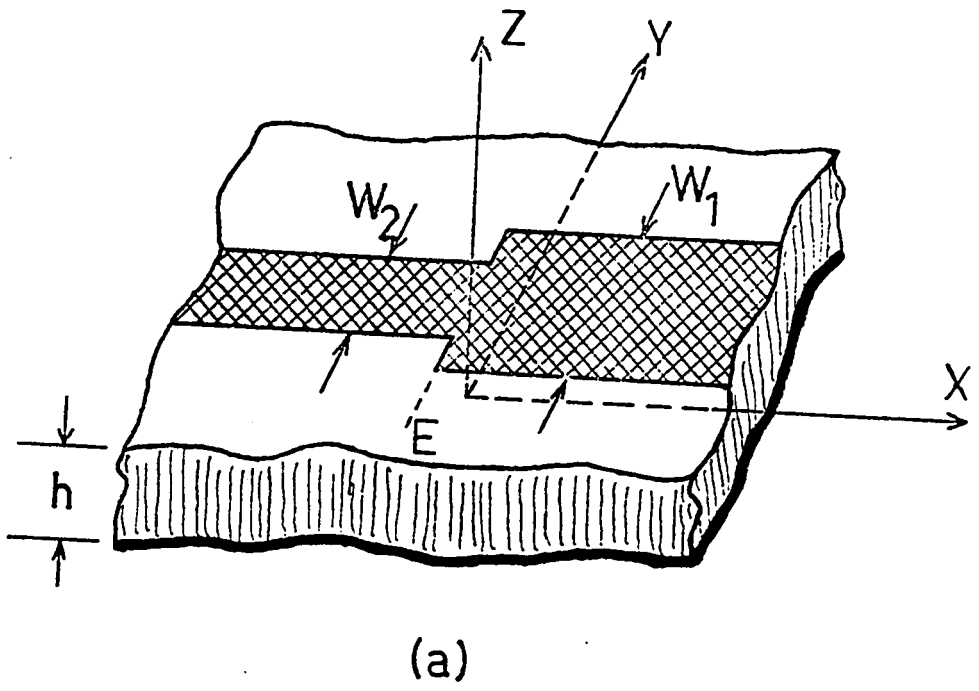

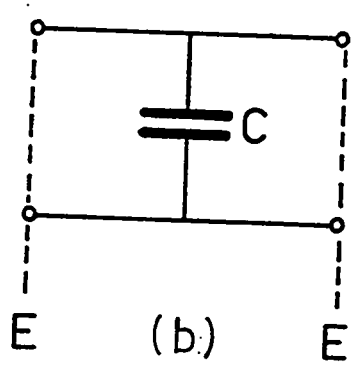

Figure 5.5.1.1 Microstrip step and shunt discontinuity capacitance model

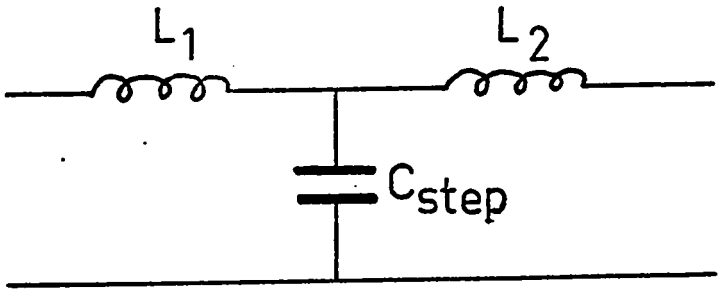

Figure 5.5.1.2 Equivalent circuit for microstrip step incorporating inductive elements

Although the charge distributions on the two half-strips are identical to those on microstrip lines of corresponding width-to-height ratios, this is not true of the potential on the strips. The superposition of these four charge distributions yields an overall potential of $\frac{1}{2}[\varphi_{\infty}^{(1)}(P_x) + \varphi_{\infty}^{(2)}(P_x) + \varphi_0^{(1)}(P_x) - \varphi_0^{(2)}(P_x)]$. As before, a certain amount of extra charge $\sigma_x^{step} = \sigma_t - \sigma_{\infty}$ must be added, to the semi-infinite microstriplike charge distributions, to raise the potential on the two half-strips to $\varphi_{\infty}^{(1)}$ or $\varphi_{\infty}^{(2)}$, as the case may be. Therefore the potential residual, producing this excess charge σ_x^{step}, is

$$\varphi_x^{step}(P) = \frac{1}{2} \begin{cases} \varphi_{\infty}^{(1)}(P) - \varphi_{\infty}^{(2)}(P) - \varphi_0^{(1)}(P) + \varphi_0^{(2)}(P) & \text{for } x > 0 \\ \varphi_{\infty}^{(2)}(P) - \varphi_{\infty}^{(1)}(P) - \varphi_0^{(1)}(P) + \varphi_0^{(2)}(P) & \text{for } x < 0 \end{cases} \qquad (5.5.2.1)$$

while the governing integral equation is

$$\varphi_x^{step}(P) = \int \sigma_x^{step}(P')\, G^{step}(P\,;P')\, dP' \qquad (5.5.2.2)$$

The indicated integration is over both half-strips. However, as in earlier instances, both excess charge and potential residuals approach zero rapidly at increasing distances from the discontinuity plane, so that integration over finite regions suffices.

5.5.3 Solution for Excess Charge and C_{step}

Much of the commentary made in Section 5.3.3 applies here, too. The excess charges are calculated directly. The potential residual is zero at the junction

of the two half-strips and rises to a maximum (falls to a minimum) moving onto the wider (narrower) of the strips and then returns to zero quite rapidly. For $\epsilon_r = 9.6$, $(w/h)_1 = 1.0$ and $(w/h)_2 = 2.0$ the potential residual is plotted in Figure 5.5.3.1 ; also shown are the typical subdivisions used for excess charge calculation.

The Green's function utilized in Equation 5.5.2.2 is the same as that given in Equation 4.2.3 with

$$f^{step}(n) = [(2n)^2 + (\frac{x-x'}{h})^2 + (\frac{y-y'}{h})^2]^{-1/2} + [(2n)^2 + (\frac{x-x'}{h})^2 + (\frac{y+y'}{h})^2]^{-1/2} \qquad (5.5.3.1)$$

where symmetry about the x-axis is included. To evaluate C_{step} use

$$C_{step} = \int \sigma_x^{step}(P')\, dP' \qquad (5.5.3.2)$$

and the integration is performed over both half-strips.

5.5.4 Results and Comparison with Existing Data

The scattering coefficients calculated by Wolff , Kompa and Mehran [72], show considerable frequency dependence. The lowest frequency at which they indicate a sharp dip in the scattering coefficient is for a step of 50 Ω to 10 Ω on a substrate thickness of 0.625 mm or 1.5 mm (there seems to be some confusion about which value was used). The width of the 10 Ω line for the 0.625 mm substrate is about 14.5 mm. At 5 GHz, since the relative phase velocity of a 10 Ω line on substrate of

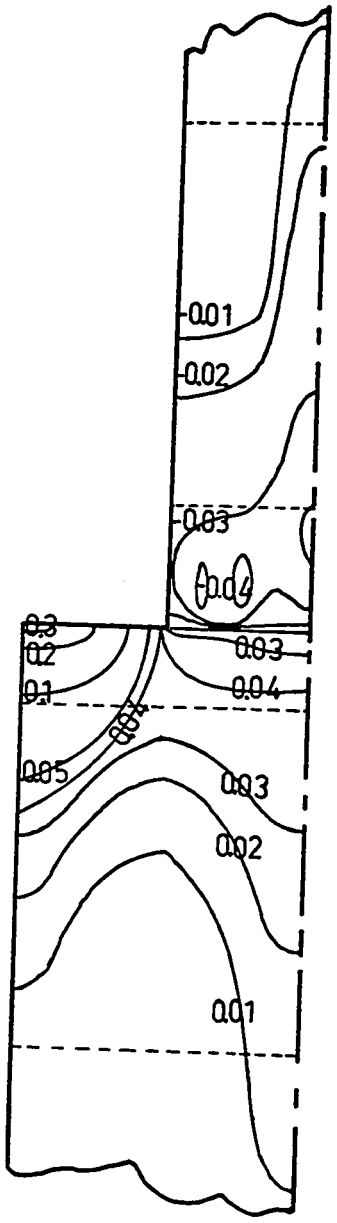

Figure 5.5.3.1 Potential residual near a microstrip step ($w_1/h = 1$, $w_2/h = 2$ and $\epsilon_r = 9.6$)

$\epsilon_r = 2.33$ is about 0.686, the strip width is comparable to a third of a wavelength. Surely, when typical dimensions are larger than onetenth of a wavelength, the electrostatic approximation is not valid. Without giving results, Wolff, Kompa and Mehran [72] indicate that for $\epsilon_r = 9.9$ the frequency dependence is negligible up to 20 GHz. This, however, supports the results obtained here. For the commonly used alumina substrate thicknesses (about 0.5 mm) realistic impedances can be obtained using small width-to-height ratios and the resulting capacitive effects are very small. Still, qualitatively speaking, the effect of the shunt capacitance, at the discontinuity plane, on the scattering coefficients is the same as predicted by Wolff, Kompa and Mehran The reason there are no experimental results available, may be partly due to this very small shunt capacitance contribution of most practical microstrip steps ; this is both difficult to measure and is not significant enough to affect seriously the performance of the overall circuit.

In Figure 5.5.4.1 calculated values are normalized to the geometric mean of the two strip widths. As expected in the case of equal width strips, i.e. no step, $C_{step} = 0$. These calculated values of step capacitance are expected to be on the low side. Typical CPU time required on the IBM S 360/75 is 1.0 minutes for $\epsilon_r = 9.6$.

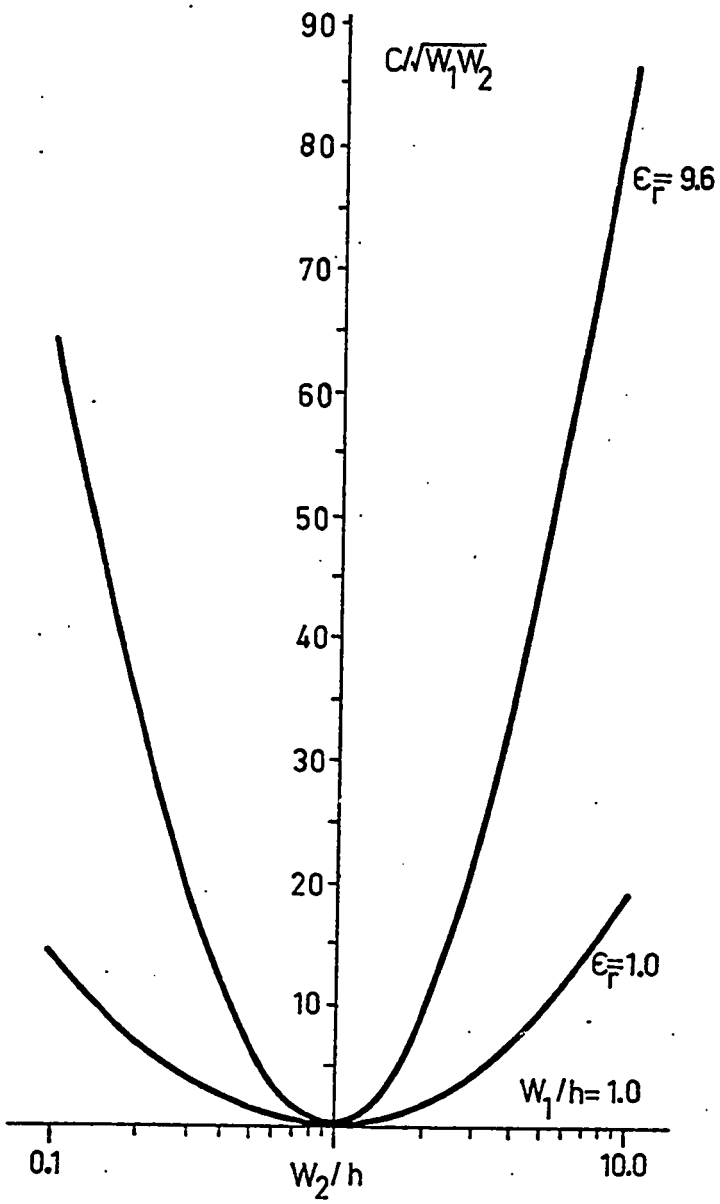

Figure 5.5.4.1 Step capacitance normalized to geometric mean width as a function of width-to-height ratio and substrate permittivity

5.6 Microstrip Right Angle Bends

5.6.1 Circuit Model and Existing Work

For the case of a microstrip right angle bend, published data are very scarce. The only data available appear to be the experimental results of Stephenson and Easter [60]. The equivalent circuit used by them includes a shunt capacitance to account for a charge accumulation at the corner and series lengths of transmission lines on either side to account for the increased current path around the corner. Their equivalent circuit, together with the reference planes used, is shown in Figure 5.6.1.1. This model is basically the same as that proposed for the microstrip step in Figure 5.5.1.2. The addition of a resistive component to the model of Figure 5.6.1.1, to account for loss due to radiation at the bend would make the model more or less complete.

Stephenson and Easter devised two types of resonant measurements : (i) two 90^{o} corners are incorporated into a closed ring resonator and (ii) a right angle bend in a symmetrical open-ended resonator. At various frequencies voltage maxima or minima occur at the corners and the two unknowns in the model can be evaluated.

5.6.2 Excess Charge Formulation

The excess charges which constitute C_{bend} are due to the potential residual, when two microstrip type charge distributions exist on the arms of a right angle bend up to terminal planes T_1 and T_2 shown in Figure 5.6.1.1a.

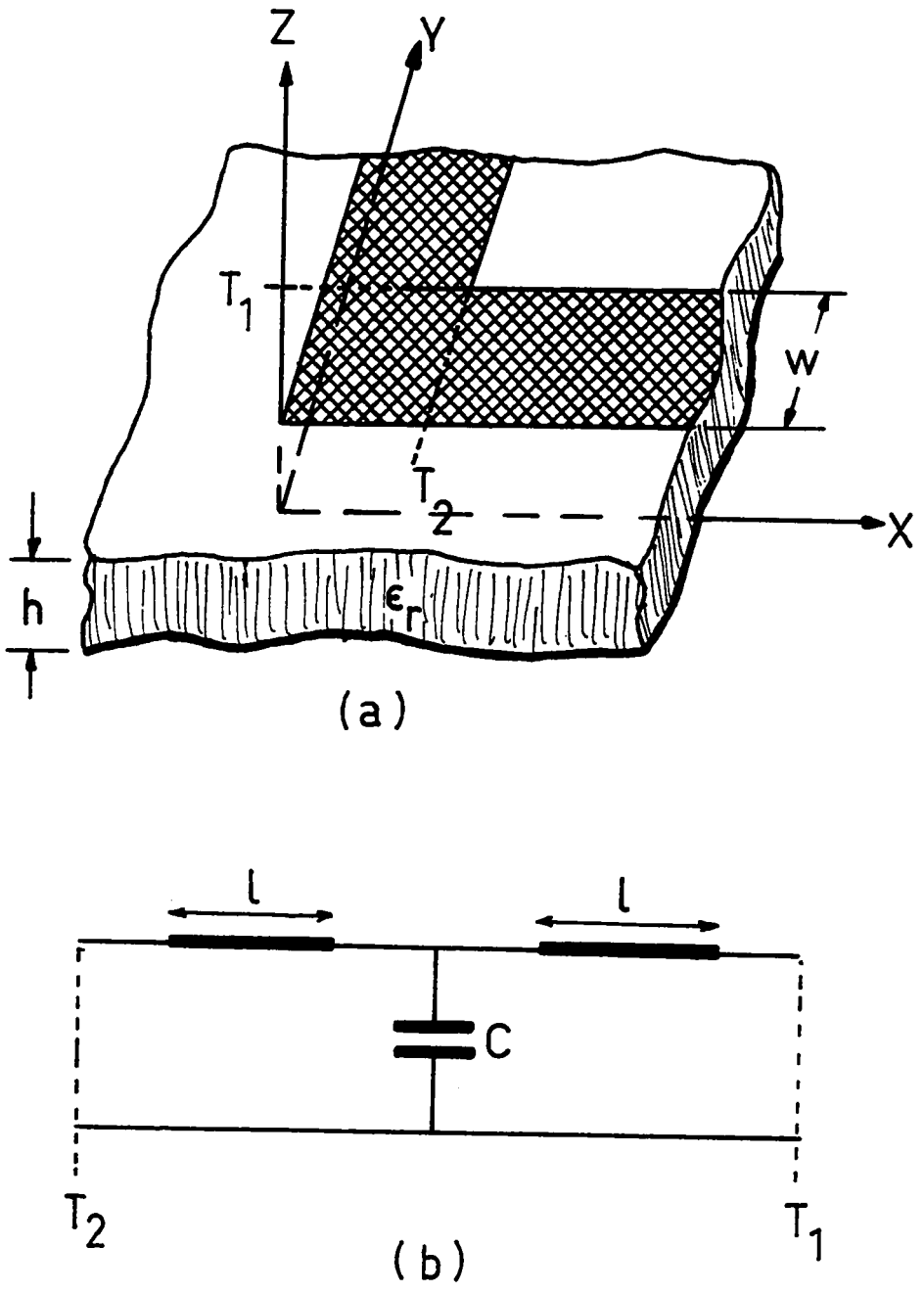

Figure 5.6.1.1 Microstrip right angle bend together with equivalent circuit proposed by Stephenson and Easter [60]

Let $\frac{1}{2}\varphi_{\infty}(P_x)$ be the potential corresponding to an infinite microstriplike charge distribution of $\frac{1}{2}\sigma_{\infty}(P'_x)$ parallel to the x-axis. Also let $\frac{1}{2}\varphi_{1.0}(P_x)$ represent the potential corresponding to a microstriplike charge distribution with a polarity reversal at $x = 1.0$. Therefore the potential corresponding to a microstriplike charge on the interval $x \in (1, \infty)$ is, by superposition, $\frac{1}{2}[\varphi_{\infty}(P_x) + \varphi_{1.0}(P_x)]$. Similarly, in the y-direction, the potential corresponding to a microstriplike charge on the interval $y \in (1,\infty)$ is $\frac{1}{2}[\varphi_{\infty}(P_y) + \varphi_{1.0}(P_y)]$. By superposition one can generate microstriplike distributions parallel to the positive x and y axes up to terminal planes T_1 and T_2. Therefore the potential residual required is

$$\varphi_x^{\text{bend}}(P) = \varphi_{\infty} - \frac{1}{2}[\varphi_{\infty}(P_x) + \varphi_{1.0}(P_x) + \varphi_{\infty}(P_y) + \varphi_{1.0}(P_y)] \qquad (5.6.2.1)$$

while the governing integral equation for the excess charge is

$$\varphi_x^{\text{bend}}(P) = \int_{\nu} \sigma_x^{\text{bend}}(P')\, G^{\text{bend}}(P\,;P')\, dP' \qquad (5.6.2.2)$$

Although the indicated integration is over the entire bend including the semi-infinite arms, both potential residual and excess charge fall to zero on moving away from the discontinuity region.

5.6.3 Solution for Excess Charge and C_{bend}

The method described in Section 5.3.3 still applies, but subject to the following changes :

Function $f^{bend}(n)$ required in the Green's function given by Equation 4.2.3 is

$$f^{bend}(n) = [\,(2n)^2 + (\frac{x - x'}{h})^2 + (\frac{y - y'}{h})^2\,]^{-1/2} \qquad (5.6.3.1)$$

and the bend capacitance is calculated from

$$C_{bend} = \int \sigma_x^{bend}(P')\, d P' \qquad (5.6.3.2)$$

A typical residual voltage for a dielectric substrate of $\epsilon_r = 1.0$ and microstrip width-to-height ratio $w/h = 1$, is shown in Figure 5.6.3.1. Not shown in this figure is that moving further away from the discontinuity some small amount of negative potential residual appears and then it dies down to zero. This is due to the interaction between the two normal microstriplike distributions and is most noticeable for small ϵ_r's and (w/h)'s . Numerical experiments indicate that the most significant part of the excess charge is located near the outer edge of the corner region. Thus, the typical discretization used is also shown in Figure 5.6.3.1. Although the symmetry about the 45° angle is not accounted for in Equation (5.6.3.1), the discretization of the region is done so that full advantage may be taken of this symmetry during computation.

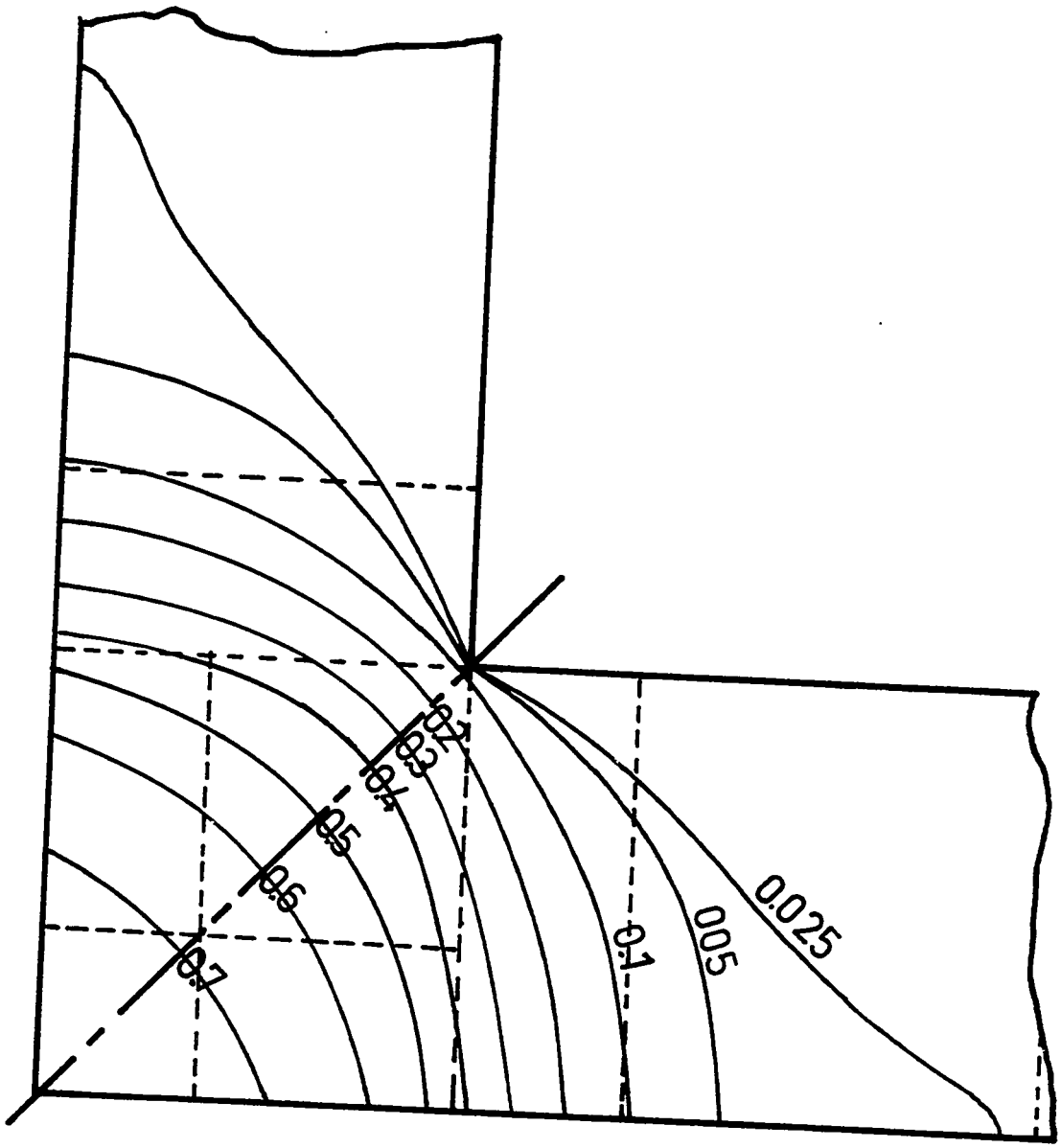

Figure 5.6.3.1 Potential residual near a microstrip right angle bend ($w_1/h = 1.0$ and $\epsilon_r = 1.0$)

5.6.4 Results and Comparison with Existing Data

The bend capacitances obtained by Stephenson and Easter [60] by means of their two resonant measurements agree with each other in order of magnitude only. However, the two types of measurements, both 90° bends and chamfered corners for a 50 Ω microstrip line on alumina substrate, indicate that the lengths of transmission line in the model of Figure 5.6.1.1 are negligible.

For various sound reasons, Stephenson and Easter conclude that the result obtained via the right angle bend in a symmetrical open-ended resonator is the better of the two. Error limits are also indicated. Their measurement, at 10 GHz on 0.5 mm Lucalox with a strip width corresponding to approximately 50 Ω characteristic impedance, is shown in Figure 5.6.4.1 together with their indicated error limits.

Also shown in Figure 5.6.4.1 are bend capacitances, calculated by this method, normalized with respect to strip width for various commonly used substrates. As expected the calculated values are lower than those obtained experimentally. Nevertheless, the close agreement between the results is an indication of the accuracy of the method. Typical computation time on an IBM S360/75 is 50 seconds for $\epsilon_r = 1.0$ and 110 seconds for $\epsilon_r = 9.9$.

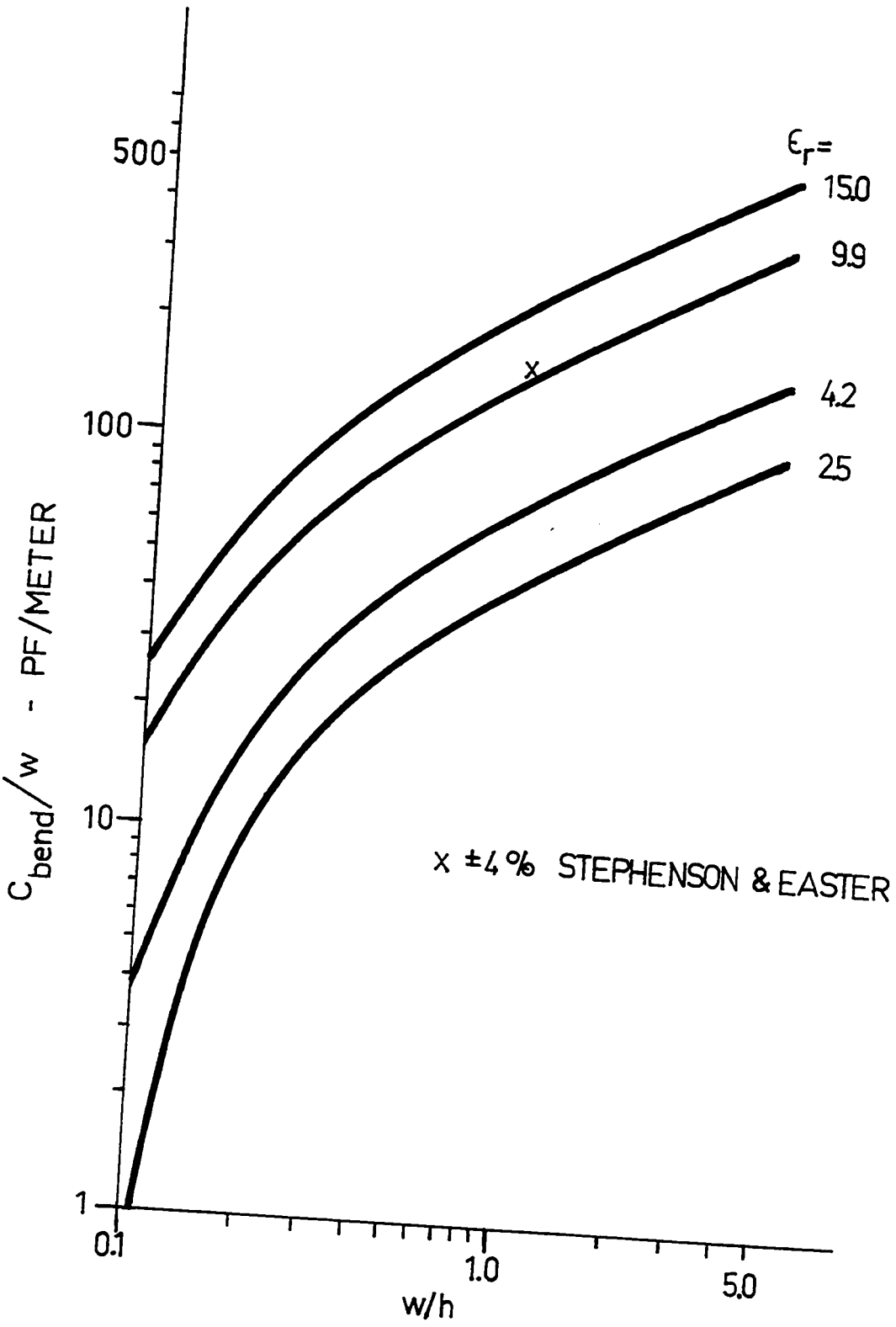

Figure 5.6.4.1 Microstrip bend capacitances normalized to strip width as a function of width-to-height ratio and substrate permittivity

5.7 Microstrip T Junctions

5.7.1 Circuit Model and Existing Work

In the case of microstrip T junctions, four sources of data were located. Stinehelfer [62] and Troughton [65] presented experimental results. They both performed transmission loss measurements on microstrip T structures to determine the electrical length of a stub ; comparing this with the physical length an "electrical defining plane" [65] for the stub can be determined. Stinehelfer presented results obtained using quarter wavelength long short circuited stubs, while Troughton used quarter and three-quarter wavelength long open circuited stubs. Both investigators indicated that a correction to the separation between two stubs is also required.

On the theoretical side Leighton and Milnes [37], as well as Wolff, Kompa and Mehran [72], used a parallel plate waveguide approximation, valid over a restricted range of parameters, with magnetic walls on the sides. Leighton and Milnes, then use a Babinet equivalent of this model to obtain a new model in which a T junction equivalent circuit has been determined by Marcuvitz [39]. Wolff, Kompa and Mehran, on the other hand, matched wave components, at the discontinuity planes and were able to obtain scattering coefficients for the T junction.

The simplest equivalent circuit for the T junction is an outcropping of the work of experimentalists. The microstrip T junction, together with this model, is shown in Figure 5.7.1.1. The lengths of transmission lines are used to correct for the electrical defining planes of the stub and main lines, while the shunt capacitor accounts for the charge surplus or deficiency at the junction.

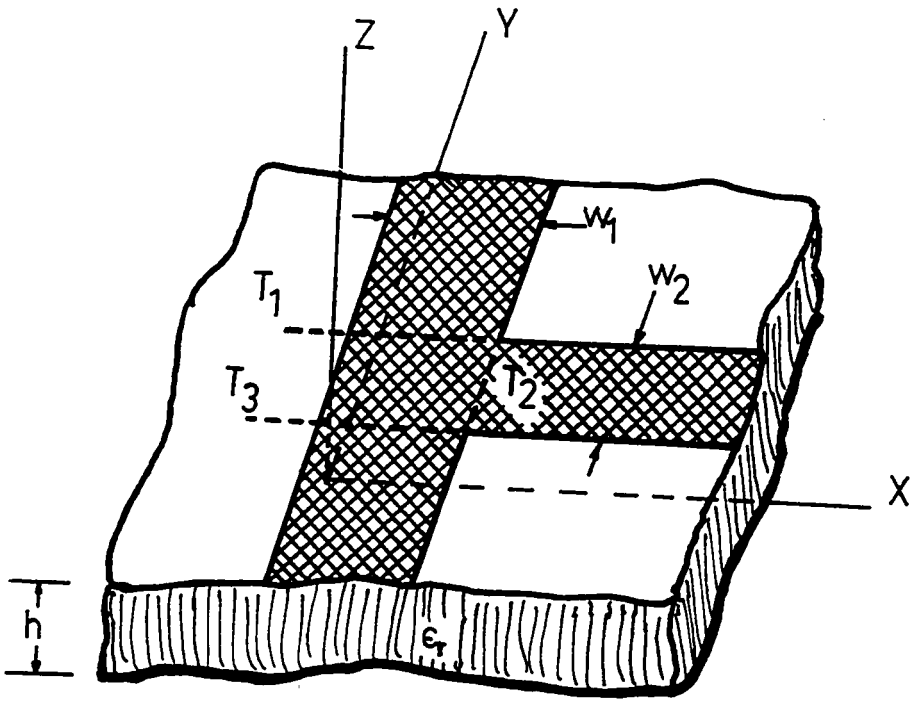

(a)

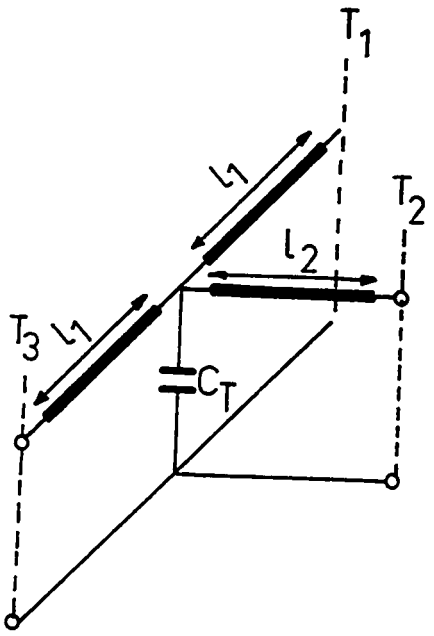

(b)

Figure 5.7.1.1 Microstrip T junction together with its equivalent circuit

5.7.2 Excess Charge Formulation

The potential residual, causing a charge surplus or deficiency at the T junction, is that due to three microstriplike charge distributions on the arms of the T structure, up to the terminal planes T_1, T_2 and T_3, shown in Figure 5.7.1.1 a. To evaluate this potential residual, take a microstriplike charge distribution $\frac{1}{2}\sigma_{\infty}^{(2)}(P'_x)$, of width-to-height ratio (w_2/h) parallel to the x-axis, with corresponding potential $\frac{1}{2}\varphi_{\infty}^{(2)}(P_x)$ given by Equation (5.2.1). Take another microstriplike charge distribution $\frac{1}{2}\sigma_{\infty}^{(2)}(P'_x)$, having a polarity reversal at $x = w_1$, with the corresponding potential $\frac{1}{2}\varphi_{w_1}^{(2)}(P_x)$, given by Equation (5.2.2). The superposition of these two distributions yields a microstriplike charge, of width-to-height ratio (w_2/h), on the interval $x \in [w_1, \infty]$ and a corresponding potential of $\frac{1}{2}[\varphi_{\infty}^{(2)}(P_x) + \varphi_{w_1}^{(2)}(P_x)]$. Similarly, in the y-direction, an infinite microstriplike charge distribution $\sigma_{\infty}^{(1)}(P'_y)$ together with charge distributions $\frac{1}{2}\sigma_{\infty}^{(1)}(P'_y)$ with polarity reversals at $y = 1.0$ and -1.0 are required. The respective potentials, by Equations (5.2.1) and (5.2.2), are $\varphi_{\infty}^{(1)}(P_y)$, $\frac{1}{2}\varphi_{1.0}^{(1)}(P_y)$ and $\frac{1}{2}\varphi_{-1.0}^{(1)}(P_y)$. The superposition of these three yields a microstriplike distribution on the two intervals $|y| > 1.0$, with corresponding potential $\{\varphi_{\infty}^{(1)}(P_y) + \frac{1}{2}[\varphi_{1.0}^{(1)}(P_y) - \varphi_{-1.0}^{(1)}(P_y)]\}$.

Now, superposing the two resulting distributions, microstriplike charges are generated on the arms of the T structure, up to the terminal planes T_1, T_2 and T_3. Therefore, the potential residual, in this case, is

$$\varphi_x^T(P) = \varphi_\infty - \{ \frac{1}{2}[\varphi_\infty^{(2)}(P_x) + \varphi_{w_1}^{(2)}(P_x)] + \varphi_\infty^{(1)}(P_y) + \frac{1}{2}[\varphi_{1.0}^{(1)}(P_y) - \varphi_{-1.0}^{(1)}(P_y)]\}$$

(5.7.2.1)

while the integral equation governing the excess charge is

$$\varphi_x^T(P) = \int \sigma_x^T(P')\, G^T(P;P')\, dP' \qquad (5.7.2.2)$$

In Equation (5.7.2.2) , both the potential residual and the excess charge fall to zero moving away from the discontinuity, so that integration over finite regions suffices.

5.7.3 Solution for Excess Charge and C_T

The changes, applicable to Section 5.3.3, in regard to a microstrip T junction are :

The function $f^T(n)$ required in the Green's function given by Equation (4.2.3) is

$$f^T(n) = [(2n)^2 + (\frac{x-x'}{h})^2 + (\frac{y-y'}{h})^2]^{-1/2} + [(2n)^2 + (\frac{x-x'}{h})^2 + (\frac{y+y'}{h})^2]^{-1/2}$$

(5.7.3.1)

and the T junction capacitance is given by

$$C_T = \int \sigma_x^T(P')\, dP' \qquad (5.7.3.2)$$

The potential residual on a dielectric substrate of $\epsilon_r = 9.9$, with main line $(w_1/h) = 1.0$ and stub line $(w_2/h) = 1.0$ is shown in Figure 5.7.3.1. In this case regions of negative residuals are much more pronounced than for the right angle bend. A typical discretization of the region is also shown in Figure 5.7.3.1.

5.7.4 Results and Comparison with Existing Data

Stinehelfer's [62] measurements, on quarter wavelength long short circuited stubs, indicate that the electrical length of the stubs is shorter than the physical length, while Troughton's measurements, on quarter and three-quarter wavelength open circuited stubs, indicate that the electrical length of the stub is longer than the physical length. Troughton also indicates that " if the stub is $\lambda/4$ and $3\lambda/4$, Δl (the correction to the physical length) is consistent, but differs from the value found from a half-wavelength stub." In addition to the specific problems in each measurement (such as accurate end effect correction in Troughton's case and difficulty of determining the exact frequency at which total transmission occurs in Stinehelfer's case and accurate phase velocity in both cases), part of the discrepancy is resolved considering the model given in Figure 5.7.1.1 b. If L denotes the physical length of the stub, in Troughton's case already corrected for the end effect, then Troughton measured the frequency at which $(l_2 + L) = \lambda/4$, while Stinehelfer measured the conditions under which $\cot\left[\frac{2\pi(l_2+L)}{\lambda}\right] = \omega C_T Z$. As a matter of fact, in principle, performing measurements on open and short-circuited

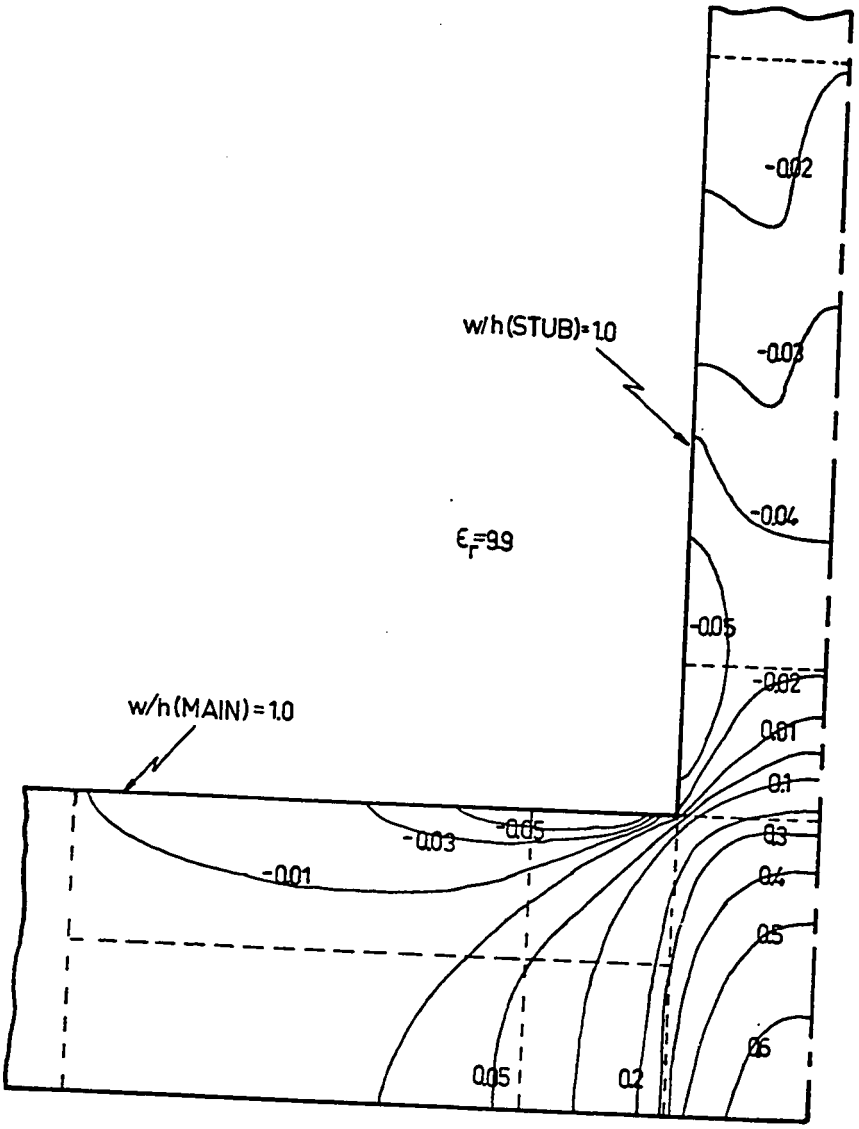

Figure 5.7.3.1 Potential residual near a microstrip T junction ($w_1/h = 1.0$, $w_2/h = 1.0$ and $\epsilon_r = 9.9$)

quarter wavelength stubs, it would be possible to determine both l_2 and C_T. This, however, may be frustrated by the difficulties already enumerated.

The theoretical results of Leighton and Milnes [37] on the approximate model of the microstrip line, are valid over a restricted range of parameters. Since both the model and the reference planes used here are totally different, no comparison was made with their data.

The approximate theoretical results of Wolff, Kompa and Mehran [72] are in terms of magnitudes of scattering coefficients of the T junction. The data given are for polyguide substrate, relative dielectric constant of $\epsilon_r = 2.33$, and they show very pronounced frequency dependence, especially above 5 GHz. This, at first sight, cannot be explained in terms of the capacitor C_T obtained here. A quick calculation, however, will indicate that at 5 GHz for $\epsilon_r = 2.33$ the wavelength is about 40 mm, while the typical dimensions required for the characteristic impedances utilized range from 4.5 mm to about 10 mm. For such structures the excess charges occupy a significant fraction of the wavelength, so that the electrostatic approximation is not valid. This argument is further substantiated by their note to the effect that the frequency dependence is small for alumina substrate ($\epsilon_r = 9.9$), where realistic impedances are obtained for smaller width-to-height ratios and the commonly available substrate thicknesses are 0.020 and 0.025 inches.

Figure 5.7.4.1 shows the capacitance C_T normalized to main line width plotted against stub line impedance. The behaviour of C_T, in that it varies from positive to negative, depending whether there is a charge deficiency or charge

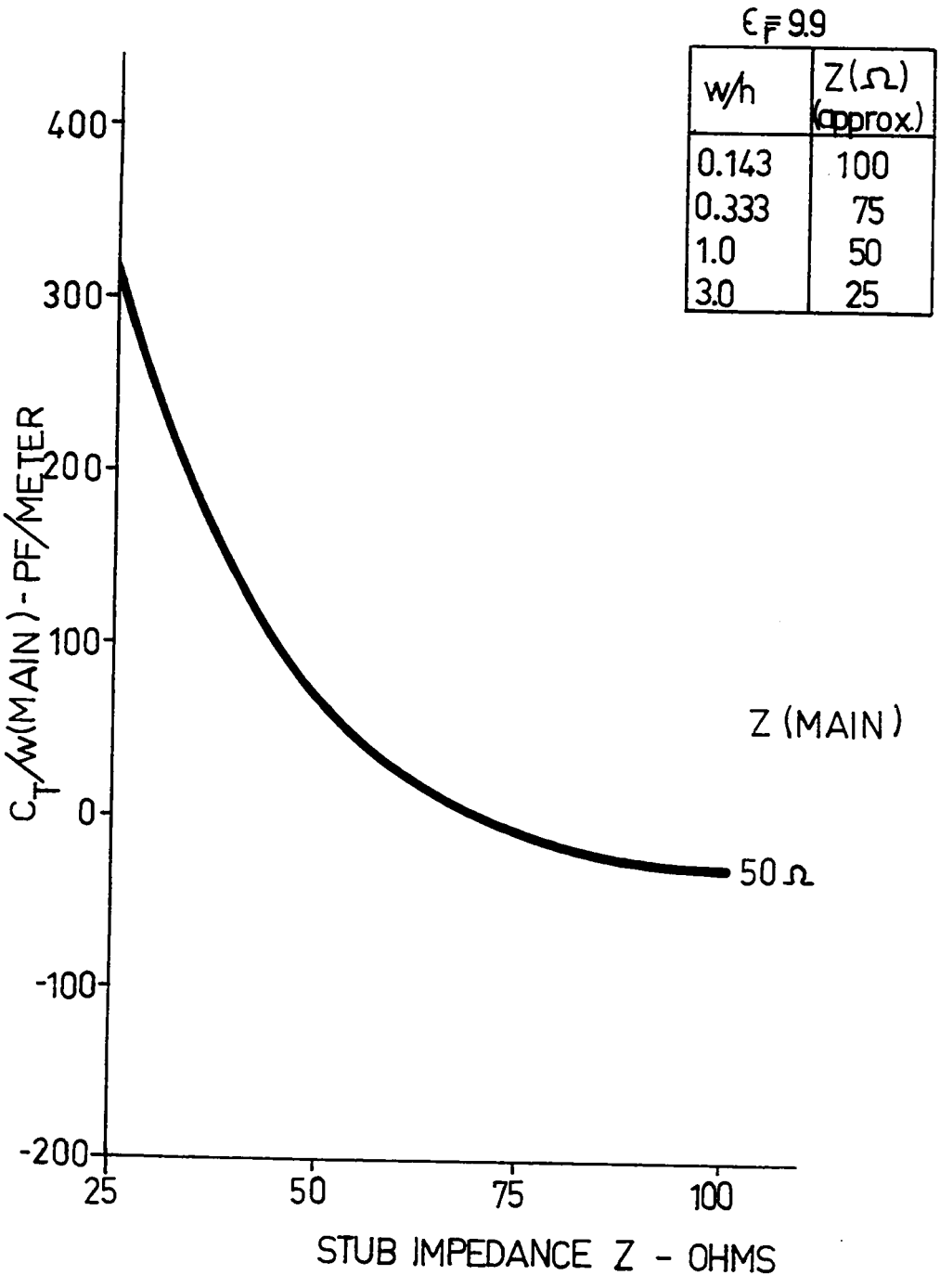

Figure 5.7.4.1 Microstrip T junction capacitances, normalized to main line width, as a function of stub line impedance

surplus, is similar to that observed experimentally by Matthaei, Young and Jones [40] in stripline. Due to the variation in the sign of the potential residual, generally speaking, the capacitances thus obtained are expected to have somewhat larger errors than, for example, in the open circuit case, where the potential residual is of uniform sign. The CPU time required, on an IBM S360/75 , to evaluate C_T on a dielectric substrate of $\epsilon_r = 9.9$ is 3.6 minutes.

5.8 Microstrip Crossings

5.8.1 Circuit Model and Existing Work

For microstrip crossings, it appears, that the only published source of data is that obtained experimentally by Stinehelfer [62] . He performed transmission loss measurements, as in the case of T junctions, on a pair of quarter wavelength short circuited stubs placed back to back, so as to determine the electrical lengths of the stubs. Similarly, a correction to the physical distance between a pair of crossings was noted.

The circuit model shown in Figure 5.8.1.1 b, for the crossing shown in Figure 5.8.1.1 a, was arrived at as a consequence of the results obtained in the above experiments. The lengths of transmission lines correct for the electrical lengths of the stubs and their electrical spacing from various other discontinuities. The shunt capacitor C_+ takes care of the charge surplus or deficiency near the crossing.

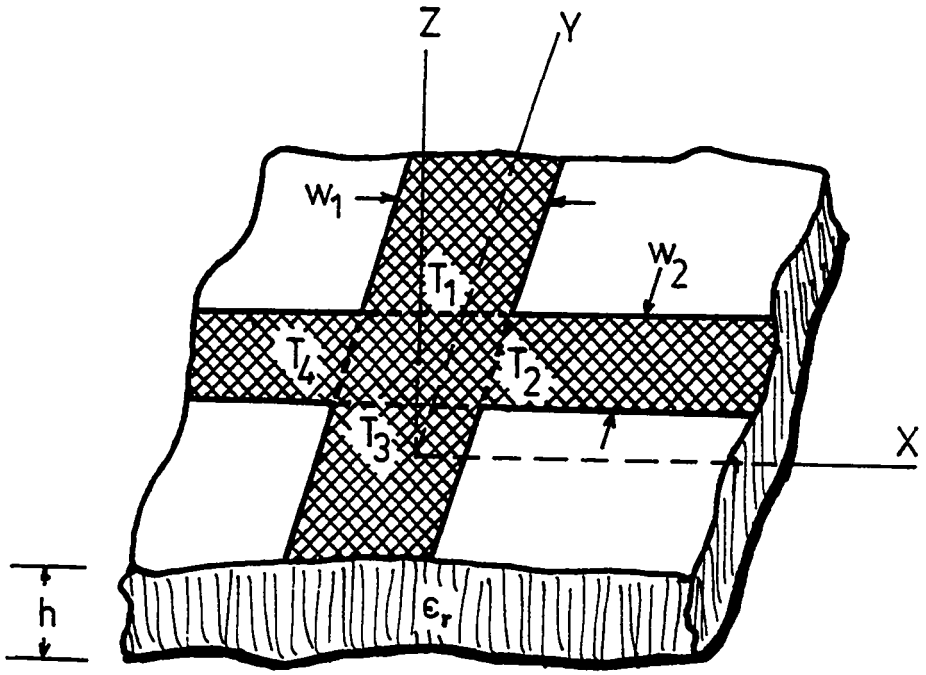

(a)

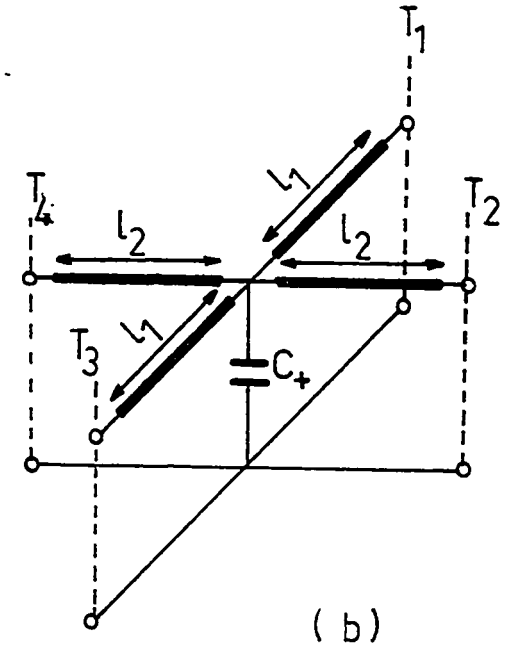

(b)

Figure 5.8.1.1 Microstrip crossing together with its equivalent circuit

5.8.2 Excess Charge Formulation

As in earlier discontinuities, the potential residual sought is obtained from the potential due to microstriplike charge distributions on the four arms of the crossing, up to the reference planes T_1, T_2, T_3 and T_4.

To obtain such a distribution, an infinite microstriplike charge $\sigma_{\infty}^{(2)}(P'_x)$ of width-to-height ratio (w_2/h) is required. Also needed are two charge distributions $\frac{1}{2}\sigma_{\infty}^{(2)}(P'_x)$ with polarity reversals at $x = w_1/2$ and $-w_1/2$. The corresponding potential distributions, given by Equations (5.2.1) and (5.2.2) are $\varphi_{\infty}^{(2)}(P_x)$, $\varphi_{w_1/2}^{(2)}(P_x)$ and $\varphi_{-w_1/2}^{(2)}(P_x)$, respectively. By superposition, microstriplike charge densities of (w_2/h) are obtained on the two intervals $|x| > w_1/2$ and the resulting potential is $\{\varphi_{\infty}^{(2)}(P_x) + \frac{1}{2}[\varphi_{w_1/2}^{(2)}(P_x) - \varphi_{-w_1/2}^{(2)}(P_x)]\}$. Similarly, the potential corresponding to microstriplike charge distribution $\sigma_{\infty}^{(1)}(P'_y)$ of width-to-height ratio (w_1/h) on the intervals $|y| > 1.0$ is $\{\varphi_{\infty}^{(1)}(P_y) + \frac{1}{2}[\varphi_{1.0}^{(1)}(P_y) - \varphi_{-1.0}^{(1)}(P_y)]\}$.

By superposition of these two resultant distributions, microstriplike charge densities of appropriate width-to-height ratios are generated, on the arms of the crossing, up to the four terminal planes. Therefore, the potential residual sought is

$$\varphi_x^+(P) = \varphi_{\infty} - \{\varphi_{\infty}^{(1)}(P_y) + \frac{1}{2}[\varphi_{1.0}^{(1)}(P_y) - \varphi_{-1.0}^{(1)}(P_y)] + \varphi_{\infty}^{(2)}(P_x) + \frac{1}{2}[\varphi_{w_1/2}^{(2)}(P_x) - \varphi_{-w_1/2}^{(2)}(P_x)]\} \tag{5.8.2.1}$$

and the integral equation governing the excess charge is

$$\varphi_x^+ (P) = \int \sigma_x^+ (P') \; G^+ (P ; P') \; d P' \qquad (5.8.2.2)$$

As in earlier instances, integration over a finite region is sufficient, since both potential residual and charge density distribution go to zero on moving away from the discontinuity.

5.8.3 Solution of Excess Charge and C_+

The comments in Section 5.3.3 are applicable to the crossing subject to the following modifications. Function $f^+ (n)$ required in the Green's function given by Equation (4.2.3) is

$$f^+ (n) = \left[(2n)^2 + \left(\frac{x-x'}{h}\right)^2 + \left(\frac{y-y'}{h}\right)^2 \right]^{-1/2} + \left[(2n)^2 + \left(\frac{x-x'}{h}\right)^2 + \left(\frac{y+y'}{h}\right)^2 \right]^{-1/2}$$

$$+ \left[(2n)^2 + \left(\frac{x+x'}{h}\right)^2 + \left(\frac{y-y'}{h}\right)^2 \right]^{-1/2} + \left[(2n)^2 + \left(\frac{x+x'}{h}\right)^2 + \left(\frac{y+y'}{h}\right)^2 \right]^{-1/2} \qquad (5.8.3.1)$$

while the crossing capacitance is given by

$$C_+ = \int \sigma_x^+ (P') \; d P' \qquad (5.8.3.2)$$

In Figure 5.8.3.1 the potential residual for a stub of $(w_1 / h) = 3$ and main line of $(w_2 / h) = 1$, on a substrate of relative dielectric constant $\epsilon_r = 9.9$, is shown. Also shown in the figure is a typical discretization of the region.

5.8.4 Results and Comparison with Existing Data

The results given by Stinehelfer [62], done on two short circuited quarter wavelength long stubs back to back, indicate that the electrical length of the stubs is shorter than the physical length. However, arguing as for the T junction, the model given in Figure 5.8.1.1 b would indicate that such a measurement in effect determines the frequency at which $2 \cot \left[\frac{2\pi (l_2 + L)}{\lambda}\right] = \omega C_+ Z$. L is the physical length of the stub. Another transmission loss measurement, on quarter wavelength long open circuited stubs, would give the frequency at which $(l_2 + L) = \lambda / 4$. From two such measurements, in principle, l_2 and C_+ may be determined. The difficulties with such an experimental approach were outlined in Section 5.7.4. Using the results given by Stinehelfer, no estimate of C_+ can be made. There appear to be no other data available for comparison.

In the computer program the computational details for the stub and main line are somewhat different. Therefore, when interchanging the width-to-height ratios of the stub and mainline left C_+ unchanged, this, in a small measure, provided a check on the program details.

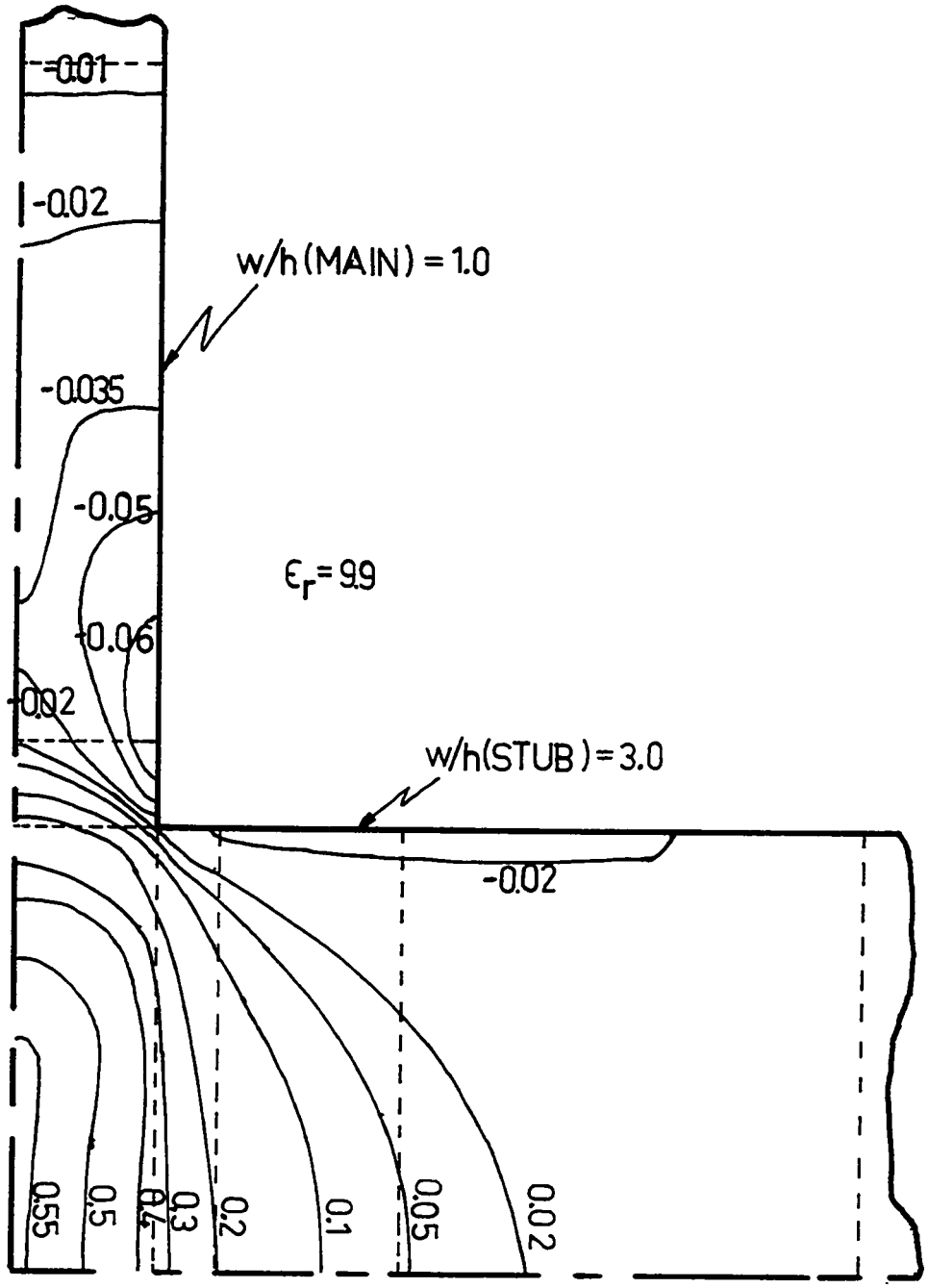

Figure 5.8.3.1 Potential residual near a microstrip crossing ($w_1/h = 3$, $w_2/h = 1$ and $\epsilon_r = 9.9$)

Figure 5.8.4.1 shows crossing capacitance values C_+ normalized to main line width for various main line impedances, plotted against stub line impedance. The stub characteristic impedances range from 25 Ω to 100 Ω. The substrate dielectric constant used is $\epsilon_r = 9.9$. As in the case of T junctions, due to the variation in the sign of the potential residual, generally speaking the errors in capacitance values can be expected to be larger than in those cases where the potential residual is of uniform sign. The computation time required on an IBM S360/75, for C_+ on a relative dielectric constant $\epsilon_r = 9.9$ is about 3.7 minutes.

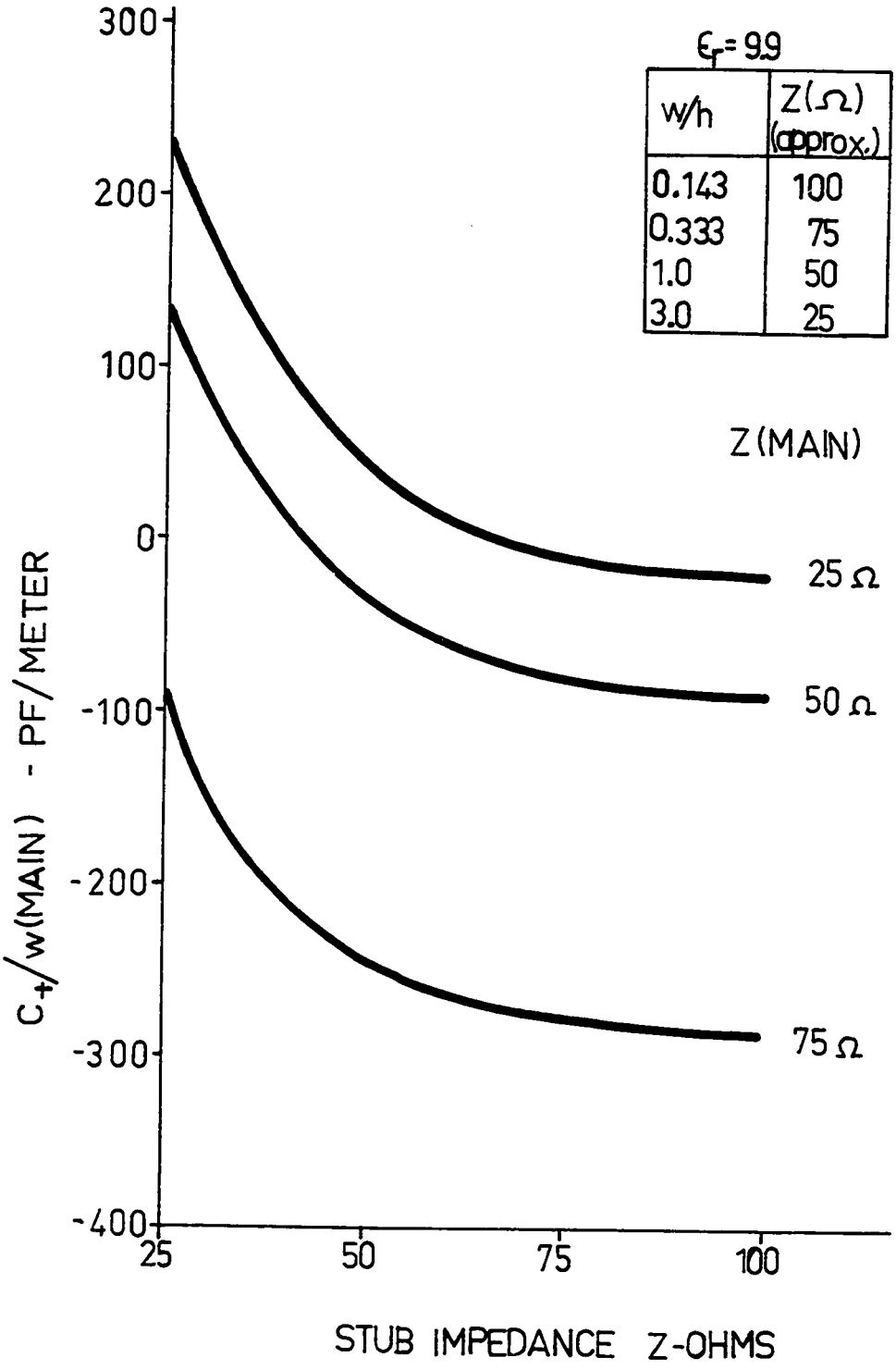

Figure 5.8.4.1 Microstrip crossing capacitances, normalized to main line width, as a function of stub line impedance

CHAPTER VI

IMPORTANCE OF DISCONTINUITY CAPACITANCES IN THE DESIGN OF AN OPEN CIRCUITED MULTISTUB MICROSTRIP FILTER

6.1 Introduction

In Section 5.4.4 it was demonstrated that calculated capacitive effects at a gap in a microstrip, were able to predict the measured transmission loss for various gaps. In this chapter, the importance of discontinuity capacitances in the design of distributed element microwave components is shown ; in particular, a five-section ten-stub microstrip filter is analyzed.

The filter under consideration, was actually built by Atwood and Stinehelfer [6] . They, however, not only covered the filter with a ground plane, but also included "mode supression walls between stubs to prevent higher order mode radiation between sections of the filter" [6] . The various filter dimensions used in their design were taken from Stinehelfer's finite difference program for the microstrip in a box [61] . Therefore it should be stressed, that the intent is not necessarily to account for the discrepancy between their ideal and measured characteristics, but rather to simply demonstrate that the inclusion of discontinuity capacitances result in changes of sufficient importance to alter the design characteristics of a microwave device.

6.2 A Two-port Network Analysis Program (NTSM)

In order to be able to analyze the behaviour of passive microwave circuits, a special purpose network analysis program, NTSM, was written. The program is based on the properties of modified transfer coefficient matrices (ABCD) for cascaded two-ports. A more general program of this nature was written earlier [18], however at that time only lossless transmission lines were considered. Since losses in microstrip are of some consequence, the present program can also account for these.

The transfer coefficients A, B, C and D provide the relationship

$$\begin{bmatrix} V_1 \\ I_1 \end{bmatrix} = \begin{bmatrix} A & B \\ C & D \end{bmatrix} \begin{bmatrix} V_2 \\ I_2 \end{bmatrix} \qquad (6.2.1)$$

between the input and output variables of a two-port network, shown in Figure 6.2.1. The overall transfer coefficient matrix for N cascaded two-ports, shown in Figure 6.2.2, is simply the matrix product of the individual transfer matrices, taken in order in which they occur,

$$\begin{bmatrix} V_1 \\ I_1 \end{bmatrix} = \left\{ \prod_{i=1}^{N} \begin{bmatrix} A_i & B_i \\ C_i & D_i \end{bmatrix} \right\} \begin{bmatrix} V_N \\ I_N \end{bmatrix} \qquad (6.2.2)$$

Transfer matrices were evaluated for a number of elemental building blocks, necessary for the present analysis, such as : series and shunt capacitors, a

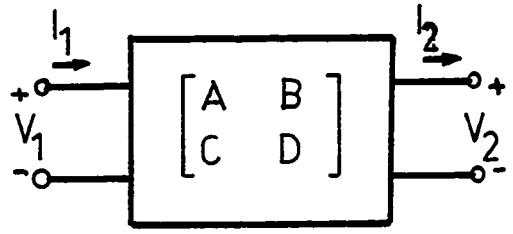

Figure 6.2.1 General two-port network

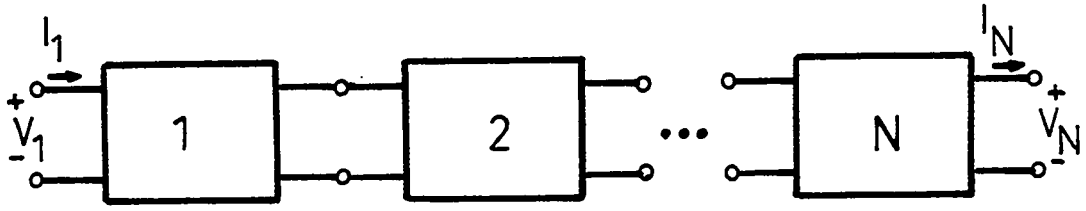

Figure 6.2.2 N cascaded two-ports

length of transmission line, open and short circuited shunt stubs and shunt stubs terminated by a capacitor. For a general purpose program of this nature, of course, other elemental two ports have to be included.

The network properties of particular interest to microwave engineers, such as transmission loss,input impedance, reflection coefficient and voltage standing wave ratio, are easily evaluated in terms of the transfer coefficients of the overall network.

6.3 Analysis of the Five-Section Ten-Stub Filter

Using results from filter theory, Atwood and Stinehelfer [6] obtained the passband filter design shown in Figure 6.3.1. This design was implemented in microstrip on a substrate of relative dielectric constant $\epsilon_r = 8.875$ and thickness of 0.020 inches. The center frequency of the filter was ideally at 9.5 GHz while its bandwidth was 1 GHz.

The first step in such a design is the determination of the relative phase velocities of the transmission lines of various characteristic impedances. The electrostatic phase velocities must be corrected for dispersion so that the physical dimensions, given in multiples of $\lambda/4$ at center frequency, can be specified as accurately as possible. Typical corrections for dispersion were measured by Troughton [67] for 25 Ω and 50 Ω lines on 0.025 inch thick alumina. He indicated 2.8 % and 2.2 % dispersion in phase velocity at 10 GHz for the 25 Ω and 50 Ω lines, respectively.

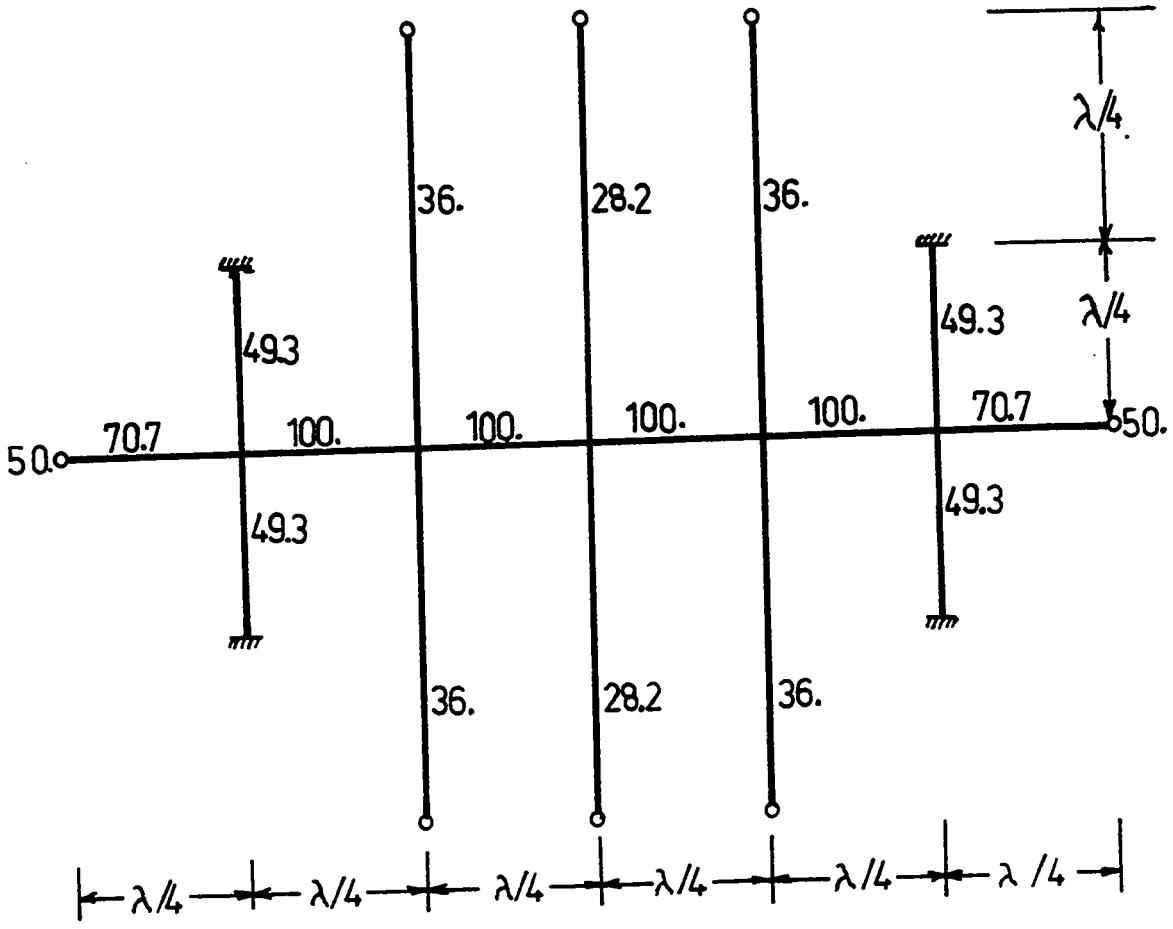

Figure 6.3.1 Atwood and Stinehelfer's [6] passband filter design

This was extrapolated to the 70 Ω and 100 Ω lines as 1.6 % and 1.0 % approximately. These extrapolations may be in error by as much as 0.5 % , however this is really irrelevant, since the results of this step are the starting point from which the discontinuity capacitances are added. Thus the effects of the discontinuities can be clearly seen by themselves.

Three types of capacitive discontinuity effects will be included in turn :

(i) crossing effects at the stubs,

(ii) end effects at open circuits,

(iii) step effect at the 50 Ω to 70.7 Ω line transition.

The discontinuity capacitance values, as calculated by the method described in Chapter V, relevant to this problem are :

C_{oc}	(28.2 Ω)	=	0.060 pF
C_{oc}	(36.0 Ω)	=	0.044 pF
C_{step}	(50 Ω and 70.7 Ω)	=	0.0015 pF
C_{+}	(100 Ω and 70.7 Ω and 49.3 Ω)	=	-0.032 * pF
C_{+}	(100 Ω and 28.2 Ω)	=	-0.030 pF
C_{+}	(100 Ω and 36.0 Ω)	=	-0.35 pF

---

* This value was obtained by linear interpolation between C_{+} (100 Ω and 49.3 Ω) and C_{+} (70.7 Ω and 49.3 Ω) .

Figure 6.3.2 a and b show the circuit model and the transmission loss for the ideal filter. Figures 6.3.3 - 6.3.5 a and b show how the successive inclusion of the various capacitive discontinuities affect filter response. And, finally, in Figure 6.3.6 the effects of line losses are indicated.

6.4 Results

In Figure 6.3.2 a and b the ideal filter model and response are indicated. As designed, the center frequency of the passband region is 9.5 GHz while the bandwidth is 1 GHz.

Figure 6.3.3 a shows the ideal circuit model modified to account for the capacitance effect of crossing discontinuities. The resulting transmission loss, as given in Figure 6.3.3 b, shows minimal changes in the passband region, however just outside passband at 9.8 GHz the transmission loss changes from 3.1 db to 1.4 db, while at 8.6 GHz it changes from 9.2 db to 12.9 db.

The circuit model is further modified to correct the open circuit end effect in Figure 6.3.4 a. In this case the transmission loss, shown in Figure 6.3.4 b, shows considerable change. First of all, the passband region now extends from 8.65 GHz to 9.75 GHz. That corresponds to a bandwidth of 1.1 GHz and a center frequency of 9.2 GHz. Secondly, the passband region shows a deterioration of about 0.2 db.

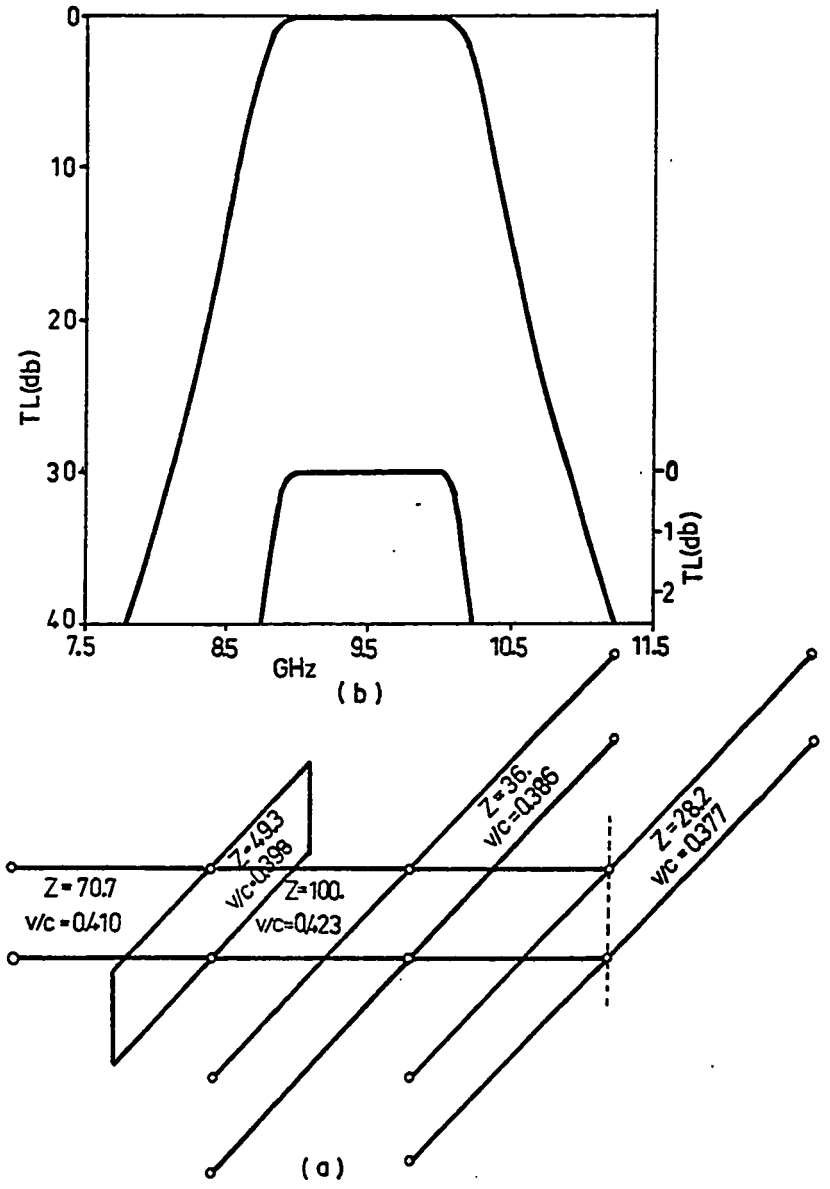

Figure 6.3.2 Circuit model and transmission loss for ideal filter design

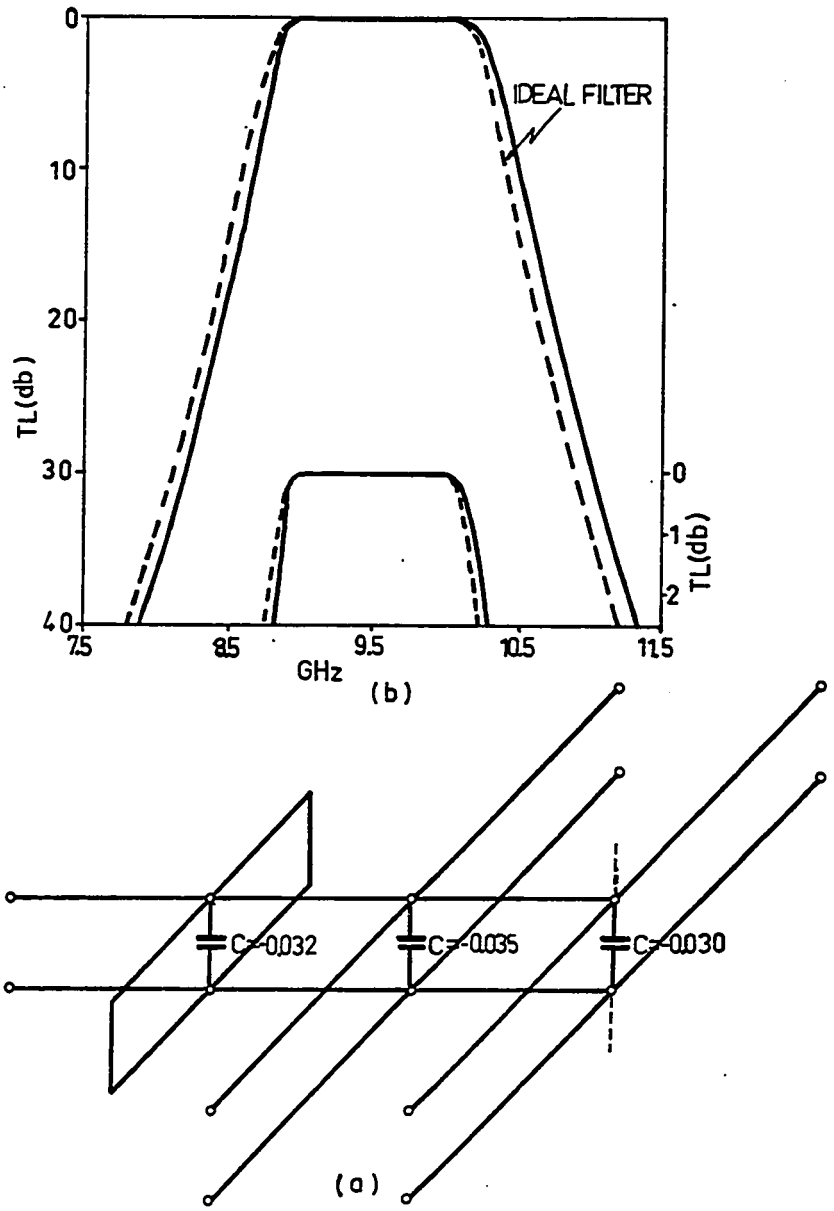

Figure 6.3.3 Filter model, modified for the effect of crossings, and transmission loss

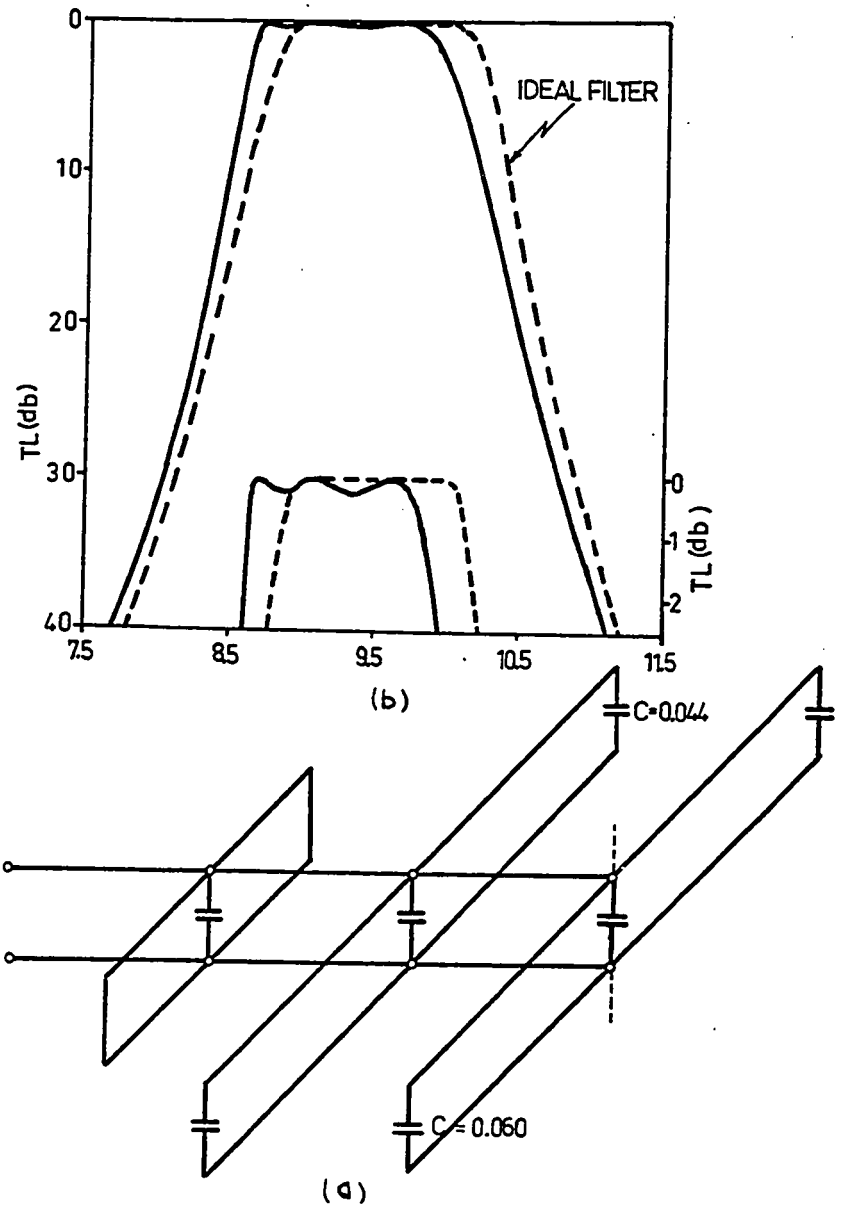

Figure 6.3.4 Filter model, modified for the effect of crossings and open circuits, and transmission loss

In Figure 6.3.5 a two step capacitances are included. These capacitances are so small that no further noticeable change in filter response, as shown in Figure 6.3.5 b , is observed.

In addition to all the capacitive discontinuities, the effect of lossy lines [77] is also included. These losses contribute, typically, 0.3 db to further deteriorate the characteristics in the passband region, as shown in Figure 6.3.6.

Atwood and Stinehelfer's [6] measured filter response shows the same type of qualitative behaviour ; a bandwidth of 1.275 GHz with center frequency of 9.25 GHz as opposed to a bandwidth of 1.1 GHz and center frequency of 9.2 GHz predicted with the discontinuities. The measured passband was, typically, 1 db worse than the predicted one. Since the physical filter included a number of further effects, such as those described in the introduction to this chapter, which are not taken account of in the analysis and are not known in detail, no precise quantitative comparisons can be made. In this light, the agreement is quite good, especially when one remembers that this is an approximate mathematical treatment of the idealized version of a physical filter.

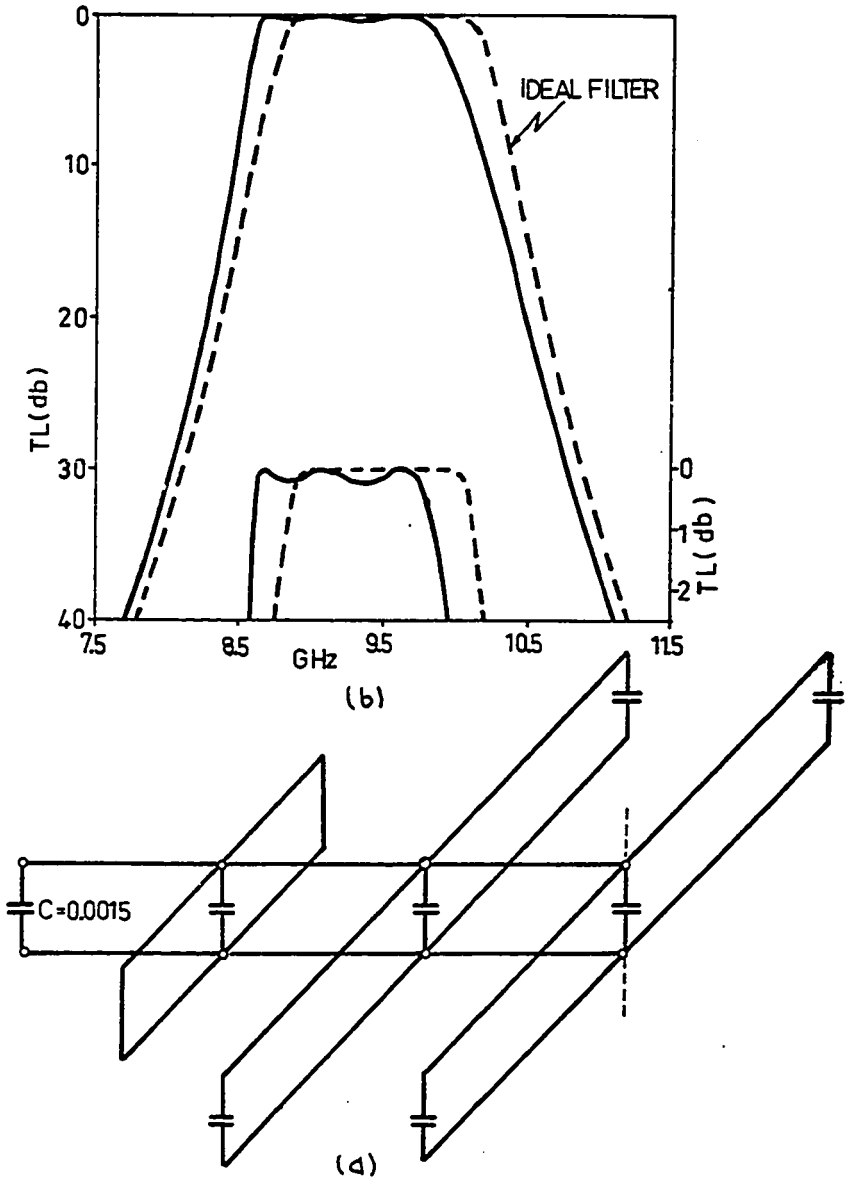

Figure 6.3.5 Filter model, modified for the effect of crossings, open circuits and steps, and transmission loss

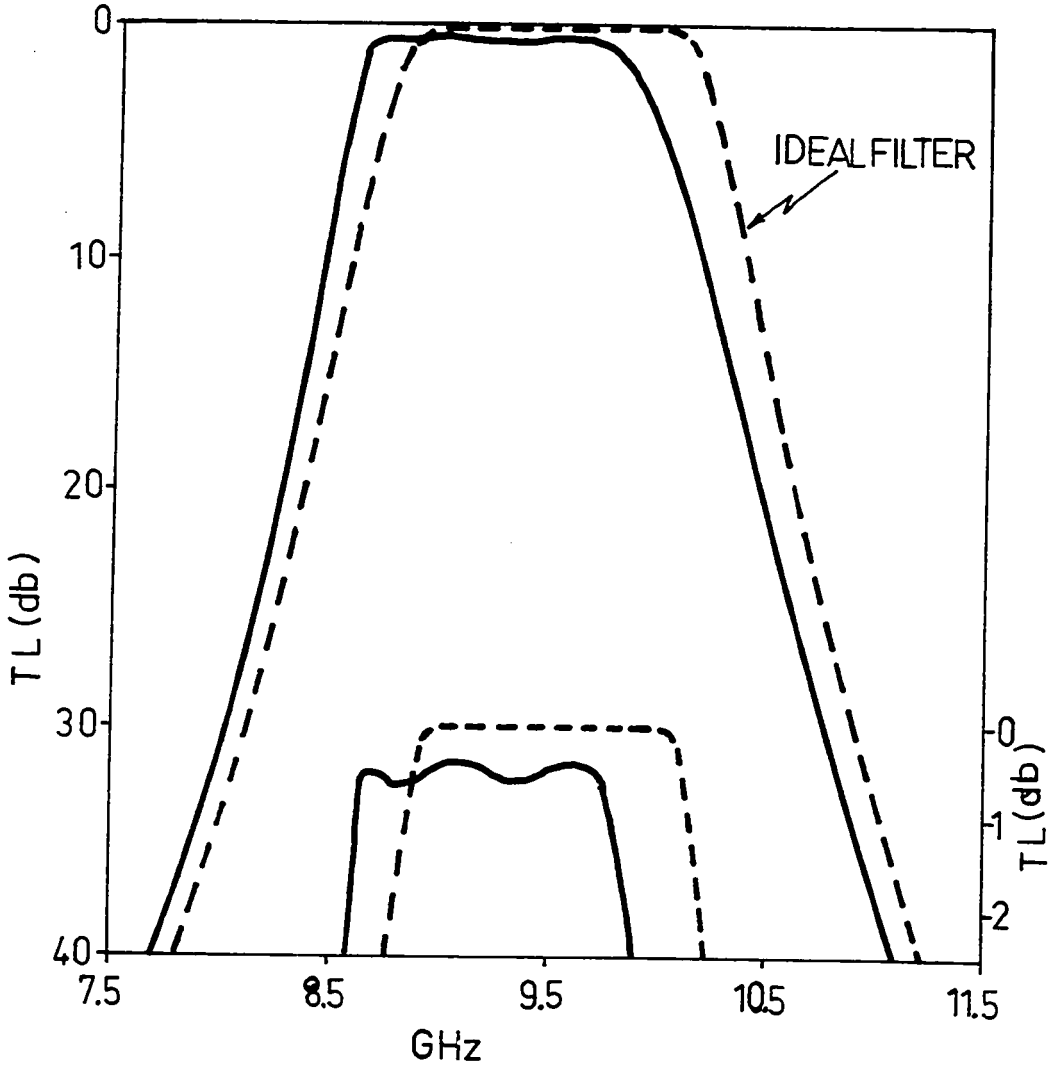

Figure 6.3.6 Filter transmission loss for the model of Figure 6.3.5 a, including the effect of lossy lines

CHAPTER VII

CONCLUSIONS

The use of trial functions which preserve the singularity in the charge distribution at the edge of the microstrip transmission line, shows that accurate determination of charge density distribution and transmission line parameters is possible with matrices as small as 2×2 .

Point matching solutions to the capacitance of rectangular plates on metal backed dielectric substrates have been obtained over the past year. However the transformations described in Section 4.2, permitted the use of fewer high-order subregions in the solution of the charge distribution on rectangular plates. This approach is readily usable to obtain the parasitic capacitance in a multiconductor system of Manhattan type (rectangular) geometry. The results presented are of interest in the design of lumped element integrated circuitry.

The methodology presented for the formulation of the excess charge distribution near various microstrip discontinuities, is readily extended to cases not discussed. This formulation is not only highly elegant but, what is more important, it is considerably more economical than the theoretical and experimental methods used by other investigators to date. The computation times required are sufficiently small to permit the calculation of extensive results of interest to the designer of distributed microwave integrated systems. In addition, an important source of error, encountered by feilow investigators in the theoretical study of microstrip open circuits, i.e. the subtraction of nearly equal large numbers, has been completely eliminated.

The experimental methods of characterizing various discontinuities are too time consuming and expensive to be used to obtain extensive data. And, the experimental results cannot guarantee accuracy to better than a few percent, which can readily be obtained by the method presented herein.

For open circuits, gaps, steps and even right angle bends on alumina substrates, the capacitive component in the discontinuity models, appears to be dominant up to frequencies as high as 20 GHz. Therefore, the capacitive models given are expected and do account greatly for the experimentally observed phenomena in these cases. For T junctions and crossings, however, the experimental evidence indicates that discontinuity series inductances are no longer negligible.

The simulation of the multistub filter in Chapter VI, clearly demonstrates the importance of these discontinuity capacitances. The inclusion of the various discontinuity capacitances affected the filter response by an amount comparable to the effect of dispersion at 10 GHz in the microstrip line. But while dispersion appears to be negligible below 5 GHz, the discontinuity capacitances are not. This was amply demonstrated for the gap in microstrip.

Although microstrip has made considerable inroads in the microwave industry due to the numerous advantages discussed in Chapter I, the high cost of engineering involved precludes its use when small quantities are involved. This problem could be overcome by completely computerizing the design of microwave integrated circuits and thus eliminating cut and try methods common today.

To this end, microstrip discontinuities have to be adequately modeled. Further study needs to be conducted in the area of discontinuity inductances and radiation losses and discontinuities, to fully characterize them. The frequency dependence of these models also needs to be studied, especially if they are to be used above 20 GHz. In the case of discontinuity capacitances, little or no dispersion is expected so long as the excess charges extend over a region smaller than one tenth of the microstrip wavelength. This is borne out by the available experimental evidence.

It is hoped that the methodology and results presented herein, bring closer the day of fully computerized microwave integrated circuit design.

APPENDIX I

A highly efficient program was written, by P. Silvester, to obtain Gaussian quadrature formulae, for almost arbitrary weight functions, of the form

$$\int_a^b w(x)\, f(x)\, dx = \sum_{i=1}^{N} W_i\, f(x_i) \qquad (I.1)$$

In this program the user must supply a subroutine capable of returning the inner products

$$\langle x^i , x^j \rangle = \int_a^b w(x)\, x^{i+j}\, dx \qquad (I.2)$$

Using these inner products and some recurrence relations [14], the polynomials orthogonal with respect to $w(x)$ can be generated. The roots of the N-th order orthogonal polynomial, correspond to the quadrature points of the N-point Gaussian quadrature formulae. To obtain rapid convergence, by Newton's method, to the roots of the N-th order orthogonal polynomial, advantage is taken of the fact that one, and only one, of the N-roots lie in each of the N-intervals determined by the two end points and the roots of the $(N-1)$-th order orthogonal polynomial. The one important requirement in the founding theorem of this approach, is that $w(x)$ must be single signed on the interval $[a, b]$. As soon as the quadrature points are known, the corresponding weights are readily calculated.

The user can specify the degree of the quadrature desired, together with tolerance limits on the quadrature points and weights. If the tolerance checks on the quadrature points and / or the weights are violated prior to reaching the desired degree of quadrature, the highest degree of quadrature, within the specified tolerance limit, is returned.

APPENDIX II

Consider a line of unit charge density, coincident with the x'-axis with a polarity reversal at the origin, as shown in Figure II.1. The primed and unprimed quantities refer to charge and potential coordinates respectively.

Let r denote the polar distance from the line of charge. The potential at some point $P(x, y, z)$ due to such a charge distribution is

$$V = \frac{1}{4\pi\epsilon} \int \frac{\pm\, dx'}{\sqrt{r^2 + (x'-x)^2}} = \frac{1}{4\pi\epsilon} \left[\int_0^\infty \frac{dx'}{\sqrt{r^2 + (x'-x)^2}} - \int_0^\infty \frac{dx'}{\sqrt{r^2 + (x'+x)^2}} \right] \tag{II.1}$$

These integrals are tabulated [17], so that

$$V = \frac{1}{4\pi\epsilon} \lim_{X \to \infty} \left\{ \left[\log \left(2\sqrt{x'^2 - 2x'x + x^2 + r^2} + 2x' - 2x \right] \right]_{x'=0}^{X} \right.$$

$$\left. - \left[\log \left(2\sqrt{x'^2 + 2x'x + x^2 + r^2} + 2x' + 2x \right] \right]_{x'=0}^{X} \right\}$$

$$= \frac{1}{4\pi\epsilon} \lim_{X \to \infty} \left\{ \log \frac{\sqrt{X^2 - 2Xx + x^2 + r^2} + X - x}{\sqrt{X^2 + 2Xx + x^2 + r^2} + X + x} \right\}$$

$$+ \frac{1}{4\pi\epsilon} \log \frac{\sqrt{x^2 + r^2} + x}{\sqrt{x^2 + r^2} - x} \tag{II.2}$$

But the first term of this sum vanishes, so that

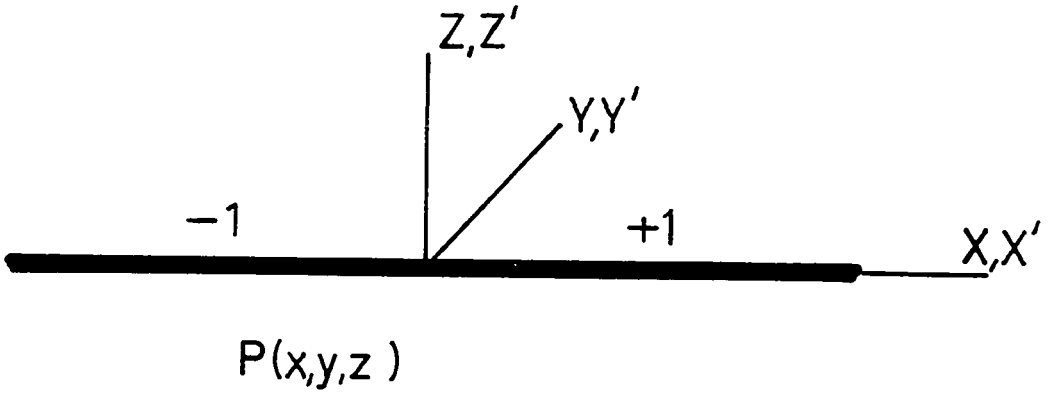

Figure II.1 Line charge with polarity reversal

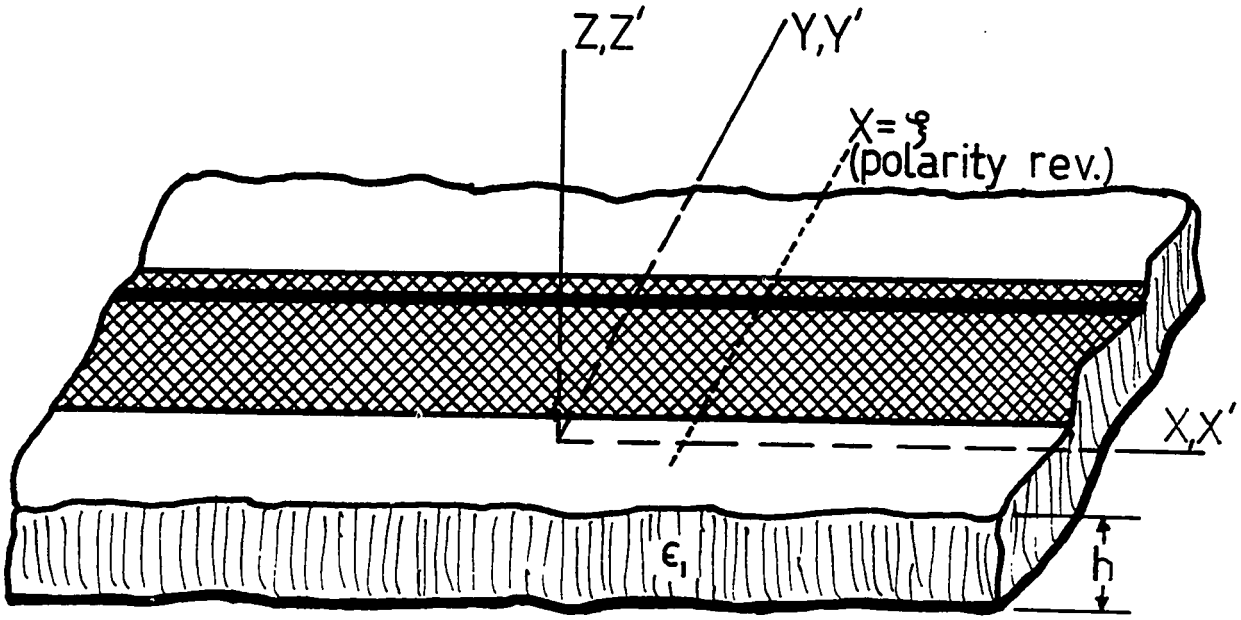

Figure II.2 Coordinate system used in the analysis of a microstriplike charge distribution with a polarity reversal

$$V = \frac{1}{4\pi\epsilon} \log \frac{\sqrt{x^2 + r^2} + x}{\sqrt{x^2 + r^2} - x} \tag{II.3}$$

Of course, if the polarity reversal occurs at $x = \xi$ instead of $x = 0$, then by a simple coordinate translation

$$V = \frac{1}{4\pi\epsilon} \log \left\{ \frac{\sqrt{(x-\xi)^2 + r^2} + (x-\xi)}{\sqrt{(x-\xi)^2 + r^2} - (x-\xi)} \right\} \tag{II.4}$$

Now, consider the microstrip line shown in Figure II.2, and in particular, the line of charge at (x', y', h). Suppose that the microstrip has a charge distribution of $\sigma_\infty(y')$, and let there be a polarity reversal at $x = \xi$. The potential due to such a line of charge in homogeneous medium, by Equation (II.4), is

$$V(x, y, z) = \frac{\sigma_\infty(y')}{4\pi\epsilon} \log \left\{ \frac{\sqrt{(x-\xi)^2 + (y-y')^2 + (z-z')^2} + (x-\xi)}{\sqrt{(x-\xi)^2 + (y-y')^2 + (z-z')^2} - (x-\xi)} \right\} \tag{II.5}$$

As in the case of the infinite microstrip [53], an infinite series of partial images can be generated for this line to account for ground plane and the air dielectric interface. Thus, the potential in the plane $z = h$, due to this line of charge on top of a metal backed dielectric substrate of thickness h, is

$$V(x, y) = \frac{\sigma_\infty(y')}{4\pi\epsilon_0} (1 - K) \left\{ f(0) - (1 - K) \sum_{n=1}^{\infty} K^{n-1} f(n) \right\} \tag{II.6}$$

where $K = (\epsilon_0 - \epsilon_1) / (\epsilon_0 + \epsilon_1)$ and

$$f(n) = \log \frac{\sqrt{(x-\xi)^2 + (y-y')^2 + 4n^2h^2} + (x-\xi)}{\sqrt{(x-\xi)^2 + (y-y')^2 + 4n^2h^2} - (x-\xi)} \tag{11.7}$$

Therefore, the potential in the $z = h$ plane due to a microstriplike charge distribution with a polarity reversal at $x = \xi$ is, by superposition,

$$V(x, y) = \int_{-1}^{1} \sigma_\infty(y')\, G_\xi(x, y; y')\, dy' \tag{11.8}$$

where

$$G_\xi(x, y; y') = \frac{1-K}{4\pi\epsilon_0} \{ f(0) - (1-K) \sum_{n=1}^{\infty} K^{n-1} f(n) \} \tag{11.9}$$

and $f(n)$ is given by Equation (11.7).

REFERENCES

[1] F.S. Acton, Numerical Methods that Work, New York : Harper and Row, 1970.

[2] A. T. Adams and J. R. Mautz, "Computer solution of electrostatic problems by matrix inversion," Proc. 1969, National Electronics Conference, pp. 198-201.

[3] H.M. Altschuler and A.A. Oliner, "Discontinuities in the center conductor of symmetric strip transmission lines," I R E Trans. PGMTT - 8, May 1960, pp. 328-339.

[4] S. Arnold, "Dispersive effects in microstrip on alumina substrates," Electronics Letters, Vol. 5, No. 26, 27th December 1969, pp. 673-674.

[5] F. Assadourian and E. Rimai, "Simplified theory of microstrip transmission systems," Proc. I R E, Vol. 40, December 1952, pp. 1651-1657.

[6] W. Atwood and H.E. Stinehelfer, Sr., "A multistub filter for microstripline," IEEE Trans. on MTT (Corresp.), Vol. MTT - 16, July 1968, pp.477-480.

[7] P. Benedek and P. Silvester, " Equivalent capacitances for microstrip gaps and steps," IEEE Trans. on MTT, to appear.

[8] P. Benedek and P. Silvester, " Capacitance of rectangular plates on metal-backed dielectric substrates," IEEE Trans. on MTT, Vol. MTT - 20, August 1972.

[9] C.W. Bostian and P.H. Wiley, " Concerning the moment method of solution for the charge distribution on a square plate," Proc. IEEE (Letters), Vol. 59, No. 11, November 1971, p. 1639.

[10] T.G. Bryant and J.A. Weiss, "Parameters of microstrip transmission lines and of coupled pairs of microstrip lines," IEEE Trans. on MTT, Vol. MTT - 16, No. 12, December 1968, pp. 1021-1027.

[11] M. Caulton, J.J. Hughes and H. Sobol, "Measurements on the properties of microstrip transmission lines for microwave integrated circuits," R C A Review, Vol. 27, 1966, pp. 377-391.

[12] W.J. Chudobiak, O.P. Jain and V. Makios, " Dispersion in microstrip," IEEE Trans. on MTT (Corresp.), Vol. MTT - 19, September 1971, pp. 783-784.

[13] P. Daly, " Hybrid mode analysis of microstrip by finite element methods," IEEE Trans. on MTT, Vol. MTT - 19, No. 1, January 1971, pp. 19-25.

[14] P.J. Davis and P. Rabinowitz, Numerical Integration, Waltham : Blaisdell, 1967.

[15] E.J. Denlinger, "Radiation from microstrip resonators," IEEE Trans. on MTT (Corresp.), Vol. MTT - 17, April 1969, pp. 235-236.

[16] E. J. Denlinger, "A frequency dependent solution for microstrip transmission lines," IEEE Trans. on MTT, Vol. MTT - 19, No. 1, January 1971, pp. 30-39.

[17] H.B. Dwight, Tables of Integrals and Other Mathematical Data, New York : Macmillan, 1947.

[18] M.A. Earle and P. Benedek, " SIMUL 5 - An extended simulation program for two-port networks," Engineering Report No. 239, R C A Victor, Montreal, July 1968.

[19] B. Easter and R.J. Roberts, "Radiation from half wavelength open circuit microstrip resonators," Electronics Letters, Vol. 6, pp. 573-574.

[20] A. Farrar and A.T. Adams, "Computation of lumped microstrip capacities by matrix methods - Rectangular sections and end effect," IEEE Trans. on MTT (Corresp.), Vol. MTT - 19, May 1971, pp. 495-496.

[21] A. Farrar and A.T. Adams, "Correction to "Computation of lumped microstrip capacities by matrix methods - Rectangular sections and end effect"," IEEE Trans. on MTT (Corresp.), Vol. MTT - 20, April 1972, No. 4, p. 294.

[22] J.A. Fuller and D.C. Chang, "On the numerical calculation of capacitance in the presence of edge boundaries," Proc. IEEE (Letters), March 1970, pp. 490-491.

[23] A. Gopinath, R. Horton and B. Easter, "Microstrip loss calculations," Electronics Letters, Vol. 6, January 1970, pp. 40-41.

[24] N.B. Haaser and J.A. Sullivan, Real Analysis, New York : Van Nostrand Reinhold Co., 1971.

[25] R.F. Harrington, Field Computation by Moment Methods, New York : Macmillan, 1968.

[26] R.F. Harrington, J.R. Mautz, C.W. Bostian and P.H. Wiley, "Comments on "Concerning the moment solution for the charge distribution on a square conducting plate"," Proc. IEEE (Letters), April 1972, pp. 448-449.

[27] J.S. Hornsby and A. Gopinath, "Numerical analysis of a dielectric loaded waveguide with a microstrip line - Finite difference methods," IEEE Trans. on MTT, Vol. MTT - 17, September 1969, pp. 684-690.

[28] J.S. Hornsby and A. Gopinath, "Fourier analysis of a dielectric loaded waveguide with a microstrip line," Electronics Letters, Vol. 5, 1969, pp. 265-267.

[29] H. Howe, Jr., "Stripline is alive and well," Microwave Journal, Vol. 14-7, July 1971, pp. 25-28.

[30] Yu. Ya. Iossel, E.S. Kochanov and M.G. Strunskiy, The Calculation of Electrical Capacitance, Foreign Technology Division Wright Patterson A F B, Ohio, AD 727 198. (Translated from the Russian, Raschet Electricheskoy Yemkosti, Leningradskoye Otdeleniye "Energiya", Leningrad 1969.)

[31] D.S. James and S.H. Tse, "Microstrip end effects," Electronics Letters, 22nd January 1972, pp. 46-47.

[32] H. Kaden, "Leitungs - und Kopplungskonstanten bei Streifenleitungen," Archiv der Electrischen Übertragung (A E Ü), Band 21, Heft 3, März 1967, pp. 109-112.

[33] H.R. Kaupp, "Characteristics of microstrip transmission lines," IEEE Trans. on E C, Vol. EC - 16, April 1967, pp. 185-193.

[34] M.K. Krage and G.I. Haddad, "Characteristics of coupled microstrip transmission lines - I : Coupled mode formulation of inhomogeneous lines," IEEE Trans. on MTT, Vol. MTT - 18, April 1970, pp. 217-222.

[35] M.K. Krage and G.I. Haddad, "Characteristics of coupled microstrip transmission lines - II : Evaluation of coupled line parameters," IEEE Trans. on MTT, Vol. MTT - 18, April 1970, pp. 222-228.

[36] M.A. Krasnosel'skii, G.M. Vainikko, P.P. Zabreiko, Ya.B. Rutitskii, and V.Ya. Stetsenko, "Priblizhennoe resheniye operatornykh uravnenii," Approximate Solution of Operator Equations), Chap. 4, Nauka, Moscow, 1969.

[37] W.H. Leighton and A.G. Milnes, "Junction reactance and dimensional tolerance effects on X - band 3 - db directional couplers," IEEE Trans. on MTT, Vol. MTT - 19, October 1971, pp. 818-824.

[38] L. Lewin, "Radiation from discontinuities in stripline," Proc. IEE, Vol. 107, pt. C, February 1960, pp. 163-170.

[39] N. Marcuvitz, Ed., Waveguide Handbook, New York : Dover 1965.

[40] G.L. Matthaei, L. Young and E.M.T. Jones, Microwave Filters Impedance-Matching Networks and Coupling Structures, New York : McGraw-Hill, 1964.

[41] K. Mehmet, M.K. McPhun and D.F. Michie, "Simple resonator method for measuring dispersion in microstrip," Electronics Letters, Vol. 8, No. 6, pp. 165-166.

[42] S.G. Mikhlin and K.L. Smolitskiy, Approximate Methods for Solution of Differential and Integral Equations, New York : American Elsevier Pub. Co. Inc., 1967.

[43] R. Mittra and T. Itoh, "A new technique for the analysis of the dispersion characteristics of microstrip lines," IEEE Trans. on MTT, Vol. MTT - 19, January 1971, pp. 47-56.

[44] R. Mittra and T. Itoh, "Charge and potential distributions in shielded strip-lines," IEEE Trans, on MTT, Vol. MTT - 18, March 1970, pp. 149-156.

[45] L.S. Napoli and J.J. Hughes, "Foreshortening of microstrip open circuits on alumina substrates," IEEE Trans. on MTT (Corresp.), Vol. MTT - 19, June 1971, pp. 559-561.

[46] A.A. Oliner, "Equivalent circuits for discontinuities in balanced strip transmission line," IRE Trans. PGMTT - 3, 2, March 1965, pp. 134-143.

[47] H.B. Palmer, "The capacitance of parallel plate capacitor by the Schwartz-Christoffel transformation," Trans. Amer. Inst. Elect. Engnrs., Vol. 56, 1937, pp. 363-366.

[48] P.D. Patel, "Calculation of capacitance coefficients for a system of irregular finite conductors on a dielectric sheet," IEEE Trans. on MTT, Vol. MTT - 19, November 1971, pp. 862-869.

[49] R.A. Pucel, D.J. Masse and C.P. Hartwig, "Losses in microstrip," IEEE Trans. on MTT, Vol. MTT - 16, June 1968, pp. 342-350 and December 1968, p. 1064.

[50] D.K. Reitan, "Accurate determination of the capacitance of rectangular parallel - plate capacitors," J. of Applied Physics, Vol. 30, No. 2, February 1959, pp. 172-176.

[51] W.W. Rogosinski, Volume and Integration, New York : Interscience Pub. Inc., 1952.

[52] P. Silvester, Modern Electromagnetic Fields, Englewood Cliffs, N.Y. : Prentice Hall, 1968.

[53] P. Silvester, "TEM wave properties of microwave transmission lines," Proc. IEEE, Vol. 115, No. 1, January 1968, pp. 43-48.

[54] P. Silvester and M.-S. Hsieh, "Projective solution of integral equations arising in electric and magnetic field problems," J. of Computational Physics, Vol. 8, 1971, pp. 73-82.

[55] P. Silvester and P. Benedek, "Electrostatics of the microstrip - Revisited," IEEE Trans. on MTT (Corresp.), to appear.

[56] P. Silvester and P. Benedek, "Equivalent capacitances of microstrip open circuits," IEEE Trans. on MTT, Vol. MTT - 20, August 1972 .

[57] H. Sobol, "Application of integrated circuit technology to microwave frequencies," Proc. IEEE, Vol. 59, No. 8, August 1971, pp.1200-1211.

[58] H. Sobol, "Radiation conductance of open-circuit microstrip," IEEE Trans. on MTT (Corresp.), Vol. MTT - 19, November 1971, pp. 885-887.

[59] I. Stakgold, Boundary Value Problems of Mathematical Physics, Vols. I and II, New York : Macmillan, 1968.

[60] I.M. Stephenson and B. Easter, "Resonant techniques for establishing the equivalent circuits of small discontinuities in microstrip," Electronics Letters, Vol. 7, No. 19, September 23, 1971, pp. 582-584.

[61] H.E. Stinehelfer, Sr., "An accurate calculation of uniform microstrip transmission lines," IEEE Trans. on MTT, Vol. MTT - 16, July 1968, pp. 439-444.

[62] H.E. Stinehelfer, Sr., "Microstrip circuit design," Tech. Rep. AFAL-TR-69-10, February 1969, (AD 848 947).

[63] A.H. Stroud and D. Secrest, Gaussian Quadrature Formulas, Englewood Cliffs : Prentice-Hall, 1966.

[64] P. Troughton, private communication (letter dated August 1971).

[65] P. Troughton, "Design of complex microstrip circuits by measurement and computer modeling," Proc. IEE, Vol. 118, No. 314, March / April 1971, pp. 469-474.

[66] P. Troughton, "High Q factor resonators in microstrip," Electronics Letters, Vol. 4, 1968, pp. 520-522.

[67] P. Troughton, "Measurement techniques in microstrip," Electronics Letters, Vol. 5, 1969, pp. 25-26.

[68] H.A. Wheeler, "Transmission line properties of parallel wide strips by a conformed-mapping approximation," IEEE Trans. on MTT, Vol. MTT - 12, May 1964, pp. 280-289.

[69] H.A. Wheeler, "Transmission-line properties of parallel strips separated by a dielectric sheet," IEEE Trans. on MTT, Vol. MTT - 13, March 1965, pp. 172-185.

[70] J.R. Whinnery and H.W. Jamieson, "Equivalent circuits for discontinuities in transmission lines," Proc. IRE, Vol. 32, No. 2, February 1944, pp. 98-114.

[71] J.R. Whinnery, H.W. Jamieson and T.E. Robins, "Coaxial-line discontinuities," Proc. I R E, Vol. 32, No. 11, November 1944, pp. 695-709.

[72] I. Wolff, G. Kompa and R. Mehran, "Calculation method for microstrip discontinuities and T-junctions," Electronics Letters, Vol. 8, No. 7, April 6, 1972, pp. 177-179.

[73] E. Yamashita and K. Atsuki, "Analysis of thick strip transmission lines," IEEE Trans. on MTT (Corresp.), Vol. MTT-19, No. 1, January 1971, pp. 120-122.

[74] E. Yamashita and R. Mittra, "Variational method for the analysis of microstrip lines," IEEE Trans. on MTT, Vol. MTT - 16, No. 4, April 1968, pp. 251 - 256.

[75] E. Yamashita, "Variational method for the analysis of microstriplike transmission lines," IEEE Trans. on MTT, Vol. MTT - 16, August 1968, pp. 529-535.

[76] G.I. Zysman and D. Varon, "Wave propagation in microstrip transmission lines," IEEE G-MTT Int. Microwave Symp. Dig., May 1969, pp. 3-7.

[77] G.D. Vendelin, "Limitations of stripline Q," Microwave Journal, Vol. 13, May 1970, pp. 63-69.

[78] M. Maeda, " An analysis of gap in microstrip transmission lines," IEEE Trans., on MTT, Vol. MTT-20, June 1972, pp. 390-396.